INDUCED ABSORPTION IN ZINC SULPHIDE DOPED WITH MANGANESE

A Thesis

presented by

J. Dreyhsig, cand. phys.

to the

University of St. Andrews

in application for the

Degree of Master of Science

Declaration

I hereby certify that this thesis has been composed by me, and is a record of work done by me, and has not previously been presented for a higher degree.

The research was carried out in the Wolfson Institute of Luminescence of the Department of Physics of the University of St. Andrews., under the supervision of Prof. J.W. Allen.

Jörg Dreyhsig

Certificate

I certify that J. Dreyhsig, cand. phys. has spent four terms at research work in the Department of Physics of the University of St. Andrews under my direction, that he has fulfilled the conditions of the Resolution of the University Court, 1967, No.1, and that he is qualified to submit the accompanying thesis in application for the Degree of Master of Science.

J.W. Allen

Research Supervisor

Acknowledgements

Firstly I have to thank the German Academic Exchange Service and the Scottish Stevenson Foundation for providing me with financial support.

I would also like to thank all the people who made this time at St. Andrews so unforgettable for me. There are others, first of all my parents, I have to thank, as they had a great influence on my previous academic career and thus made it possible for me to come to St. Andrews.

I thankfully acknowledge the help of Prof. H.E. Gumlich, Berlin, whose contacts to St. Andrews were the basis of my academic endeavour. Most of all I have to thank my supervisor, Prof. J.W. Allen, for his advice, encouragement and patience throughout the entire time of the project. I would like to express my gratitude to Prof. W. Sibbett and his research group for having been allowed to use their spectra-physics Ar-ion laser.

Finally, I should like to thank Babette, for although having been apart her love has stayed with me and encouraged me throughout this year.

Abstract

The experimental tool of induced absorption from a populated excited level was employed to investigate electronic high energy excitation states of Mn impurities in ZnS. The sample used had a doping of 0.5 at% Mn, the spectral range was 350 - 2700 nm. All experiments were performed at room temperature.

First, white light served as inducing light to consider any other induced processes that do not directly involve the Mn centres. A broad band in the visible was found, giving absorption under blue light, increased transmittance under red light illumination.

Next, by pumping the first excited state of the Mn centres, $^4T_1(G)$, by an Ar-ion laser a lot of structures were found. With the aid of frequency response the features were specified. Five structures seemed to be correlated to the Mn centres: bands at 650, 830 and 1270 nm as had been observed in a former work by Kushida et al [1,2], a band near 1910 nm and a threshold in the region 390 - 520 nm.

The possibility of a photo-ionization of the $^4T_1(G)$ state, any assignments of the bands according to crystal field theory and models for the other processes are discussed.

Für meine Eltern

(To my parents)

CONTENTS

1 INTRODUCTION

The technical usefulness of semiconductor phosphors is obvious. By means of different exciting processes there is the possibility of constructing light emitting devices. Flat panel electroluminescent devices are relevant in particular. ZnS phosphors have been very promising materials hitherto. Pioneer work was done by Destriau [3] in 1936, but reliability problems halted any commercial interest in the 1950's. Later on new breakthroughs brought industrial feasibility back. Although some firms dropped out again, actual devices made of a ZnS phosphor (ZnS:Mn) and working by electroluminescence are now available.

Though a lot of work has been spent on ZnS:Mn in the past 50 years there are still a lot of remaining questions. Even the actual exciting process that is responsible for the electroluminescence has not been thoroughly understood.

On the other hand it is well known that the Mn luminescence is due to an internal transition of the d^5 subshell of the Mn centres. In terms of crystal field theory the transition is labelled $^4T_1(G) \rightarrow {}^6A_1(S)$. The luminescence corresponds to a transition from the ground state to the first of five bands seen in direct absorption. Among the disputed questions are the problems whether there are any excited states above the five bands and, above all, how deep the $^6A_1(S)$ ground state lies within the bands of the host lattice since an absorption threshold indicating the removal of one electron

to the conduction band has not been seen yet. The latter is quite essential for any theory of electroluminescence.

To have access to higher energy excitations than the intrinsic band gap absorption, a method was extended from works on Cr impurities in ruby to ZnS:Mn by Kushida et al [1,2]. If an excited level of the impurity is populated sufficiently, subsequent absorption to higher states could be detected. Since the energy difference of these two excited states is smaller than for a direct transition from the ground state, this induced absorption can reveal levels that are usually hidden by the band gap absorption. Compared to the other known states that decay non-radiatively to the $^4T_1(G)$ state the latter has a rather long lifetime of about 2 ms because the radiative transition to the ground state is spin-forbidden. If this level is sufficiently pumped, it could be possible to see induced absorption structures.

Kushida et al [2] had to use modulated pumping by laser light and to use lock-in techniques to enhance the sensitivity of the system as the signals were still very weak. They looked at the region 350 - 2000 nm and found bands around 655, 830 and 1280 nm. Temperature dependent broadening and decay characteristics were investigated as well as any dependence on the impurity concentration. Finally they assigned the bands to internal Mn transitions by the aid of crystal field theory. Unfortunately their work lacks a display of a whole spectrum of the induced processes. Although they mentioned relative intensities a direct comparison would have been of interest. Any photo-ionization threshold was not observed.

More than 10 years passed without any confirmation or further evidence of those results. Obviously the performance of the experiments is quite difficult. The expected signals are very weak (unfortunately the Japanese work lacked any absolute values) and one has to take care that the crystal is not 'blown up' by the laser beam.

The object of this thesis was to repeat that experiment. Just one sample (0.5 at% Mn) was used and all experiments were carried out at room temperature. Main emphasis was put onto the actual existence of any induced process and on related dynamical behaviours among the revealed structures to see whether the features had the same origin. It was also tried to obtain spectra of as large a spectral region as possible. Furthermore white light was employed as inducing light source as well to look for any other processes that could perturb the laser experiments. Ordinary absorption and photoluminescence (excited by the laser) experiments served to check the usual optical properties a ZnS:Mn sample should have.

The thesis has been divided into eight chapters. After this introductory one the next chapter tells about basic theoretical knowledge that is of importance for this work. Chapter 3 deals with the optical properties of Mn centres in ZnS. The experimental outline of the experiments is explained in chapter 4. Following, the experimental results are shown in the fifth chapter. Chapter 6 discusses these results in order to distinguish between Mn correlated and other structures and tries to use crystal field theory for any

assignments. A structure that could represent the photo-ionization of the $^4T_1(G)$ state is considered in terms of a theory outlined in chapter 2. Chapter 6 also gives suggestions about future experiments. Finally a summary is given in chapter 7.

2 THEORY

2.1 INTRODUCTION

The main topic of this thesis is about optical properties of an impurity within a crystal. In particular internal transitions within an electronic shell are of importance. For this purpose section 2.2 deals with the so-called crystal field theory. Since all experiments were carried out at room temperature section 2.3 considers the influence of phonon interaction. Finally, as there is the possibility of photo-ionization, section 2.4 gives some basic background of this phenomena.

2.2 CRYSTAL FIELD THEORY

2.2.1 INTRODUCTION

Already for free atoms it is impossible to achieve an exact theory for the description of the line spectra. Perturbation theory and approximations have to be used. The conditions are much more complicated in the case of an impurity sited within a solid. A

consideration of the interactions with all the other atoms is beyond any calculation. Even if one takes only nearest neighbours into account one will hardly be able to develop a theory to describe the experimental results a priori. However, it is possible to work out some qualitative properties just because of the symmetry of the impurity site. In a second step one employs time independent perturbation theory and fits the results to the experimental data. Thus no exact knowledge of the interaction forces is needed.

The problem was first approached by considering the influence of electrostatic fields of the ligands. The energies of ordinary atomic orbits can split by first order perturbation theory but the wavefunctions have still the same radial dependence as the atomic orbits. However, in a lot of crystals it turns out that the electrostatic fields are too weak to explain the observed levels. Covalency has to be taken into account. A detailed treatment requires more specifications about the wavefunctions. However, if the radial parts of the different orbitals wavefunctions are still the same, one gets the same results (matrix elements) as for the electrostatic fields. The splitting parameter is now regarded to be mainly empirical. Even the values describing the Coulomb interaction among the electrons in a many electron system can change relative to the values of the free atom.

There are different terminologies in use: ligand field theory is used for the more general problem, whereas the expression crystal field theory arose with the first considerations about electrostatic effects (Bethe [4]). I shall use the latter expression.

Introductory literature can be found in works by eg Gliemann and Schlaefer [5], Ballhausen [6], Tanabe, Sugano and Sukumoto [7] or McClure [8]. Here a brief description will be given.

2.2.2 THE FREE ATOMIC SPECTRA

First the free atom is considered. The full Hamiltonian in space representation (indicated by the superscript x) neglecting spin orbit interaction (s. section 2.2.3) is

$$H^{x} = -\frac{\hbar^2}{2m}\sum_j \nabla_j^2 - \sum_j \frac{Ze^2}{4\pi\varepsilon_o r_j} + \sum_{j>k} \frac{e^2}{4\pi\varepsilon_o r_{jk}} \qquad (2.2.2.1)$$

where j is numbering the electrons, Z is the nuclear charge number, r_j the distance of the jth electron to the centre and r_{jk} the distance between the jth and kth electron. The eigenvalues of (2.2.2.1) cannot be found directly. In a first approximation the third term is considered by replacing Z in the second term by an effective charge Z_j, taking into account the shielding of the core charge by the other electrons. These Z_j's are obtained by the self-consistent field treatment. The result yields nl-orbitals similar to the hydrogen case, but orbitals with different l are no longer degenerate. A specific nl-orbital is still (2l+1) manifold indicated by the magnetic quantum number m_l. Introducing the spin the degeneracy rises by a

factor 2.

Suppose an atom has a $1s^2 2s^2 2p^3$ configuration. The 2p subshell is the only unfilled one. The electron-electron interaction splits the degeneracy of a subshell so that transitions within the 2p subshell are possible. Since the other shells are filled and to a certain amount well separated in energy, one can reduce the optical treatment for small enough energies to the 2p electrons.

Of course, this treatment is valid for any other subshell as long as other configurations are not very close in energy. Now j in (2.2.2.1) is only labelling the electrons of the appropriate subshell and Z becomes the effective charge for these. The third term is regarded as perturbation. Carrying out the secular equation one finds that the energy levels split into so-called terms. In the case of small spin-orbit interaction (as here considered), the Russell-Saunders or LS coupling scheme is obtained. The electron-electron interaction mixes all states with same total angular momentum L and total spin S. A term is (2L+1)(2S+1) manifold. Both s and l are no longer good quantum numbers because their operators do not commutate with H. They are now replaced by the good quantum numbers L and S. The nomenclature for a term is ^{2S+1}L, eg L = 1 and S = 1 => ^3P.

To obtain the matrix elements of the perturbation one has to use antisymmetric wavefunctions because of the Pauli principle. It turns out that the integrals of the form

$$\langle \varphi_1 | H_{int} \varphi_2 \rangle = \int \varphi_1^*(\underline{x})\ H_{int}^{\underline{x}}\ \varphi_2(\underline{x})\ d^{3n}r,$$

where the $|\varphi_{1,2}\rangle$ are many-electron eigenfunctions, get separated into integrals with single-electron eigenfunctions. There are different notations but a very convenient method was developed by Racah [9]. Using the 'Racah-parameters' A, B and C one gets eg for a d^5 configuration the energy values listed in Tab. 2.2.2.1.

2.2.3 CRYSTAL FIELDS

For an impurity in a crystal one gets an additional term V in (2.2.2.1) describing the influence of the environmental atoms, mainly the nearest neighbours. Thus the entire Hamiltonian including spin-orbit coupling is:

$$H^{\underline{x}} = -\frac{\hbar^2}{2m}\sum_j \underline{\nabla}_j^2 - \sum_j \frac{Ze^2}{4\pi\varepsilon_0 r_j} + \sum_{j>k} \frac{e^2}{4\pi\varepsilon_0 r_{jk}} + V + \sum_j \xi_j(r)\ \underline{l}_j \cdot \underline{s}_j \qquad (2.2.3.1)$$

There are different cases of importance [6]:

- $V < \xi_j(r)\ \underline{l}_j \cdot \underline{s}_j$ — complexes of rare earths
- $\xi_j(r)\ \underline{l}_j \cdot \underline{s}_j < V < e^2/(4\pi\varepsilon_0 r_{jk})$ — complexes of the first transition group
- $e^2/(4\pi\varepsilon_0 r_{jk}) < V$ — 'covalent' complexes

Tab. 2.2.2.1: Energies of the terms of a d^5 configuration in form of Racah parameters A, B and C

term	energy	term	energy
^6S	10A-35B	$^2G'$	10A+3B+10C
^4G	10A-25B+5C	^2F	10A-9B+8C
^4F	10A-13B+7C	$^2F'$	10A-25B+10C
^4D	10A-18B+5C	^2D	10A-4B+10C
^4P	10A-28B+7C	$^2D''$	$10A-3B+11C \pm 3(57B^2+2BC+C^2)^{1/2}$
^2I	10A-24B+8C	^2P	10A+20B+10C
^2H	10A-22B+10C	^2S	10A-3B+8C
^2G	10A-13B+8C		

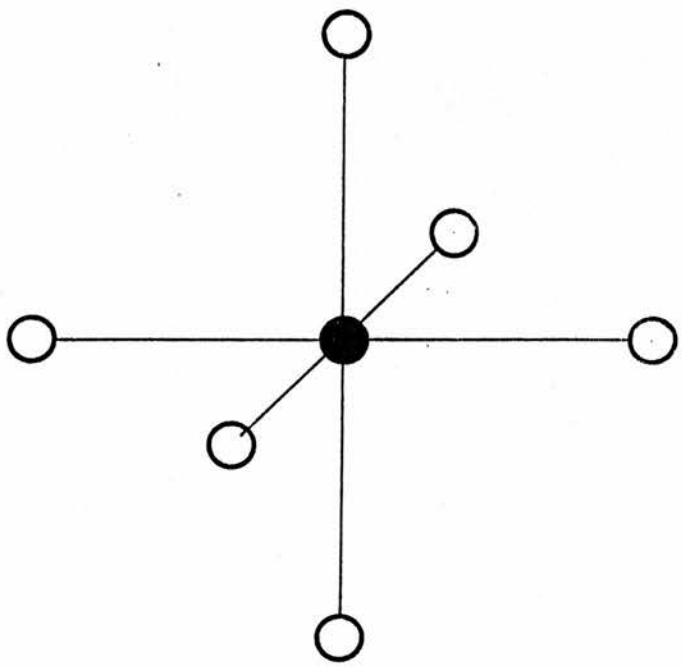

Fig. 2.2.3.1: Atom surrounded by an regular octahedron (O_h point symmetry)

In this thesis I am concerned with the second group. Thus spin-orbit coupling is neglected (as already done in section 2.2.2). The energy levels are now evaluated by figuring out the matrix elements of the third and fourth term in (2.2.3.1).

Before passing to this more general treatment it is convenient to consider the properties of the perturbation V first. Suppose an impurity is surrounded by 6 nearest neighbours as drawn in Fig. 2.2.3.1. The site of the impurity has the symmetry of the O_h point group. In contrast to the free atom Hamiltonian its symmetry is now reduced. First H was invariant against every rotation around any axis through the centre, now there are only a few rotations left. This is lifting some of the degeneracy of the electronic levels.

Assuming R to be an operator for a symmetry transformation, $|\varphi_i\rangle$, $i = 1,n$ a set of degenerate eigenfunctions for an eigenvalue E of the Hamiltonian H, one has

$$H\,|\varphi_i\rangle = E\,|\varphi_i\rangle,$$

$$H = R\,H\,R^{-1}$$

$$\Rightarrow \quad R\,H\,|\varphi_i\rangle = R\,E\,|\varphi_i\rangle$$

$$\Rightarrow \quad H\,R\,|\varphi_i\rangle = E\,R\,|\varphi_i\rangle\ .$$

$\Rightarrow R\,|\varphi_i\rangle$ is again an eigenfunction for the eigenvalue E. Therefore it must be a linear combination of the $|\varphi_i\rangle$'s:

$$R\,|\varphi_i\rangle = \sum_j \Gamma_{ji}(R)\,|\varphi_j\rangle\ .$$

All the symmetry operators R for a specific situation form a group. Obviously the $\Gamma_{ji}(R)$'s satisfy the group axioms, too. They are a so-called representation of the group with the base of the $|\varphi_i\rangle$'s. The representation is called reducible, if it has the form of 'submatrices' as illustrated in Fig. 2.2.3.2. Otherwise it is an irreducible representation. A matrix can be reducible though it does not look like one shown in Fig. 2.2.3.2. This can happen because of an inconvenient choice of the base. By applying a unitary operation (eg to rotate the wavefunctions) a reducible matrix can always be transferred into the shape of Fig. 2.2.3.2. By means of 'characters', the sum of the diagonal elements in $\Gamma(R)$, it is possible to decide whether $\Gamma(R)$ is reducible or not.

Now the following statement can be made: in case of a reducible matrix $\Gamma(R)$ the degeneracy will split into m levels, m being the number of irreducible representations within $\Gamma(R)$. The appropriate eigenfunctions are given by the separated sets of the new base. A still existing degeneracy beyond this is accidental. This can be understood as follows: a degeneracy arises because different locations are equivalent. In the case in which no symmetry operation is able to mix different eigenfunctions they are not equivalent. Thus they should not necessarily have the same energy eigenvalue.

One problem is still left: in (2.2.3.2) it was assumed that the eigenvalue problem is already solved. In most cases this is impossible. However, the treatment gives qualitative information and helps to calculate matrix elements. The latter are of the form

*	*	*	*	*	0	0	0	0	0	0	0	0	0
*	*	*	*	*	0	0	0	0	0	0	0	0	0
*	*	*	*	*	0	0	0	0	0	0	0	0	0
*	*	*	*	*	0	0	0	0	0	0	0	0	0
*	*	*	*	*	0	0	0	0	0	0	0	0	0
0	0	0	0	0	*	*	*	0	0	0	0	0	0
0	0	0	0	0	*	*	*	0	0	0	0	0	0
0	0	0	0	0	*	*	*	0	0	0	0	0	0
0	0	0	0	0	0	0	0	*	0	0	0	0	0
0	0	0	0	0	0	0	0	0	*	*	*	*	0
0	0	0	0	0	0	0	0	0	*	*	*	*	0
0	0	0	0	0	0	0	0	0	*	*	*	*	0
0	0	0	0	0	0	0	0	0	*	*	*	*	0
0	0	0	0	0	0	0	0	0	0	0	0	0	*

Fig. 2.2.3.2: Reducible matrix

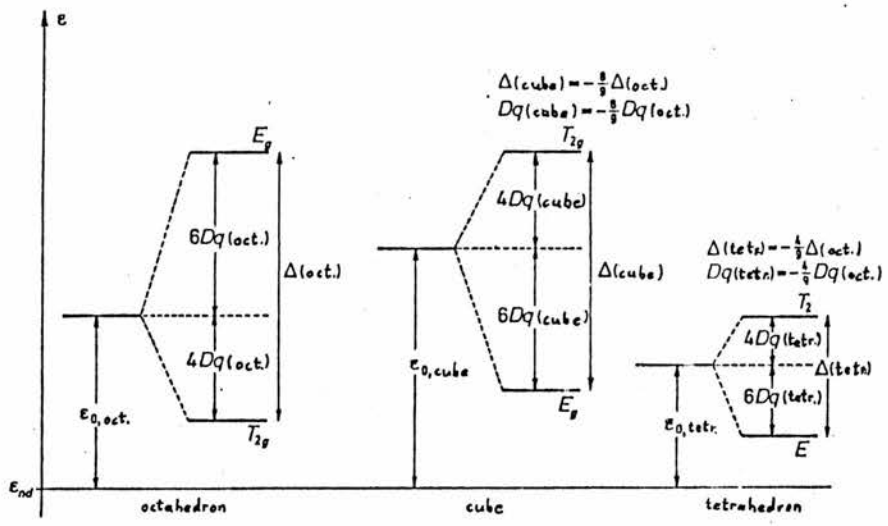

Fig. 2.2.3.3: Splitting of a d orbital in an octahedral, cubic and tetrahedral crystal field [5]

$$H_{ij} = \langle \varphi_i | H \varphi_j \rangle .$$

If this is subjected to a symmetry transformation it can hold that $|\varphi_i\rangle$ belongs to a representation Γ_i and $|\varphi_j\rangle$ to Γ_j. H is invariant by the symmetry operation, it is transformed according to the identity operation Γ_1. Hence $|H \varphi_j\rangle$ transforms like Γ_j since the direct product gives $\Gamma_j \otimes \Gamma_1 = \Gamma_j$. In the case $\Gamma_i \neq \Gamma_j$ the two vectors in the scalar product are in different representation spaces. Hence they are orthogonal and $H_{ij} = 0$. Thus the secular equation of first order perturbation theory becomes extremely simplified.

For the representations there are some nomenclatures in use. I shall use Mulliken's, where A and B stand for one-dimensional, E for two-dimensional and T for three-dimensional representations. Small letters are used for orbitals.

If one does the perturbation calculation for one d electron for O_h symmetry, it turns out that the fivefold degeneracy for single electron orbits (spin neglected) is removed giving a twofold 'e_g' level and a threefold 't_{2g}' level (the suffix is for even parity). The energy difference between these levels is $\Delta \equiv 10Dq$. D and q are parameters that represent the electrostatic fields of the ligands (s. section 2.2.1). Δ is used for the more covalent approach. The splitting is shown in Fig. 2.2.3.3. The calculation was done for a regular octahedron. In the case of a cubic or tetrahedral environment (O_h and T_d point symmetry), the representations are the same but in T_d there is no inversion centre and any suffix g or u is dropped. The resulting one electron levels are again $e_{(g)}$ and $t_{2(g)}$ but the

difference between them has changed (Fig. 2.2.3.3).

As already mentioned it is nearly impossible to calculate Δ a priori. Therefore, Δ is used as an empirical parameter (s. also section 2.2.1). The same procedure is applied for the shift of a multiplet.

In a many-electron system many-electron functions have to be constructed out of these one-electron functions. As in a free atom the electron-electron interaction has to be considered and a splitting can occur because the representation of a many-electron function, as a product of irreducible representations, is often reducible. Tab. 2.2.3.1 shows a multiplication table for the groups T_d. Since the spin S is still a good quantum number, a term is written $^{2S+1}\Gamma$ eg $S = 2$, $\Gamma = T_2 \Rightarrow {}^5T_2$.

There are different possibilities to distinguish how to treat both perturbations, the crystal field and the electron-electron interaction:

1) The electron-electron interaction is much stronger than the perturbation by the crystal field. Thus first the terms ^{2S+1}L are determined and then the crystal field is treated as a perturbation upon each of the terms. This is the <u>weak field case</u>.

2) In this case the crystal field is dominant, the electron-electron interaction is weak. Now the configurations by the crystal field are split separately by the other perturbation. This is the <u>strong field</u>

Tab. 2.2.3.1: Multiplication table for products of representations of the T_d point group

$\Gamma_i \times \Gamma_j$	A_1	A_2	E	T_1	T_2
A_1	A_1	A_2	E	T_1	T_2
A_2	A_2	A_1	E	T_1	T_2
E	E	E	A_1+A_2+E	T_1+T_2	T_1+T_2
T_1	T_1	T_1	T_1+T_2	$A_1+E+T_1+T_2$	$A_2+E+T_1+T_2$
T_2	T_2	T_2	T_1+T_2	$A_2+E+T_1+T_2$	$A_1+E+T_1+T_2$

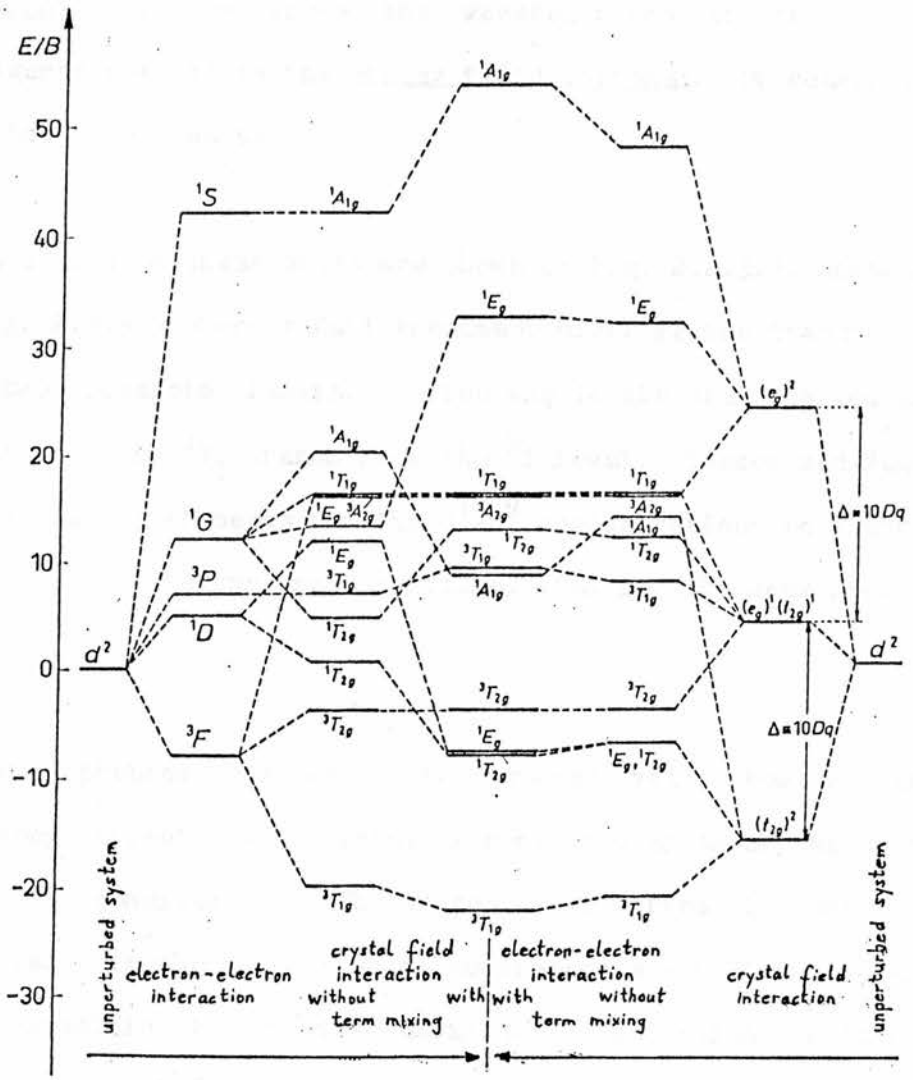

Fig. 2.2.3.4: Weak and strong field case and approach for a d^2 configuration in a octahedral field (C/B = 4, Δ = 10Dq = 20B) [5]

case.

3) Both interactions are of comparable strength. Thus equal terms obtained by 1) or 2) are mixed considerably in either case by the second perturbation and the negligence of some off-diagonal matrix elements as done in 1) and 2) is no longer reasonable. Instead one has to figure out all matrix elements. There are two possible ways to simplify the calculation: if one starts with the wavefunctions of the terms of the electron-electron interaction one performs the weak field approach, if one takes the wavefunctions of the crystal field configurations it is the strong field approach. Of course both ways give the same results.

For a d^2 system these cases are shown in Fig. 2.2.3.4. Another example is Fig. 2.2.3.5 where a full treatment displays the transition between the two possible limits. Often the levels are labelled eg $^3T_1(F)$, indicating the $^3T_1$ branch from the ^3F level. Tanabe and Sugano have listed matrix elements for the d^1-d^9 configurations in a strong field approach [10] whereas Orgel published them for the weak field approach [11].

One problem has not been covered yet: how strong are any covalency effects beyond this? A more general theory about covalency is quite complicated. Therefore, one tries to use simplified theories. In the case in which covalency is not too strong it is quite sensible to consider covalency by a distinct treatment of the different electronic orbitals, here the t_2 and e orbitals. In particular the radial part of the wavefunction should be altered such

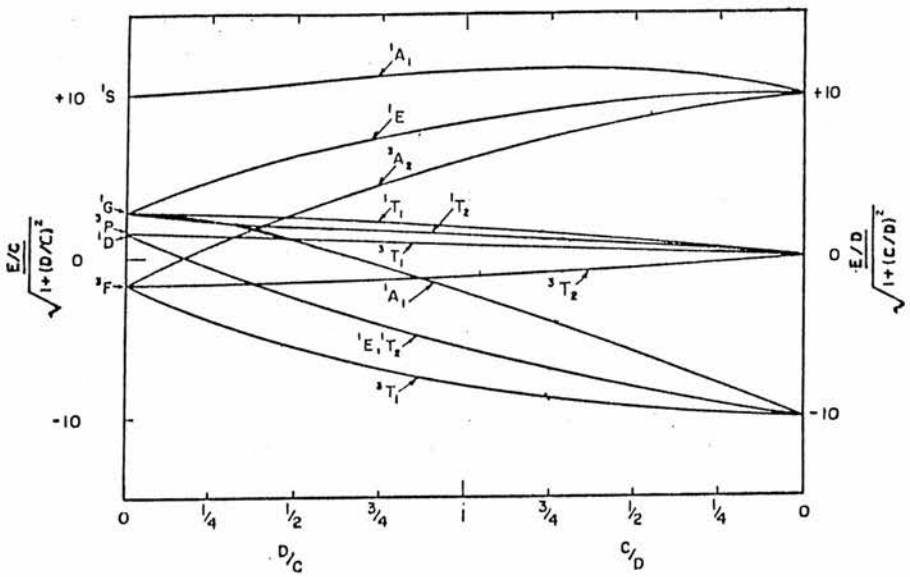

Fig. 2.2.3.5: Correlation between crystal field and electron-electron interaction for a d^2 configuration in a octahedral field (C/B = 4.5) [8]

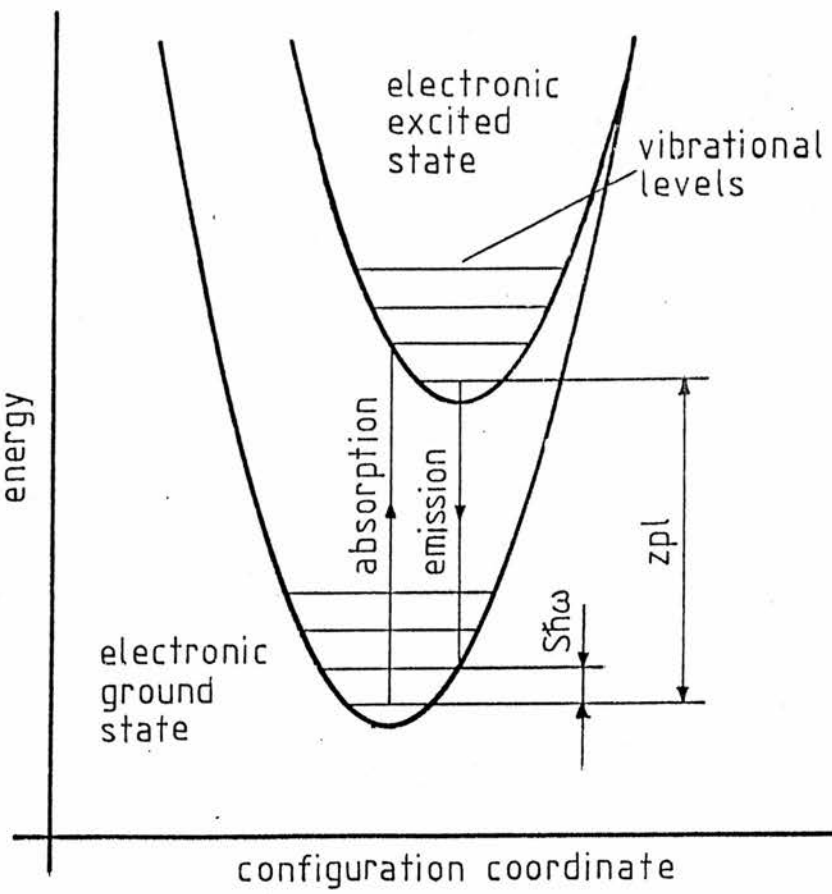

Fig. 2.3.1: Configuration coordinate diagram for an electronic ground and excited state showing the zero phonon line (zpl) and the Stokes parameter S

that they are 'stretched' differently according to the influence by the ligands. Basic work was done by Koide and Pryce [12]. Recently O'Neill [13] and Zunger [14] worked out theories resulting in actual energy level calculations particularly for $3d^n$ impurities. Summarized one has to expect a possible splitting of still accidentally degenerate levels and changes of the differences between the levels.

2.3 PHONON INTERACTION

Though there is a lot of literature about this topic, it is hard to find basic articles. However, Allen [15] has given a review of this subject.

An impurity, depending on whether it has got similar properties to the host material, gives rise to local phonons or is resonant with the crystal phonons. In the case of electronic transitions there might be some phonon interaction involved since the electrons are moving in a field caused by the nuclei. Usually the nuclei are far too slow in contrast to the electronic movements so that they sense only a constant average field by the electronic motion. This is the Born-Oppenheimer approximation where a wavefunction for both nuclear and electronic state is separated into a nuclear and an electronic part:

$$\Psi(\underline{r},\underline{R}) = \varphi(\underline{r},\underline{R})\,\phi(\underline{R})$$

electrons nuclei

where $\underline{r}$ stands for the electronic and $\underline{R}$ for the nuclear coordinates. The Hamiltonian gets the form

$$H^{X} = -\frac{\hbar^2}{2}\sum_{\alpha}\frac{\underline{\nabla}_{\alpha}^2}{M_{\alpha}} - \frac{\hbar^2}{2m}\sum_{\beta}\underline{\nabla}_{\beta}^2 + V(\underline{r},\underline{R}),$$

α numbering the nuclei and β the electrons. In a harmonic approximation for the phonons one gets for the sum of electronic and phonon energy a so-called configuration coordinate diagram (Fig. 2.3.1). The parabolas represent the harmonic approximation and the different curves stand for different electronic states.

First a more localised mode will be discussed. If the mode is strongly localised the normal coordinate q for the localised phonons is proportional to the positional coordinate of the impurity. Still, there can be a small contribution to q from the coordinates of other atoms so that the expression of a 'positional' coordinate should be handled with caution. It is not essential that the normal coordinates for the two states are the same. Though, in a lot of cases it is reasonable to assume that. The shift between the minima in Fig. 2.3.1 means that for the two states there are different positions where the impurity has its minimum energy.

For T = 0 K a transition classically happens such that the electron leaves the ground state in the minimum and terminates at the excited state directly above it. In this approximation, the Franck-Condon approximation, the nuclei are too slow to follow the electronic transition. After the transition, however, the system relaxes to the minimum by giving phonons to the lattice. Therefore a following emission would lead to a line (same process the other way around) less in energy than that in absorption. This is known as Stokes' rule.

Quantum-mechanically the quantization of phonons and the zero point energy have to be taken into account. This is indicated in Fig. 2.3.1. Treating the radiation field classically and calculating electronic dipole transition probabilities, one gets with the help of the Condon approximation that the appropriate matrix elements are proportional to the overlap of the vibrational modes. Supposing T = 0 K only the lowest vibrational state of the ground electronic state is occupied, but for a transition several vibrational states of the excited state are now possible. Thus the absorption spectrum consists of a series of lines with the maximum near to the classical Franck-Condon value. A similar consideration can be applied to the emission process.

If the curvatures are the same, some easy results are obtained. Emission and absorption (after a certain normalization) show a spectrum symmetrical about the zero phonon line (zpl)(mirror rule). For T = 0 K the shape function of the lines is a Poisson

distribution. If the mean number of phonons that are produced by a transition is S, where $S\hbar\omega$ is half the classical Stokes' shift (Fig. 2.3.1), then the Poisson distribution can be approximated by a Gaussian if S is greater than about 2. Anharmonic effects broaden the lines for high S so a continuous Gaussian band can be seen. For small S only a few lines are visible whereas in an intermediate range the zpl and the first phonon replicas are masked or flanked by a Gaussian band. At $T > 0$ K the thermal occupation of states of the initial level must be considered, and at high temperatures one gets a Gaussian band increasing in width by $T^{1/2}$ and peaking at the classical Frank-Condon value.

In case of the non-localised phonons the situation is quite different. After a simplified treatment by Huang and Rhys who assumed that all phonon modes have the same energy one striking result is that here a lot of phonon modes are distributing by changing their occupation number by 1 whereas in the previous case one mode changes by a certain amount. However, the spectral shape of the absorption turns out to be exactly the same as in the localised case.

2.4 PHOTO-IONIZATION

Under photo-ionization one defines the process where an electron/hole is transferred from a localised state of an impurity to a state of the conduction/valence band. Unfortunately, there is no basic theory on this field [16,17]. However, there are some

approaches by Allen [16,17], from which basic characteristics are reducible.

To get the spectral dependent probability for a transition from the initial state $|\varphi_i\rangle$ to the final state $|\varphi_f\rangle$ one has to start with Fermi's Golden Rule Nr.2:

$$W = 2\pi/\hbar \; |\langle\varphi_i|H_{int}\varphi_f\rangle|^2 \, \varrho(E,d\Omega) \; , \quad (2.4.1)$$

where $H_{int} = i\hbar e/(mc)\, \underline{A}\cdot\underline{p}$ and $\varrho(E,d\Omega)$ is the density of states at $|\varphi_f\rangle$ for the solid angle $d\Omega$ from the impurity. If one takes the dipole approximation which is valid as the wavelength of the light is far larger than the treated space on atomic scales, one gets for the optical cross-section for the absorption process with (2.4.1):

$$\sigma(h\nu,d\Omega) = \frac{\gamma^2 2\pi e^2\hbar^2}{n m^2 \nu c} \; |\langle\varphi_i|D\;\varphi_f\rangle|^2 \, \varrho(E,d\Omega) \; , \quad (2.4.2)$$

where D in space representation is given by $D^{\chi} = \underline{\Pi}\cdot\underline{\nabla}$, $\underline{\Pi}$ being a unit vector in the polarization direction, and γ is the effective field ratio, n the refractive index. There are now different possibilities of how to continue. From now on only the transfer of an electron to the conduction band is subject of the considerations since this is of interest for this work. Holes are treated similarly. Fig. 2.4.1 shows the transition of interest: the initial localized state is in the band gap, the final state in the conduction band. The initial state is more or less d-like for 3d electrons near the impurity, but

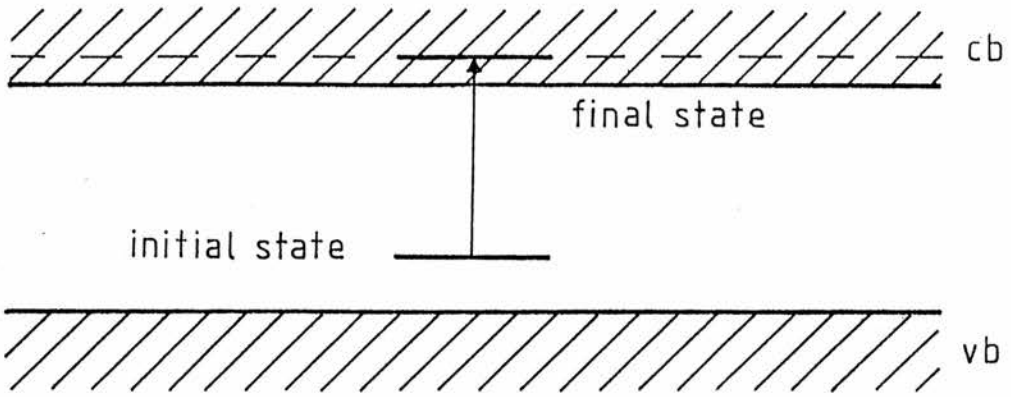

Fig. 2.4.1: Transition from a localized initial state to a less localized final state in the conduction band

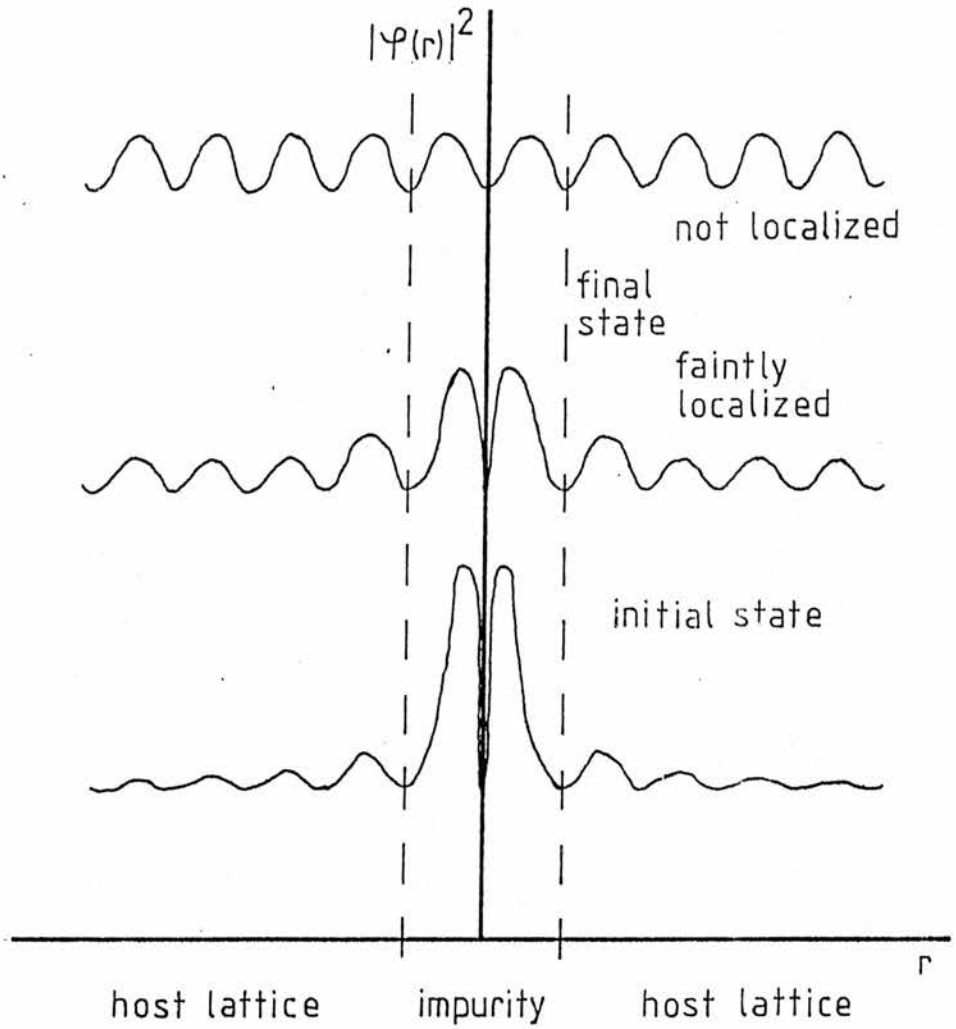

Fig. 2.4.2: Radial dependence of wavefunctions of the localized initial state and the less or not localized final state (strongly schematic!)

unlike the free atom it spreads over some crystal spacings, getting modulated by the latter and decaying with distance (Fig. 2.4.2). This region is called the tail region. On the other hand the final state has a wavefunction in the tail region that is not decaying at all. It remains periodic with the lattice. However, at the impurity site it can have a slight maximum because of a faint localization (Fig. 2.4.2).

By evaluating (2.4.2) there are two extreme situations that are used to simplify the calculation:

a) the final state is not localised, thus the matrix element is mainly dependent on the wavefunctions outside the impurity cell, $|\varphi_f\rangle$ can be approximated by a Bloch wave or even by a plane wave, $|\varphi_i\rangle$ by a decaying function, that can be modulated by Bloch waves;

b) the final state is more localised, thus the matrix element is mainly dependent on the wavefunctions values at the impurity site, $|\varphi_i\rangle$ and $|\varphi_f\rangle$ can be approximated by atomic functions.

a) has been treated in [16]. First $|\varphi_f\rangle$ is approximated by a plane wave. Taking $\underline{\Pi}$ along the z-axis one gets for the matrix element in (2.4.2):

$$\langle\varphi_i|D\varphi_f\rangle \sim \int\varphi_i(\underline{r})\ \underline{\Pi}\cdot\underline{\nabla}\ e^{i\underline{k}\cdot\underline{r}}\ d^3r = ik_z\int\varphi_i(\underline{r})\ e^{i\underline{k}\cdot\underline{r}}\ d^3r$$
$$\sim ik_z\ (2\pi)^{3/2}\ F_i(\underline{k})\ . \qquad (2.4.3)$$

$F_i(\underline{k})$ is the Fourier transform of the initial bound state wavefunction. If one takes $F_i(\underline{k})$ and $\varsigma(E,d\Omega)$ to have spherical symmetry one has with (2.4.2) and (2.4.3):

$$\sigma(h\nu) \sim k^2 \nu^{-1} |F_i(k)|^2 \varsigma(E) \quad . \quad (2.4.4)$$

There is now an important conclusion: if $F_i(k)$ stays constant over a range of k near the threshold, one can obviously simplify (2.4.4). Eventually this characteristic of $F_i(k)$ turns out, if one approximates $\varphi_i(r)$ by an exponential decaying function tail function. Since near to the threshold there is $\varsigma(E) \sim E^{1/2}$ and $k^2 \sim E$ one has for (2.4.4):

$$\sigma(h\nu) \sim \nu^{-1} E^{3/2} = \nu^{-1}(h\nu - h\nu_{threshold})^{3/2} \quad . \quad (2.4.5)$$

If one tries to fit an experimental curve by (2.4.5) it is possible to estimate the 'ionization energy' $h\nu_{threshold}$ by the intercept of the fitting. It is interesting to note that (2.4.5) even holds in some cases when the wavefunctions are modified by Bloch functions [16].

Case b) has been discussed in [17]. By expressing $|\varphi_f\rangle$ by a Bloch function

$$\varphi_f(\underline{r}) \sim u_{\underline{k}}(\underline{r})\, e^{i\underline{k}\cdot\underline{r}} \,,$$

it can be shown that $u_{\underline{k}}(\underline{r})$ can be expressed by a mixture of $|s\rangle$ and $|p\rangle$ orbitals for a zincblende structure with sp^3 bonding. If one uses these properties of $|\varphi_f\rangle$ over the spatial extent of the 3d functions one finally has

$$\sigma(h\nu) \sim E^{3/2} (E+E_p)^{-1} , \quad (2.4.6)$$

where $E_p = 2m^* P^2/\hbar^2$, P is the momentum matrix element connecting the conduction and the valence band (parabolic isotropic bands assumed). If one has a material where $E << E_p$, (2.4.6) can be approximated by (2.4.7),

$$\sigma(h\nu) \sim \nu (h\nu - h\nu_{threshold})^{3/2} , \quad (2.4.7)$$

which is similar to (2.4.5) except for the power of ν.

Till now phonon interaction was excluded. In fact phonon interaction that is too strong does not allow a similar qualitative analysis. However, as long as it is weak the above theory is somewhat applicable. Fig. 2.4.3 shows a configuration coordinate diagram for the initial and the final states. According to section 2.3 phonon interaction gives a Poisson/Gaussian distribution for a transition. Surprisingly it turns out that a Gaussian widening does not change the shape of the straight line of the absorption coefficient except near the threshold. This is illustrated in Fig. 2.4.4. The intercept E_{ic} is not the real difference E_{min} between the conduction band and the initial state but E_{cc} in Fig. 2.4.3. At low temperatures, however, one can try to estimate E_{min} by a log(absorption coefficient) against $h\nu$ plot so there is a large threshold near E_{min} (Fig. 2.4.5).

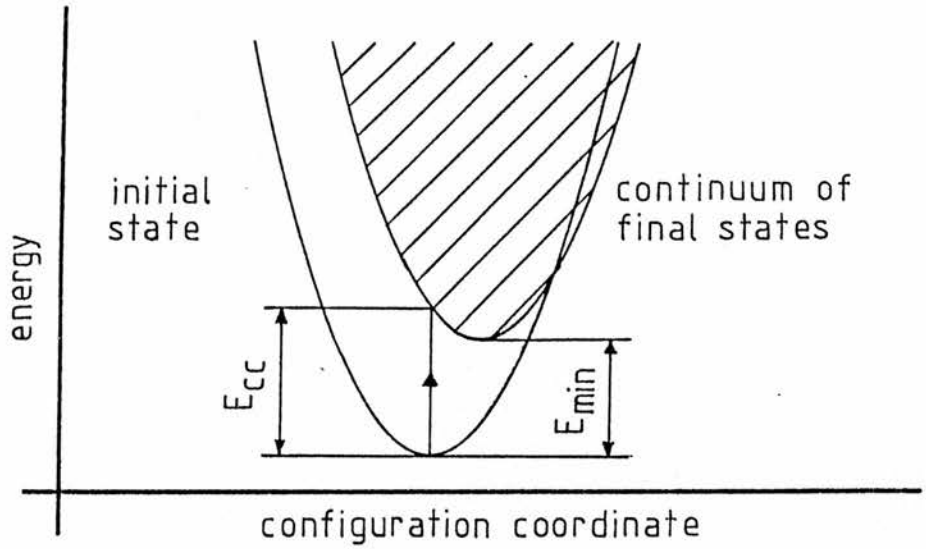

Fig. 2.4.3: Configuration coordinate diagram for a transition to the conduction band

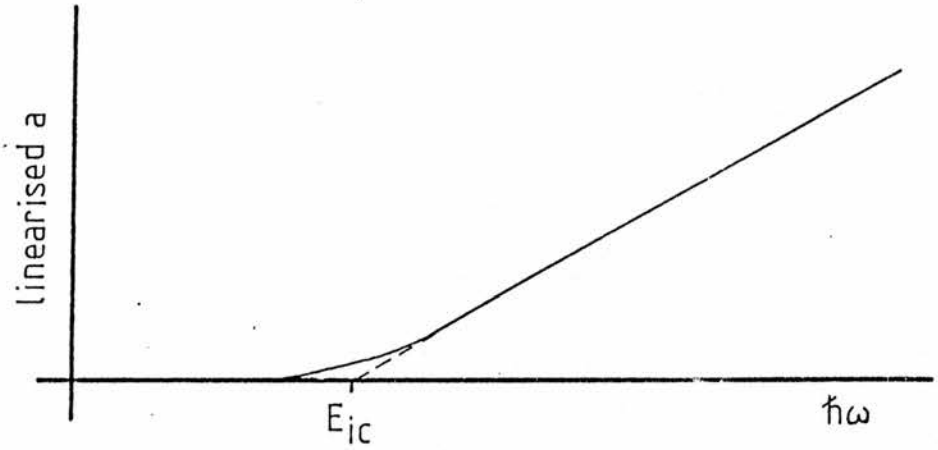

Fig. 2.4.4: Deviation of the absorption coefficient of a photo-ionization transition from a straight line plot because of Gaussian broadening of each single transition

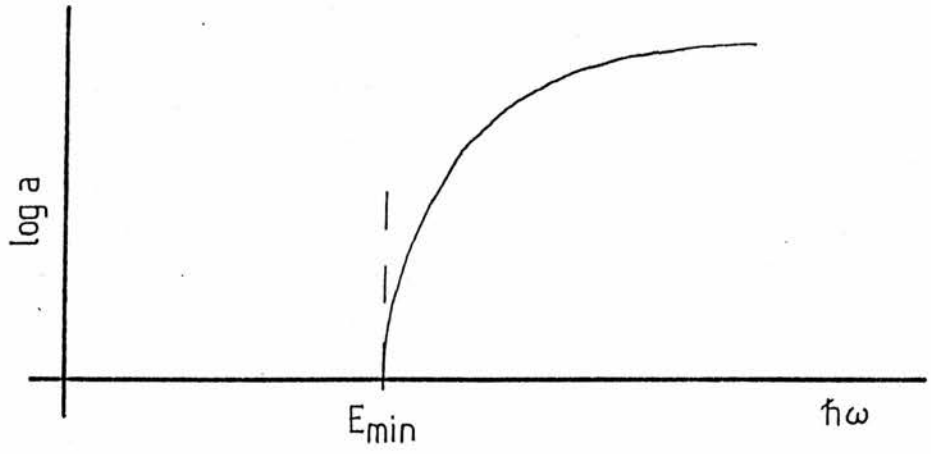

Fig. 2.4.5: Threshold of a log(a) plot of the absorption coefficient of a photo-ionization transition, showing the distance E_{min} of Fig. 2.4.3 at low temperatures

3 OPTICAL PROPERTIES OF Mn IMPURITIES IN ZnS

3.1 ENERGY LEVELS

ZnS crystals are based on S atoms tetrahedrally surrounded by Zn atoms and vice versa. There are two regular crystal structures, cubic and hexagonal. It is well known that Mn impurities are situated on substitutional Zn sites within the ZnS host lattice, eg [18]. The outer shells of a free Mn atom consist of a $3d^5 4s^2$ configuration. In the crystal the two s-electrons are involved in bondings. Hence a basic treatment of the optical properties of Mn in ZnS has to deal with the half filled 3d subshell. Any configuration mixing can be neglected since the energy difference to the next configuration ($3d^4 4p$) is large [19] (although these data were for the free ion they should not be that different for the crystal).

Compared to the free atom case the symmetry of the surroundings of the Mn is now lowered by the lattice. Thus crystal field theory as briefly outlined in section 2.2 is applicable. In cubic ZnS each atomic site has tetrahedral symmetry (point group T_d) (Fig. 3.1.1). Taking into account only nearest neighbours this is still valid in hexagonal ZnS as the Mn is surrounded by a tetrahedron of four S atoms. The free atoms terms of the d^5 configuration are listed with their splittings according to section 2.2 in Tab. 3.1.1 . For a full treatment of the perturbation it must be considered that states with

Tab. 3.1.1: Splitting of the Mn terms (d^5 configuration)

term	representation (level)
$^{6,2}S$	$^{6,2}A_1$
$^{4,2}P$	$^{4,2}T_1$
$^{4,2}D$	$^{4,2}E, ^{4,2}T_2$
$^{4,2}F$	$^{4,2}A_2, ^{4,2}T_1, ^{4,2}T_2$
$^{4,2}G$	$^{4,2}A_1, ^{4,2}E, ^{4,2}T_1, ^{4,2}T_2$
^{2}H	$^{2}E, ^{2}T_1, ^{2}T_2$
^{2}I	$^{2}A_1, ^{2}A_2, ^{2}E, ^{2}T_1, ^{2}T_2$

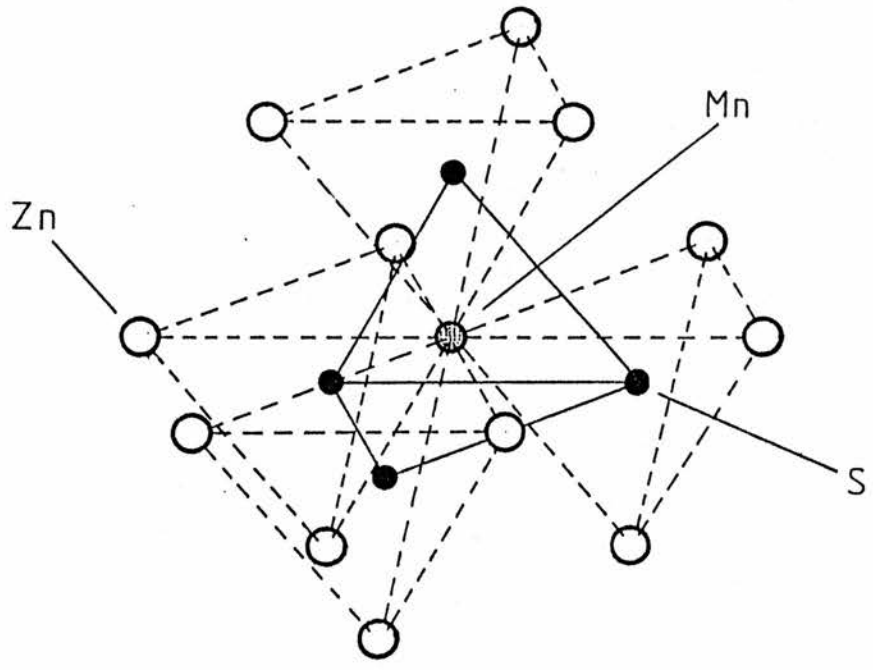

Fig. 3.1.1: Mn impurity on Zn site in cubic ZnS

the same representation are mixing.

At room temperature five broad bands are observed for ZnS:Mn in direct absorption, that are not to be seen in pure ZnS. Fig. 3.1.2 shows an absorption spectrum by Kushida et al [2] at 77 K. The threshold on the left hand side is due to intrinsic band-to-band transitions. On the other hand only one band near 580 nm is obtained both in photo- and electroluminescence. The band is displayed in Fig. 3.1.3 (according to [2]).

Although four of the absorption bands were first recognized by Kroeger 50 years ago [20] some assignments are still controversial. For the three low energy bands there is general agreement to label them with the following transitions [18]: $^6A_1(S) \rightarrow {}^4T_1(G)$, $^6A_1(S) \rightarrow {}^4T_2(G)$, $^6A_1(S) \rightarrow {}^4E(G)$. The last state is degenerate with the $^4A_1(G)$ state within a simple crystal field treatment. However, there is evidence that the observed transition terminates at the $^4E(G)$ state [18]. The radiative transition is assigned to $^4T_1(G) \rightarrow {}^6A_1(S)$ whereas the shift from the appropriate absorption can be explained by a configuration coordinate scheme. For the two remaining bands in absorption there are differing assignments by various authors. A list is given in Tab. 3.1.2 . An energy level diagram calculated by Kushida et al [2] according to Tanabe-Sugano's model [10] is shown in Fig. 3.1.4.

Tab. 3.1.2: Assignments of fourth and fifth band of Mn in ZnS

band near 395 nm	band near 430 nm	author
$^4E(D)$	$^4T_2(D)$	[2,21,22,23,24]
$^4T_2(D)$	$^2T_2(I)$	[25]
$^4E(D)$	$^2T_2(I)$	[26]
$^4E(D), ^4T_2(D)$	$^4T_1(P)$	[27,28]
$^4T_2(D)$	$^4A_1(G)$	[13] (third band -> $^4E(G)$, degeneracy lifted by special theory)

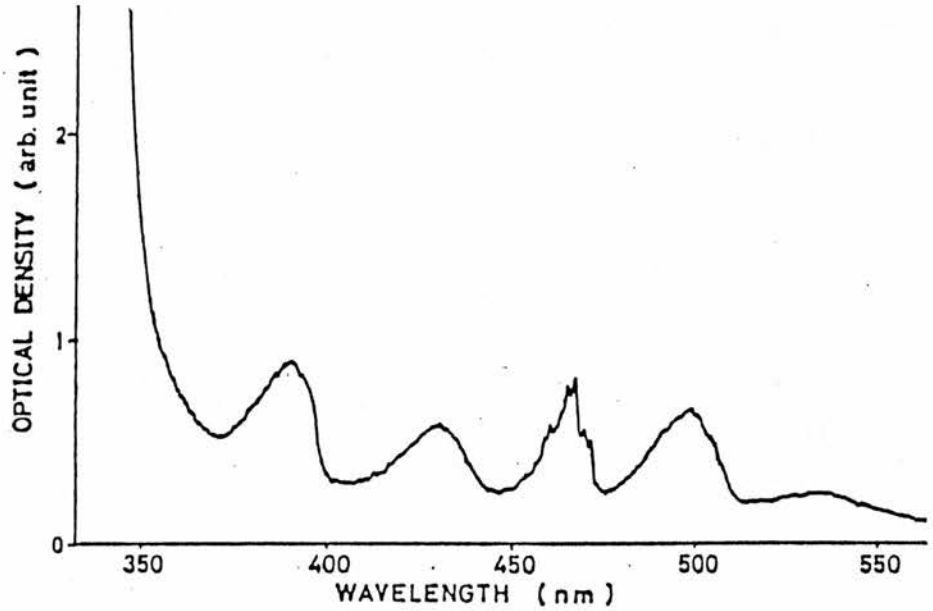

Fig. 3.1.2: Absorption spectrum of ZnS:Mn (3 mol%) at 77 K by Kushida et al [2]

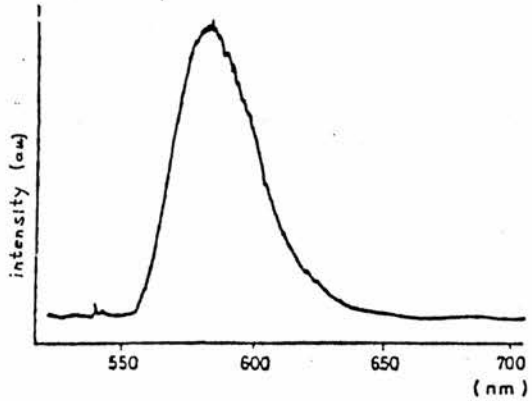

Fig. 3.1.3: Luminescence of ZnS:Mn (3 mol%) at 77 K by Kushida et al [2]

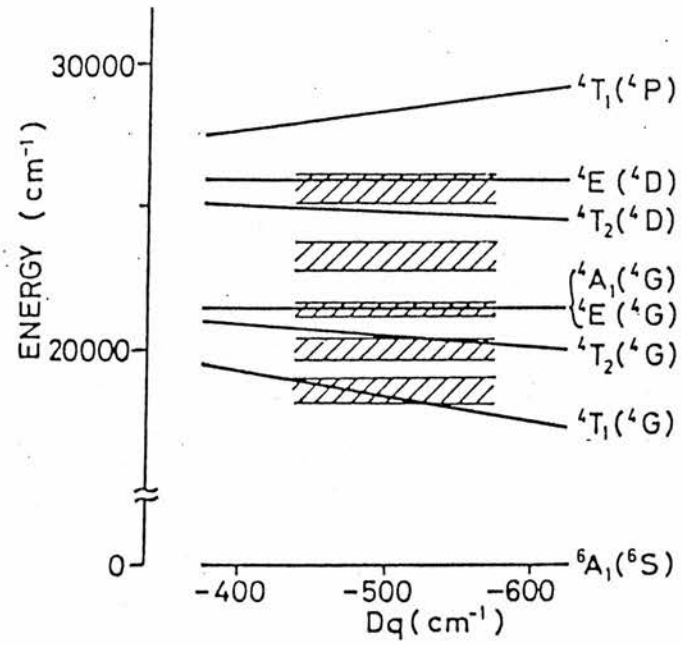

Fig. 3.1.4: Calculated energy level diagram for Mn ($3d^5$ configuration) in ZnS by Kushida et al [2], the shaded area shows the observed bands in absorption

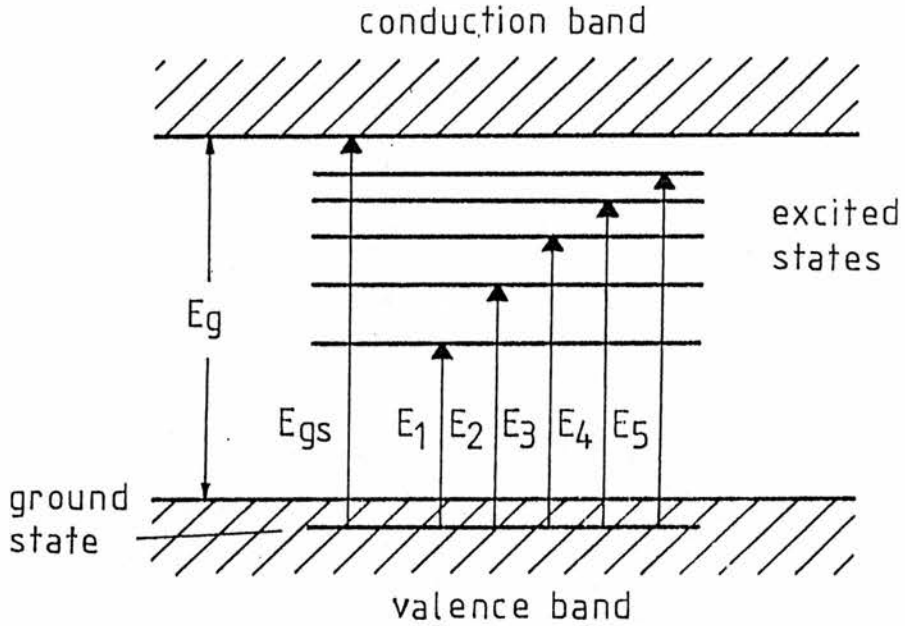

Fig. 3.1.5: Mn levels within the electron bands of the ZnS host lattice

The position and the absorption coefficient of the bands do not seem to be dependent whether the crystal structure is cubic or hexagonal [24].

Zero phonon lines (zpls) have been found for the first three bands by Langer and Ibuki [25] and for the fourth by Pohl et al [22]. The zpls are split by different crystal environments such as cubic or hexagonal ZnS or stacking faults [18,22]. This splitting as well as splitting by spin-orbit coupling is small compared to the width of the broad bands observed at room temperature. Therefore, it has no major influence on the work that is presented in this thesis. Additionally it justifies the assumption of section 2.2 to neglect spin-orbit coupling.

A point that has not been mentioned yet is the position of the Mn levels within the band scheme of the ZnS lattice. Since in the free ion case the energy of the ground state is set relative to the energy where an electron is transferred to infinity it is quite reasonable to proceed for the crystal in a similar way: the energy of the ground state is defined relative to the conduction band edge as a transition where one electron is transferred to the conduction band. This is illustrated in Fig. 3.1.5 where E_{gs} corresponds to the energy of the ground state, E_{1-5} to the internal transitions observed in absorption and E_g to the band gap (≈ 3.7 eV in cubic ZnS).

There have been several attempts to determine E_{gs}. Supposing it lay in the band gap one should be able to see a photo-ionization threshold in direct absorption. This is not observed. Hence the ground state has to be below the top of the valence band or at least very near to it (it would be difficult to distinguish between this feature and the regular band threshold in this case). Early rough considerations by Gumlich et al [24] showed the ground state to be 10 eV below the bottom of the conduction band. Langer et al [29] using X-ray induced electron emission found a value of 3 eV for the ground state being below the top of the valence band. However, their results are somewhat unreliable as their Mn3d signal was superposed on a signal due to the ZnS valence band. On the other hand Allen [30] obtained by his estimates 0.1 eV, the ground state being above the valence band.

Xue-yin and co-workers [31] used the following model to explain their photoconductivity results on ZnSe:Mn : they got one additional peak to the intrinsic band-to-band transition peak, that was strongly dependent on temperature. The model is based on the idea that the Mn being excited from the $^6A_1(S)$ to the $^4T_1(G)$ state by the incident light is thermally ionized. Their final result shows the $^4T_1(G)$ state being positioned very near to the conduction band edge. This would result in a ground state ≈ 2 eV below the conduction band. However, the possibility of energy transfer (s. section 3.3) was never considered. Recently [32] this work was extended to samples of $ZnSe_{1-x}S_x$:Mn ($x = 0.0$-0.1). Unfortunately their results are quite inconsistent because of a model which is too simple. Apart from the

neglect of energy transfer they did not consider the conduction band consisting of a continuum of states but represent it by a single state. For the energy difference of the $^4T_1(G)$ state and the conduction band they found it extremely rapidly varying with x. One would expect a more linear behaviour as the bands vary nearly linearly with x. In contrast they got a somehow stable position of the second excited state towards the conduction band indicating a strongly differing difference of these two states. Therefore, there is no sense in extrapolating the figures for ZnS:Mn.

Photoconductivity spectra of ZnS:Mn crystals have been obtained by Borisenko and Kodzhespirov [33]. They discovered peaks near to the 395 nm and 428 nm peaks in excited absorption spectroscopy. An additional peak at shorter wavelengths they did not attribute directly to Mn transitions. They concluded that an ionization of the Mn is possible. Again the problem of energy transfer was not borne in mind. In general the latter seems to render the interpretation of photoconductivity or photocapacitance measurements much more difficult.

3.2 Mn PAIRS

When high Mn concentrations are used it is quite probable that on a nearest neighbour Zn site to a Mn impurity another Mn is situated. Then the question of exchange coupling arises. Some simple calculations assuming random distribution of the impurities show the

fraction of Mn atoms assembled in 'pairs' depending on the Mn concentration. The values were tabled by Behringer [34] for different crystal environments. Fig. 3.2.1 displays a diagram worked out by McClure [27] showing that Mn pairs already gain importance at 2 at% Mn. At higher concentrations even clusters have to be considered.

McClure [27] observed a lot of sharp lines in the 470 nm band at low temperatures. He developed a model of exchange coupled Mn pairs. Still, his results are a bit controversial since he did not include phonon satellites into his considerations.

Busse et al [35] used time resolved spectroscopy to distinguish possible zpls due to pairs from those due to 'singles'. The decay time of the luminescence was expected to be much faster for pairs than for singles as the spin selection rule is weaker. For the $^6A_1(S) \rightarrow {}^4E(G)$ transition in excitation the authors were able to decompose each of one line thought to be the zpl for singles and pairs into three exponentials for the luminescence resulting in three decay times. They ascribed them to transitions within singles, pairs and some sort of less effective coupling. However, the ratio of the intensities of the lines were strongly dependent on the excitation energy. Tab. 3.2.1 shows their results clearly indicating a decay much faster for pairs. The shift between the found zpls is again small compared to the broadening at room temperature. Furthermore the authors suggest that any possible energy exchange between singles and pairs is quite small as this is essential for the whole experiment.

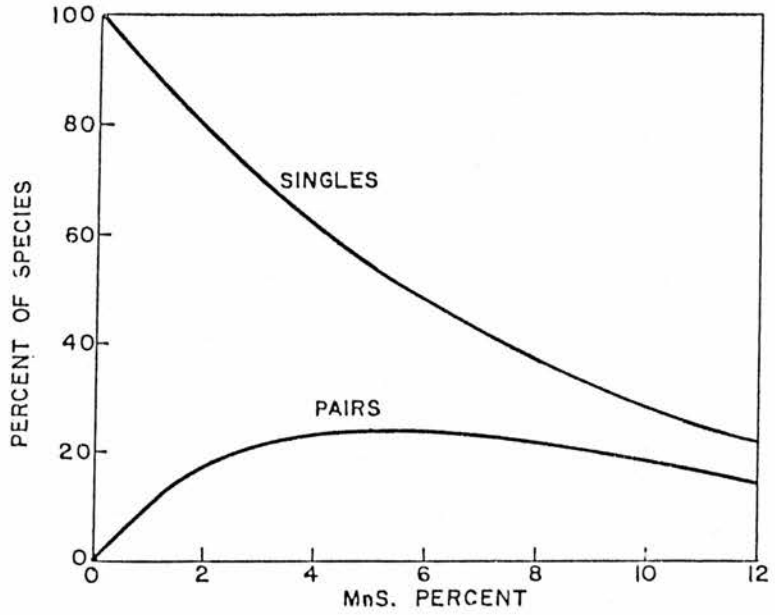

Fig. 3.2.1: Fraction of Mn impurities in ZnS sited as 'singles' or as 'pairs' according to [27]

Tab. 3.2.1: Decay constants τ for the Mn luminescence in ZnS:Mn [35]

Mn content (nominal)	Statistics (Behringer) [16]			decay constants [ms] T = 78 K excitation single: 21225 cm^{-1} (s) excitation pair : 21448 cm^{-1} (p)						T = 4.2 K excitation single: 21230 cm^{-1} (s) excitation pair : 21410 cm^{-1} (p)					
	singles	pairs	cluster	τ_1		τ_2		τ_3		τ_1		τ_2		τ_3	
gMn/gZnS	%			s	p	s	p	s	p	s	p	s	p	s	p
1×10^{-4}	99.9	0	0	1.94	1.98	0.48	0.46	–	(0.03)	–	–	–	–	–	–
8×10^{-4}	99	0	0	1.97	1.99	0.47	0.48	(0.03)	(0.09)	1.80	1.80	0.55	0.54	?	(0.04)
4×10^{-3}	95.3	4.5	0.2	1.37	1.19	0.40	0.40	0.09	0.09	1.89	1.69	1.0	0.44	0.08	0.08
8×10^{-3}	90.1	8.3	0.6	1.46	1.24	0.68	0.55	0.22	0.22	1.65	1.58	0.52	0.33	0.07	0.07
1×10^{-2}	88.6	10	1.4	1.01	0.95	0.41	0.38	0.13	0.11	1.62	1.41	–	0.24	0.11	0.09
3×10^{-2}	69.3	20.8	9.9	(0.98)	0.63	–	–	0.15	0.13	(1.29)	(0.58)	0.36	–	0.14	0.18

3.3 OTHER OPTICAL PROPERTIES

A very important aspect is the possibility of energy transfer to other centres. Suppose there is a transition from the first excited state to the ground state within the Mn centres (Fig. 3.3.1). Instead of radiating the loss of energy the latter is transferred non-radiatively to another centre that is getting excited or even ionized.

That these processes are occurring in ZnS:Mn has been observed by different authors. Rigby [36] has shown that energy is both transferred into and out of the Mn centres after flash excitation. She took into account van der Waals-interaction between the Mn and the resonant centres. Goede et al [37] used the appearance of a second, red emission band for $c_{Mn} > 1$ mol% to work out an effective lifetime model for the $^4T_1(G)$ state. They succeeded in describing their results by suggesting a resonance energy transfer from the excited Mn via other Mn centres to centres responsible for the red emission and non radiative centres. According to their model the process of energy transfer changes the effective lifetime of the $^4T_1(G)$ state already for $c_{Mn} > 0.1$ mol%. In [38] Goede et al investigated the non exponentiality of the ZnS:Mn luminescence getting a non exponential decay for short times for small c_{Mn} (< 8 mol%). Using a more detailed expression of the interaction with the non radiative centres they got consistent results.

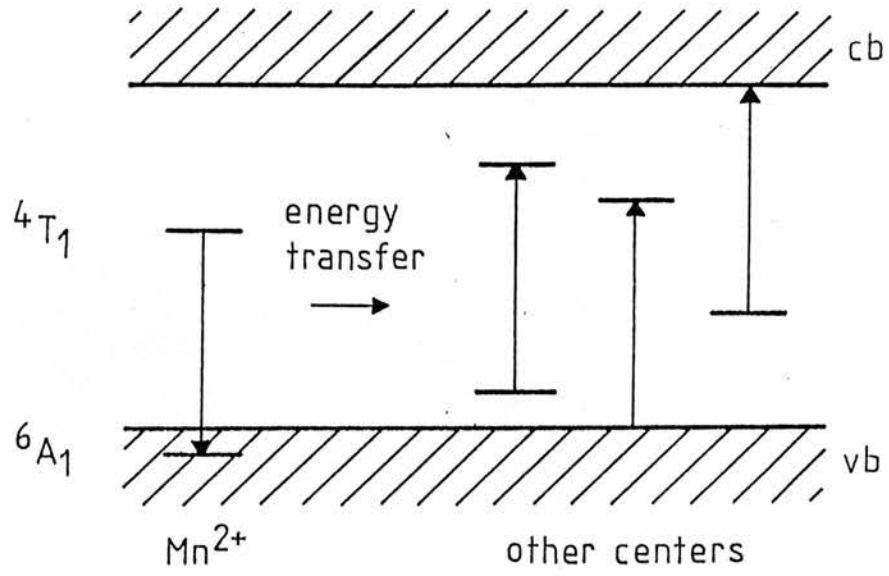

Fig. 3.3.1: Possible energy transfer process from excited Mn centres to other centres

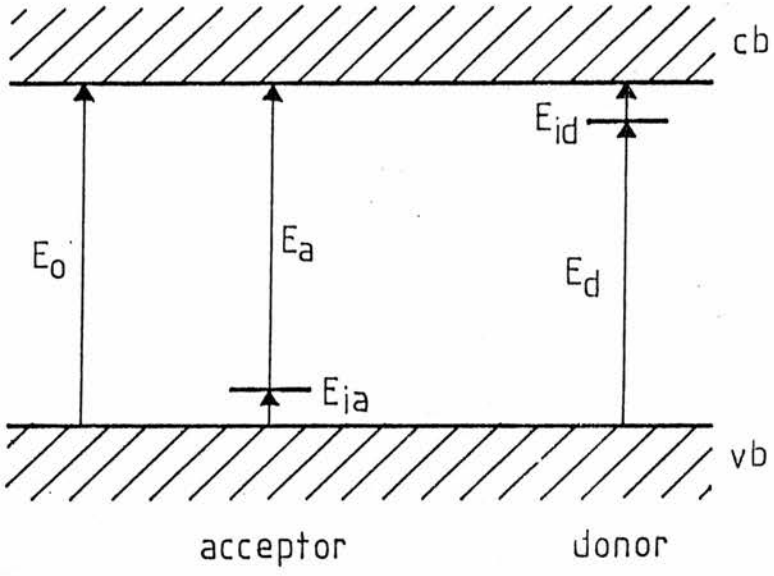

Fig. 3.3.2: Induced absorption due to charge transfer according to [43] (see text for explanation)

About the nature of the red radiating centres very little is known. Goede and Thong [37] suggested a possible MnS_6 cluster. According to Gumlich [18], Neumann [26] was looking at low energy emission bands occurring for $c_{Mn} > 4$ at%. He saw two bands with peculiar temperature dependence. The decay times were found to be larger than the one for the orange luminescence. Since these bands were linearly dependent on c_{Mn} and had nearly the same excitation spectra as the orange emission it is likely that the origin of these bands is correlated to the Mn. Although Neumann proposed pair interaction this is quite improbable because of the slow decay (as stated in [18]).

Another effect is the light induced darkening. As this work deals with induced absorption any other induced processes have to be considered. Light induced darkening of ZnS due to surface effects was studied by Sviszt [39]. The effect was found to be caused by chemical decomposition on the surface of the crystal and could only be seen with UV irradiation by Hg lines beyond the fundamental band gap energy. Simmonds and Eaves [40] took ZnS (Mn: 0.4 at%, Cu: 0.05 at%) powder and irradiated it by UV light resulting in induced absorption within 400 - 1000 nm. Beyond 2.4 μm the induced component was found to be negligible. Here again the effect was only possible to be observed if the UV light was of higher energy than the intrinsic band gap. Furthermore the darkening was dependent on the condition of the ZnS powder as well as of c_{Mn}. Noras [41] observed quasi periodic fluctuations in the transmission of polycrystalline ZnS under white illumination at 6 K. He also detected spontaneous changes in

transmission not reproducible in detail by heating and cooling from 7-70 K. He found similar effects for ZnS:Mn [42]. In particular he looked at the spectral dependence of the induced absorption showing a broad band from E ≈ 4000 cm^{-1} to 14000 cm^{-1}. The inducing process behaved quite peculiarly. The band was nearly one order stronger at 6 K than at 77 K. This band is probably the band Kushida et al [2] discovered as they were looking for induced states of the Mn at 4.2 K.

Dieleman et al [43] took attention to processes of charge transfer causing induced absorption in ZnS doped with several impurities. They assumed the existence of one acceptor and one donor level compensating each other (Fig. 3.3.2). After illuminating with E_0, E_d or E_a a charge transfer is possible resulting in a trapped electron at the donor and a trapped hole at the acceptor. This causes induced absorption for E_{id}, E_{ia}, E_d and E_a. The authors used Cl, I, Al, Sc, In, Cu and Ag for the dopants.

Kukimoto et al [44] observed infrared absorption due to shallow electron traps in ZnS (Cu: 0.04 mol%, Al: 0.04 mol%). The band was masking the region 3-14 μm and was stimulated by UV. The excitation spectrum was similar to that of photoconductivity having a broad maximum around 420 nm. Though better visible at LNT the effect was still to be seen at room temperature. There the decay of the induced absorption was of the order of seconds.

3.4 CONCLUSION

At room temperature the main optical features of Mn in ZnS are five bands in absorption and one in luminescence. For higher concentrations red luminescing centres are observed. Spin-orbit coupling and splitting due to different crystal environments are small. The same is found for the splitting by pair interaction. However, in pairs the decay time is much shorter. The Mn ground state lies near or below the top of the valence band. Energy transfer and darkening effects must be considered when interpreting processes like induced absorption.

4 EXPERIMENTAL

4.1 THE EXPERIMENT

The idea of the work presented here was to investigate induced absorption in ZnS:Mn due to energy levels of the Mn centres. It was also to confirm the results of Kushida et al [2]. Since the latter showed that there was still large broadening for the observed bands at 77 K all experiments carried out here were done at room temperature. This had also the effect to avoid induced bulk darkening (s. section 3.3) that occurs at low temperatures.

A weak light source was used for the transmittance of the sample and shone onto a monochromator. The signal was detected at the other slit of the monochromator. For the induced light an Ar-ion laser (λ = 514.5 nm) was taken. The beam was chopped so that a signal connected to the inducing beam could be recovered by a lock-in amplifier.

To discuss the point whether there are any other induced processes going on that are not necessarily due to the Mn centres a normal tungsten halogen bulb was also employed as inducing light source whereas the direct beam was chopped. The induced signal was achieved by the difference between the signal with/without inducing light thus permitting a longer time scale for the induced process.

The ordinary optical properties of the sample were checked by direct absorption measurements and by photoluminescence that was excited by the Ar-ion laser.

In the late part of the experiments another experiment was performed. It was tried to quench the laser excited luminescence by spectral dependent illumination. The idea of the experiment will be explained later.

4.2 THE SAMPLE

During all the experiments only one sample was used. It consisted of ZnS doped with Mn and was grown from the melt by the Eagle-Picher Company. The Mn concentration was 0.5 at% according to the suppliers. Concerning the crystal structure it was thought to be mainly sphalerite. To avoid too much heating and possible darkening effects (s. section 3.3) by laser illumination the size of the chosen crystal was rather big. Besides, this made the experiments more handy. The size was about 9x7x13 mm^3 though the planes were not strictly perpendicular. Fig. 4.2.1 shows a photograph of the sample. Just the clear part on the right hand side was used for the experiments.

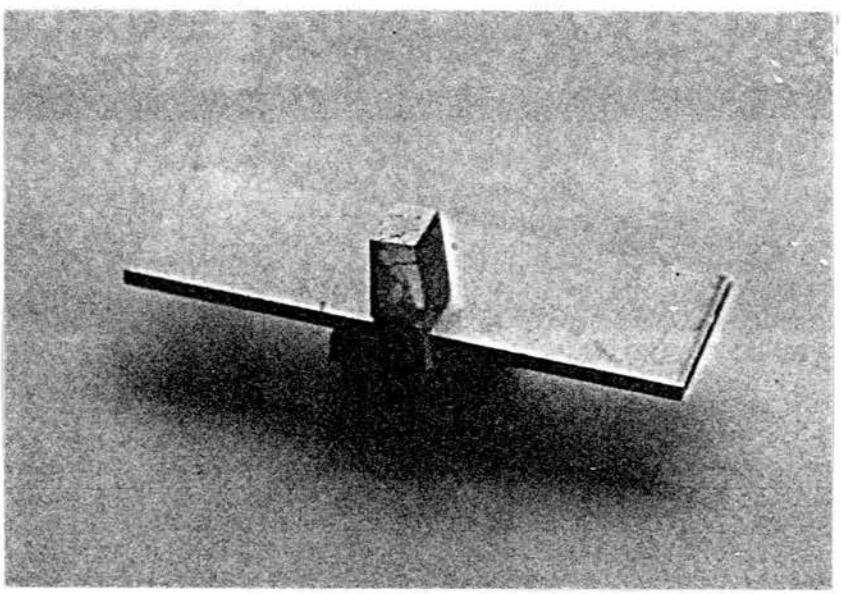

Fig. 4.2.1: Sample (ZnS:Mn), just the large clear fraction on the right hand side was used for the experiments

Since spectra of the sample were recorded it is essential to know the spectral dependence of the refractive index of cubic ZnS. I assume that the Mn impurities do not change the characteristics significantly. The wavelength dependence of the refractive index n for cubic ZnS is shown in Fig. 4.2.2 and Fig. 4.2.3 according to [45]. Fig. 4.2.2 displays results of Pikhtin and Yas'kov and of DeVore. Values in the short wavelength range by Cardona and Harbecke are drawn in Fig. 4.2.3, as well as data they obtained for the absorption index k. For comparison some data of Fig. 4.2.2 were included in Fig. 4.2.3.

The figures show that k can be neglected compared to n. On the other hand the values for n spread over a range of 2.7 down to 2.25 for 350 nm $< \lambda <$ 2800 nm. However most of the change occurs in the short wavelength part.

4.3 EXPERIMENTAL ARRANGEMENT

The basic outline of nearly all the experiments is shown in Fig. 4.3.1. As probe light source a tungsten halogen bulb Wotan 64150-01, H1, 12 V, 55 W was used run by a Farnell G12-10S power supply. The actual input power was around 49 W.

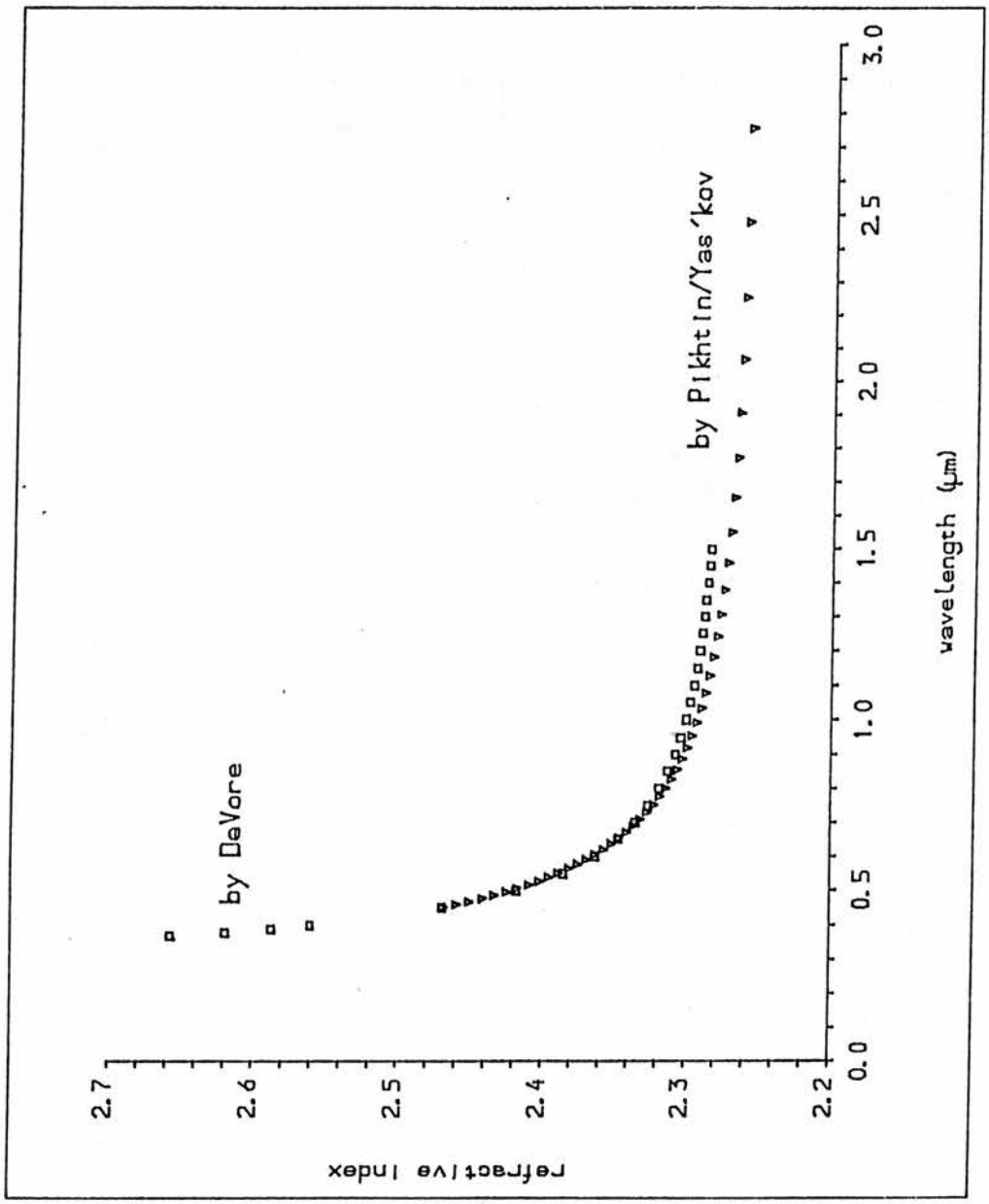

Fig. 4.2.2: Refractive index of cubic ZnS [45]

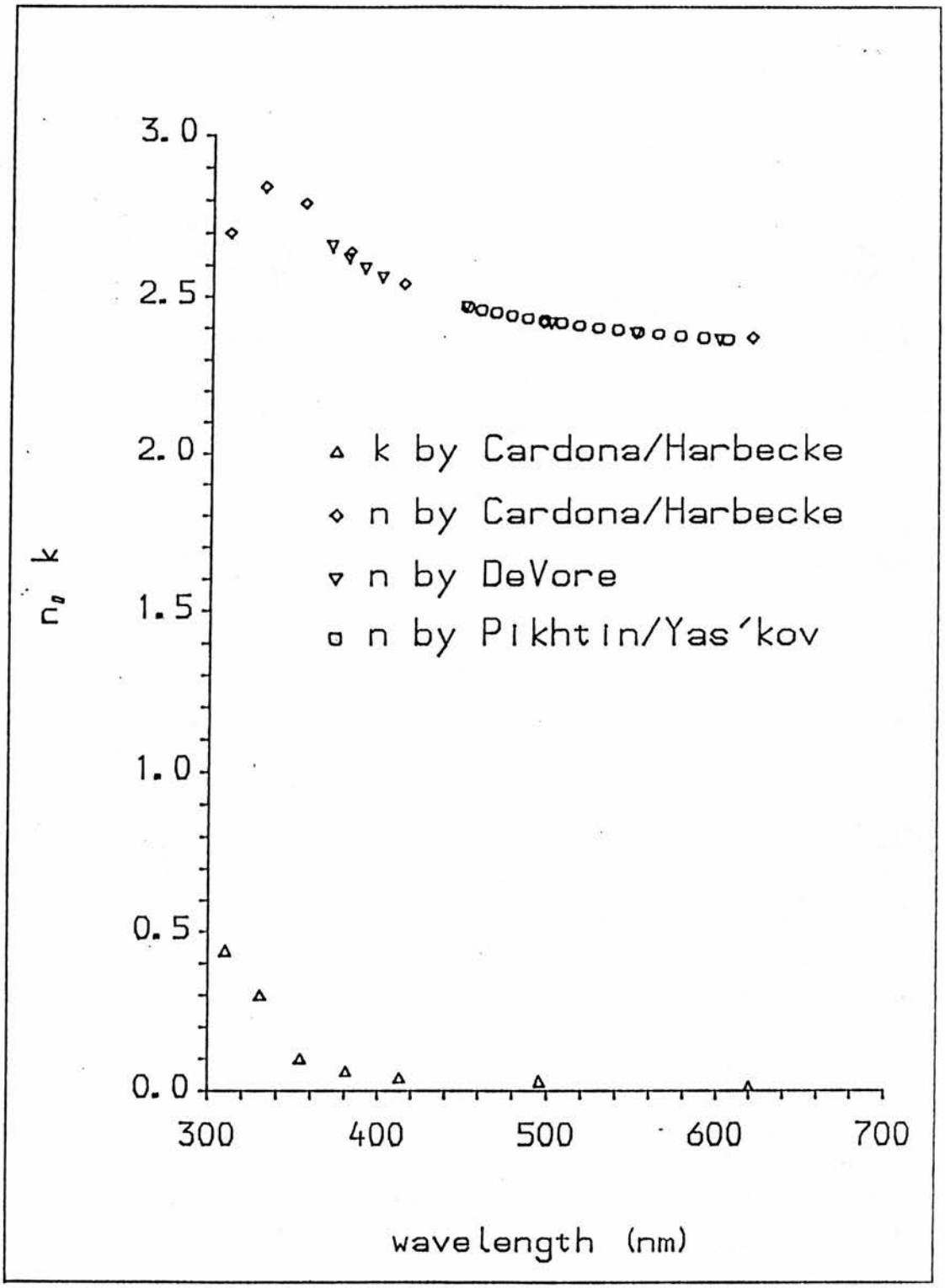

Fig. 4.2.3: Refractive and absorption index of cubic ZnS [45]

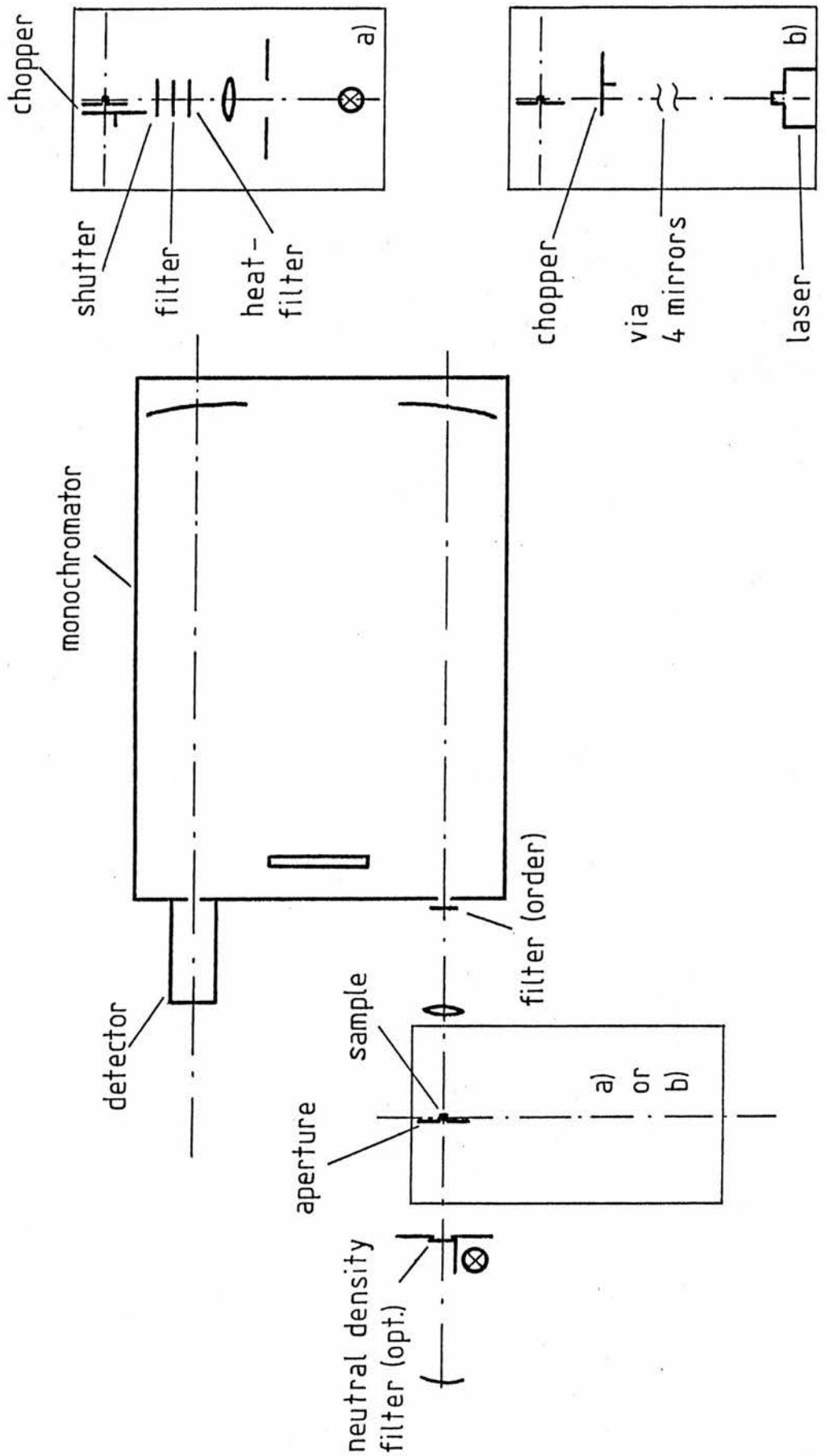

Fig. 4.3.1: Basic outline of the experiments

After hitting a mirror the light was focused on an aperture near to the sample. A neutral density filter (Kodak, density 0.8) could be inserted. For the size of the aperture see Fig. 4.3.2. The arrangement towards the sample is shown in Fig. 4.3.3. Hence only a part of the sample of size 4x3x9 mm^3 was used. This bulk area was nearly free of visible damage in contrast to the rest of the material. For the experiments described in 5.2 and 5.3 a slightly different area was used as for those from 5.4 and 5.5. where a part 'nearer' to the laser light was chosen.

The sample was stuck on a removable part of plastic. In the laser experiments an aluminium plate was put between this part and the sample to assure efficient cooling. A second aperture of the same size as the first one was mounted behind the sample in some of the laser experiments.

The light was then either focused on the entrance slit or on the first mirror of the monochromator. For the latter a nearly homogeneous illumination of the entrance slit was achieved as the distance lens-sample/image of the bulb was about the focal length of the lens. In some cases this was advantageous as the monochromator showed variations of the image on the exit slit caused by the mechanical movements resulting in variations of the signal at the detector site.

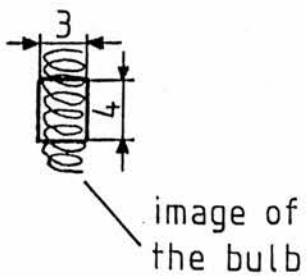

Fig. 4.3.2: Aperture in front of the sample with the image of the probe light bulb

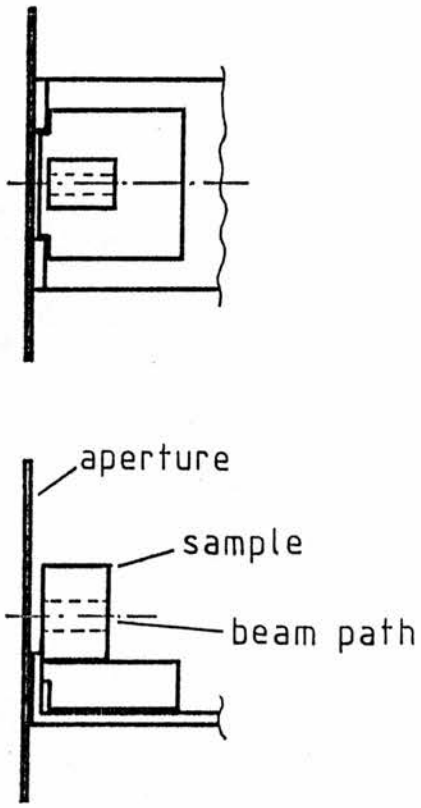

Fig. 4.3.3: Sample mounting

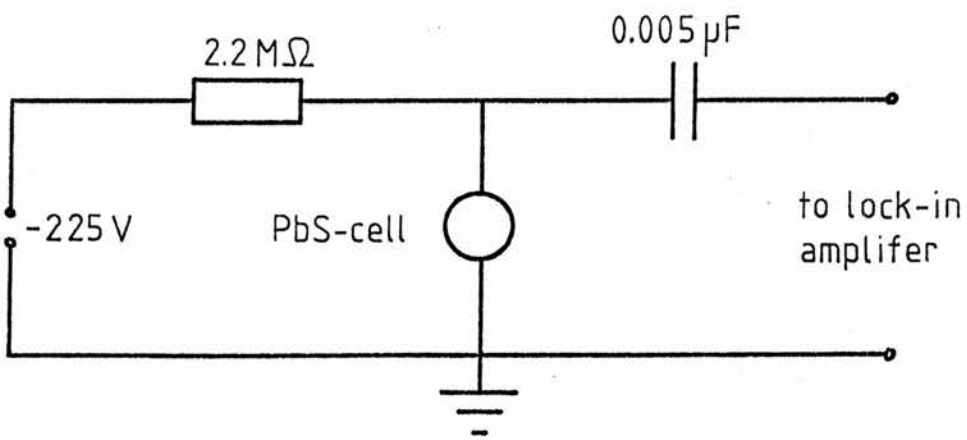

Fig. 4.3.4: Circuit for PbS-photocell

As detector a RCA 1P28 (only for the absorption spectrum 350 nm - 600 nm, Fig. 5.1.1.2) and a Thorn EMI 9558B photomultiplier as well as a Mullard 62SV PbS-photocell were employed. A Oltronix B2.2K-25HR served as power supply. The voltages for the pm tubes were 1000 V (1P28) and 1260 V (9558B).

The PbS-cell was wired within a circuit drawn in Fig. 4.3.4. Any small drop ΔR_c of the cell resistance R_c is proportional to the incident light intensity. As long as this drop is small against the sum of the load resistance R_l and R_c it causes a proportional voltage drop ΔU_c of the cell voltage U_c. Suppose the supply voltage is U, the current I, one obtains

$$U_c = I R_c = \frac{U R_c}{R_l + R_c}$$

$$\Rightarrow \quad U_c - \Delta U_c = \frac{U (R_c - \Delta R_c)}{R_l + R_c - \Delta R_c}$$

$$\Rightarrow \quad \Delta U_c = \frac{U R_c}{R_l + R_c} - \frac{U (R_c - \Delta R_c)}{R_l + R_c - \Delta R_c}$$

$$\Rightarrow \quad = \frac{U R_l \Delta R_c}{(R_l + R_c)(R_l + R_c - \Delta R_c)}$$

$$\Rightarrow \quad \approx \frac{U R_l \Delta R_c}{(R_l + R_c)^2} \quad .$$

In the case when chopped light is shone on the cell an AC signal is passing the capacitor. As the maximum signals were around 1 V compared with U = 225 V there were no linearity problems (R_c was of the order of R_l). The reason to include the capacitor was to block a DC current from passing through the following lock-in amplifier (type Brookdeal 9501). The pm tubes were connected directly. Finally the signals were measured by either a chart recorder or a digital voltmeter.

A Monospek 1000 was employed as monochromator. Gratings D410-C100, D410-D100 and D410-E100 were alternatively mounted to cover a spectral region from 350 nm to 2700 nm. In front of the entrance slit filters were attached to remove high order signals. The spectral resolution was varying depending on the gratings and experiments. For that see the data in chapter 5.

As second light source either a tungsten halogen bulb Thorn A1/216, FCS, 24 V, 150 W (Fig. 4.3.1 a)) or the 514.5 nm line of an Ar-Ion laser Spectra-physics 170 (Fig. 4.3.1 b)) with the power of 1 W were installed.

The bulb was run by a Valradio 250RU/12/10 power supply resulting in $\approx$ 84 W input power. The light was focused down on the sample by a lens in order to get an ideal cross-section with the probe light beam (Fig. 4.3.5). Two heat filters Ealing 26-3053 avoided overheating of the sample (these filters have a cut off near 750 nm). Colour filters were used to get spectral dependent illumination. A shutter provided

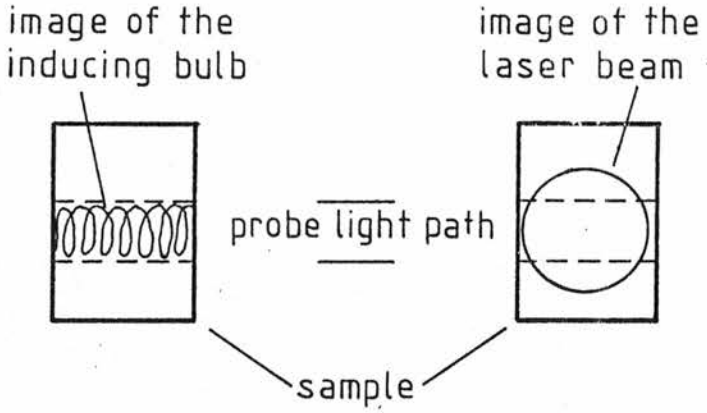

Fig. 4.3.5: Illumination of the sample by second bulb

Fig. 4.3.6: Illumination of the sample by laser beam

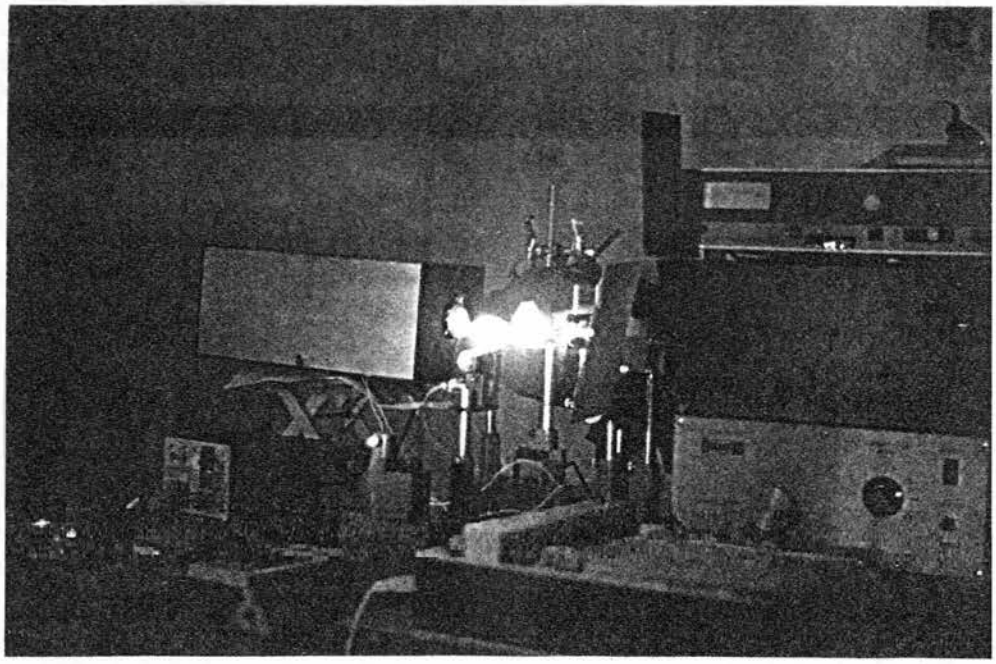

Fig. 4.3.7: Experiment showing laser illumination

an easy possibility to interrupt the illumination.

The laser beam was guided by four mirrors towards the sample. Unfortunately these had to be aligned and sometimes even to be changed in between the experiments since the laser was the property of another research group. The total beam path was around 6 m causing a considerable beam widening. Thus an illumination illustrated in Fig. 4.3.6 was achieved. Taking a beam diameter of 8 mm the beam density is approximately 2 Wcm^2. However it has to be stated again that the illumination conditions were slightly varying from experiment to experiment.

For chopped light purposes a Bentham 218 chopper provided with several disks was used. It was mounted either in front of the first sample aperture or somewhere on the laser path, depending on the experiment. The lower the number of slots in a disk was, the better a square wave signal was achieved.

Fig. 4.3.7 shows a photograph of an experiment with laser illumination.

At the very last stage of the experiments the experimental set-up changed slightly for an experiment explained in section 5.5.4. Fig. 4.3.8 gives the schematic outline: the chopped beam of an ordinary halogen-tungsten bulb (probe light lamb of the former experiments) and the laser beam were shone in opposite directions onto the sample, the apertures on each side of the sample guaranteeing an optimal cross-section. The bulb's light beam passed an interference

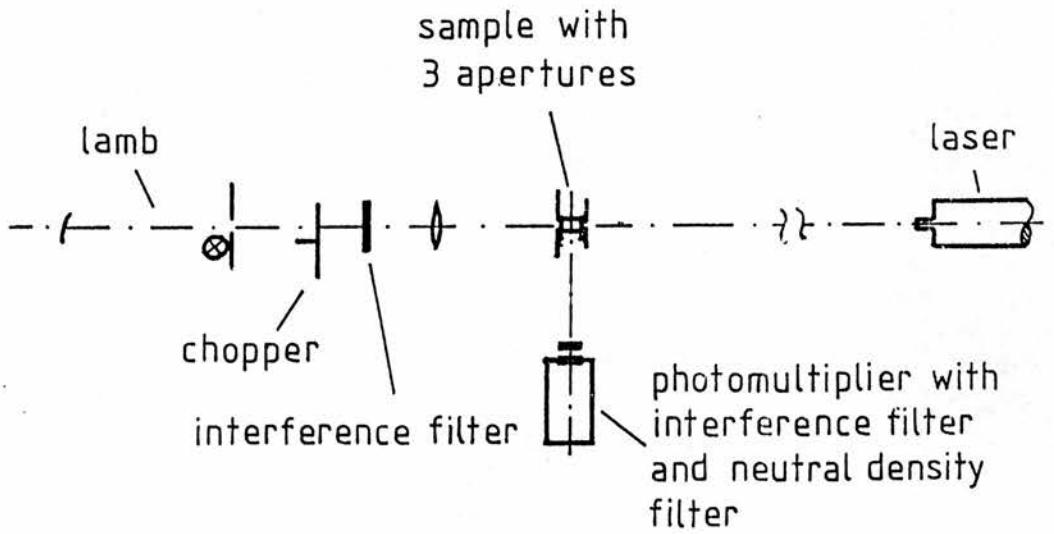

Fig. 4.3.8: Experimental outline of the experiments of section 5.5.4

filter of the set 'Oriel G-522-11', centred at 400, 420, 440, 460, 480 or 500 nm and having a FWHM of 10 nm each. The beam was then focussed onto the sample by a lens. The section of the sample that was crossed by the two beams was screened by a third aperture towards the EMI 9558B pm-tube in front of which a 580 nm interference (FWHM: 10 nm) of the above set and a neutral density filter (d = 0.8) were mounted. For this experiment the laser output power was 250 mW. To calibrate the bulb's intensity a thermopile (Hilger-Schwarz FT/17A) was placed at the samples place alternatively.

5 RESULTS

5.1 INTRODUCTION

In this chapter all experimental results are listed. The motivation for each series of experiments is explained in the beginning of each section. However, there will be no discussion since this is dealt with in chapter 6.

5.2 ORDINARY OPTICAL PROPERTIES OF THE SAMPLE: ABSORPTION

Direct absorption measurements were done with the experimental arrangement shown in Fig. 4.3.1, the probe light beam being chopped. The chopping frequency was 780 Hz (10 slot disk). The RCA 1P28 photomultiplier was used for the spectral range of 350 - 600 nm whereas the Mullard 62SV PbS-cell was employed for up to 2.7 μm. It was not aimed to derive exact absorption data in the sense of very absolute figures. However, the measurements were thought to show qualitatively whether the sample did indicate the usual ZnS:Mn properties or not.

The probe light source had to be turned to compensate the refraction by the slightly not parallel planes of the sample. Although this would affect measurements concerning the value of the absorption coefficient it does not harm more qualitative results as long as the refractive index n stays approximately constant with wavelength. The same argument applies for any path variation caused by the incident light beam not being strictly parallel (as it is focused onto the sample). Referring to Fig. 4.2.2 one sees that for the used spectral range n varies only monotonic between 2.25 and 2.7. It has, therefore, no considerable influence on the results. Furthermore any small damages of the sample in the optical path should not provide any problems. Some additional error sources arose because of a kind of instability of the signal. It is thought to have been due to small variations of some optical parts by vibrational resonance to chopper vibrations. To control this a signal of a certain wavelength was recorded before and after each scan (these variations were quite slow and monotonic).

The experiments were performed first by measuring the signal obtained by the light source directly and second by fitting the sample onto its place, replacing the light source as mentioned above, and repeating the procedure. I worked with the light source being focused on the first mirror of the monochromator. Since the light beam was chopped there were no disturbing scattered lights. Zero-signals by light scattered directly to the detector (though this was shielded) did not disturb the results since a shutter on the entrance slit of the monochromator provided an easy possibility to indicate the

zero-signal. Any difference in the phase of the two cases of measurements as the light source was moved changes the absorption by a multiplication factor close to 1. The final data were derived as follows: referring to Fig. 5.2.1 the absorption $a_{\%}$ by the sample is obtained by:

$$a_{\%}(\lambda) = ((1-r(\lambda))^2 I_1(\lambda) - I_{ZnS}(\lambda))/(1-r(\lambda))^2/I_1(\lambda) \quad . \quad (5.2.1)$$

Since the absorption index k is small against n (s. section 4.2), r can be evaluated as

$$r(\lambda) = (n(\lambda)-1)^2/(n(\lambda)+1)^2 \quad . \quad (5.2.2)$$

Strictly (5.2.2) is only valid for perpendicular illumination. Since the deviation to this ideal situation was small it is still a useful formula. With the aid of (5.2.1) and (5.2.2) $a_{\%}$ was derived. $a_{\%}$ was not transformed into the absorption coefficient a,

$$a_{\%}(\lambda) = e^{-a(\lambda)x} \quad , \quad (5.2.3)$$

where x is the thickness of the sample, because any feature is already visible for $a_{\%}(\lambda)$. It was not worthwhile to calculate r for each λ. For any spectrum the whole experiment was divided into, one value of n was chosen. Tab. 5.2.1 contains these data and the spectral resolutions for the obtained spectra. For the second spectrum it must be added that there were second order influences for λ = 800-900 nm, but these were quite small.

Tab. 5.2.1: Refractive index n, resulting reflection r and spectral resolution $\Delta\lambda$ for the different spectra

region [nm]	n	r	$\Delta\lambda$[nm]
350 - 600	2.4	0.17	0.09
550 - 900	2.35	0.16	1.5
900 - 1750	2.28	0.15	3
1700 - 2700	2.26	0.15	6

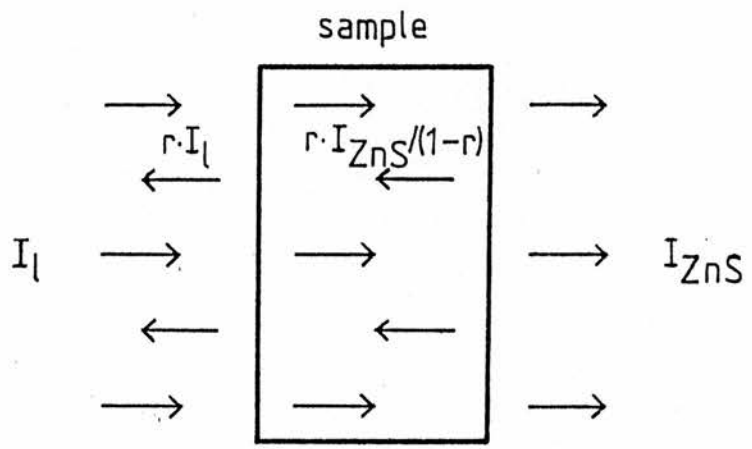

Fig. 5.2.1: Absorption by the sample: the incoming flux I_l and the transmitted flux I_{ZnS} are measured, light gets reflected on both surfaces, multiple reflection is not considered

Fig. 5.2.2-5 show the final absorption spectra. The scale for the absorption is the same on each spectrum. The error bars were obtained from the reading errors only, thus giving a rough estimate.

Additional problems arose in some infrared regions because of water vapour absorption bands. The spectral regions are shown in Fig. 5.2.4 and 5.2.5. Before and after each scan the intensities of these bands were controlled, too, to provide a measure of the stability of these bands.

5.3 INDUCED CHANGE IN TRANSMISSION BY ILLUMINATION WITH BULB LIGHT

5.3.1 INTRODUCTION

The change of the chopped transmission signal by illumination with a second bulb as shown in Fig. 4.3.1a) was investigated. The reason for these experiments were less to find any Mn correlated absorption. It was more to see whether there are any other processes with different origin and thus maybe disturbing the interpretation of the later laser experiments. The experiments were divided into two parts: studies of long and of short time exposure.

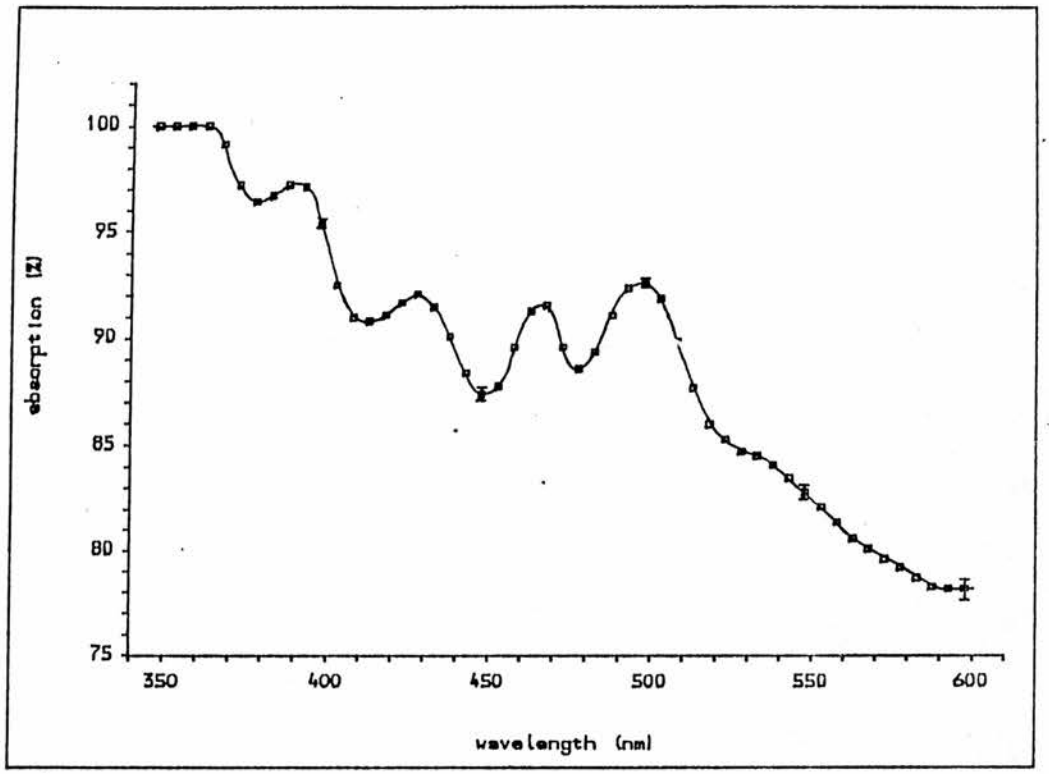

Fig. 5.2.2: Absorption spectrum of the sample for λ = 300 - 600 nm

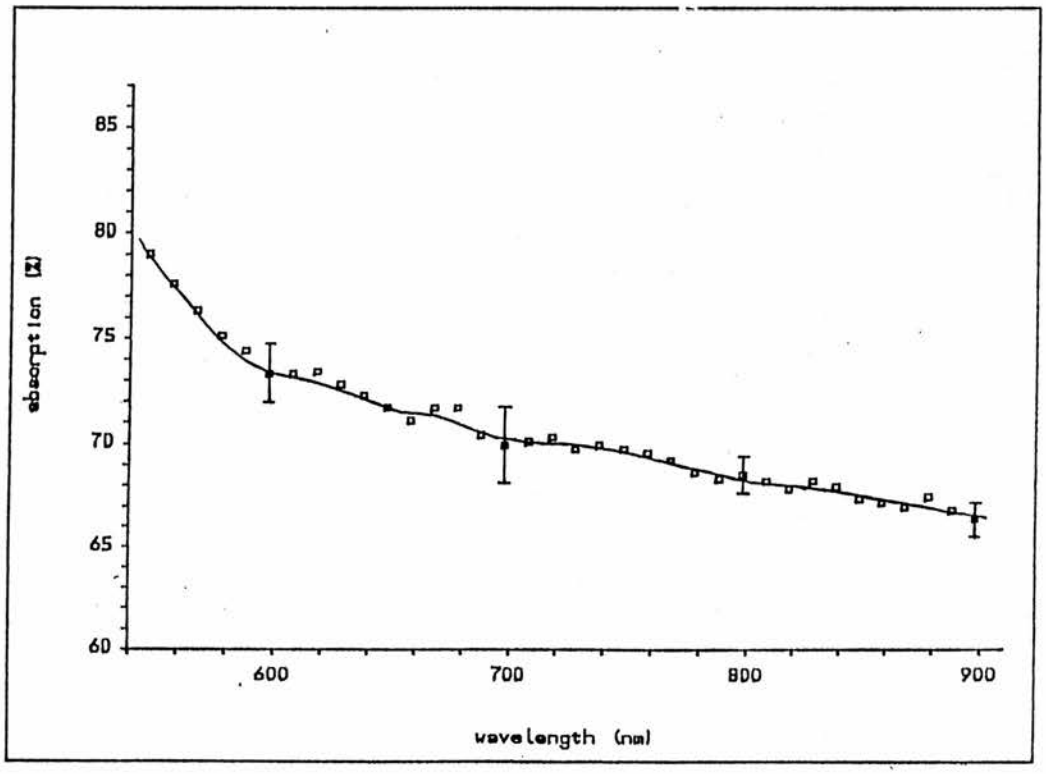

Fig. 5.2.3: Absorption spectrum of the sample for λ = 550 - 900 nm

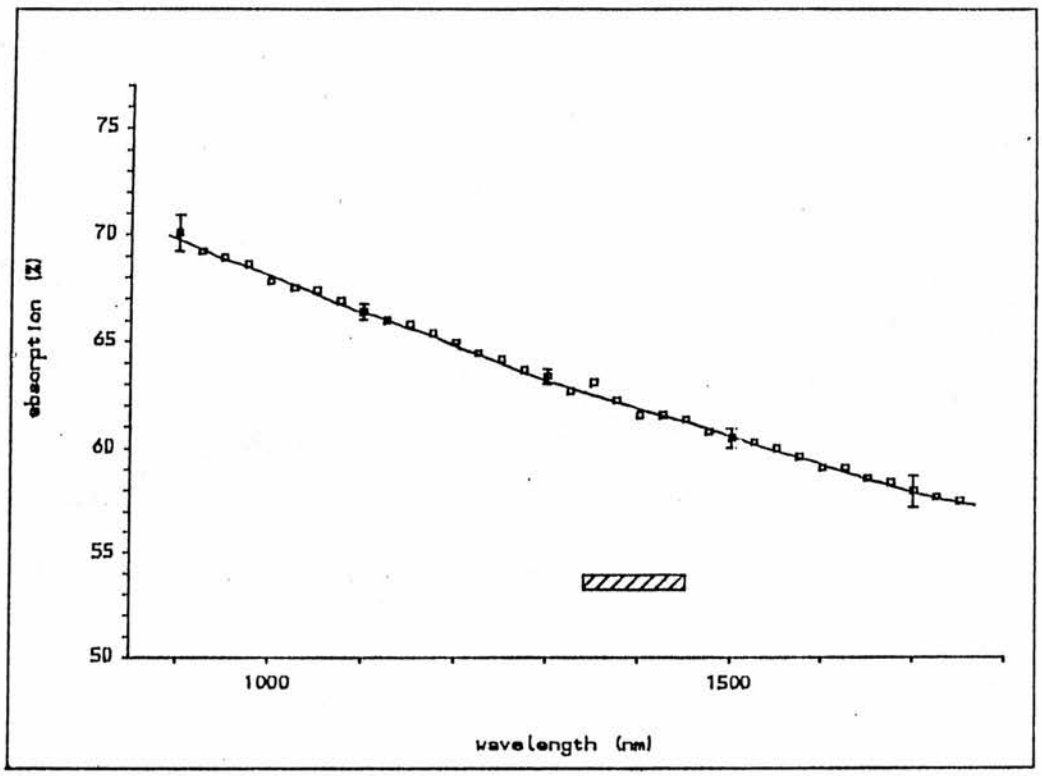

Fig. 5.2.4: Absorption spectrum of the sample for λ = 900 - 1750 nm, water vapour bands are indicated by the shaded area

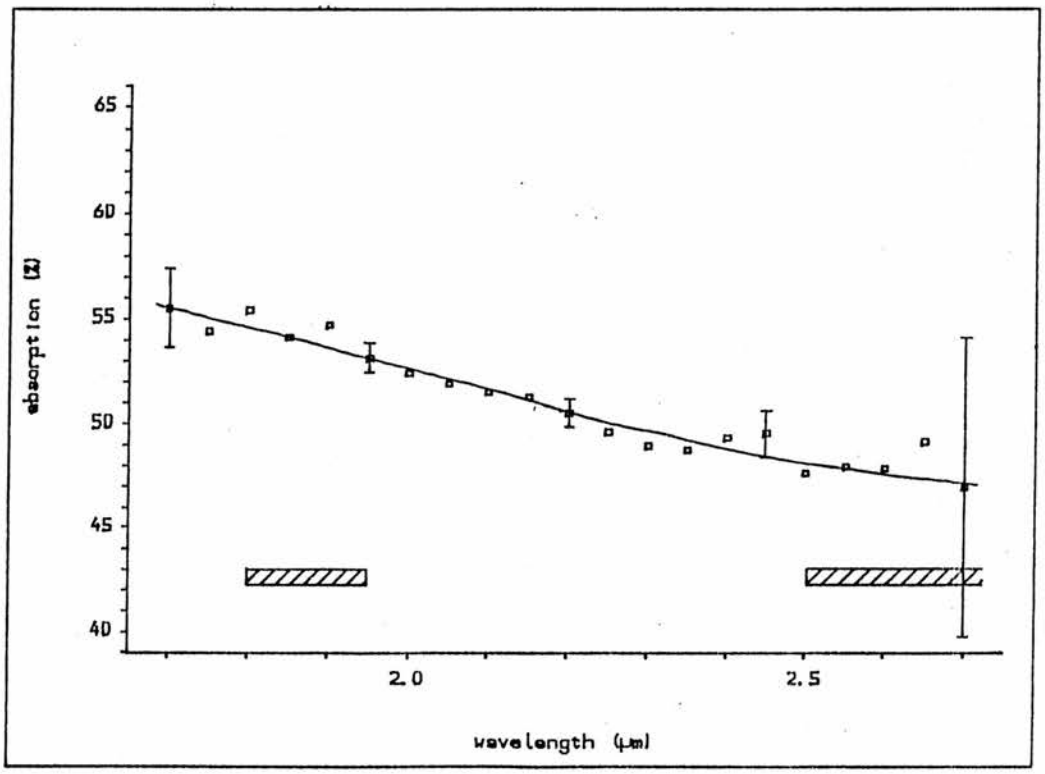

Fig. 5.2.5: Absorption spectrum of the sample for λ = 1700 - 2700 nm, water vapour bands are indicated by the shaded area

The density of the incoming power was quite small. Neglecting the absorption by the heat-filter and the lens it was around 0.04 Wmm^{-2}. Since the heat-filter absorbs the biggest part of the bulb light one recognizes easily how small the inducing power was (compared to the laser light where 0.02 Wmm^{-2} was achieved). The intensity of the probe light was rather small as the input power was less than that of the other one, not the whole picture of the bulb was used, the spatial part of the light directly coming from the bulb was smaller and a neutral density filter (d = 0.8) was mounted. Up to 800 nm the EMI 9558B photomultiplier served as detector, later on the Mullard 62SV PbS-cell was used. The spectral resolutions were the same as in Tab. 5.2.1. Only for the photomultiplier it differed, now having been around 2 Å. The chopper worked with a frequency of 780 Hz (10 slot disk).

5.3.2 LONG TIME EXPOSURE

The experimental procedure was performed as follows: the transmission signals were scanned without illumination, then the sample was illuminated for a time of 5 h and finally the transmission signals were scanned again. During the 5 h the intensity of one particular wavelength was recorded. Before the experiment the sample has not been illuminated by the second light source for less than a night (> 12 h).

As the experimental time was quite long the instabilities of the signal had a greater effect than before. Therefore, the change of the signals after 5 h showed a certain shift. Since there were no spectral dependent features visible I suggest I have not seen any induced process exceeding the error bars. A general darkening can be excluded because in separate experiments such declines were visible for the bare bulb signal as well. A further reason for this argument was a bad reproducibility. In the worst case the change of the signal was up to 10 % after 5 h.

5.3.3 SHORT TIME EXPOSURE

For these experiments it was possible to enhance the sensitivity by looking just at discrete points in the spectrum. With the aid of zero-shift facilities I was able to detect very small changes of the signal. The inducing light was simply switched by a manual shutter. I chose an exposure and relaxing time of 3 min.

Induced signals were found for the region where the photomultiplier served as detector. Every time the inducing light was shone onto the crystal the transmittance dropped instantly. When it was shut off again the transmittance gained the original value with a decay of the order of 0.5 min. Since this has to be seen relative to a time resolution of 1 s (time constant of lock-in amplifier), there is no doubt that the second process was taking considerably more time

than the first one. Fig. 5.3.3.1 shows an example. Observations over longer time periods did show that the arbitrary time interval of 3 min was sufficient for the study of the effect. As far as noise and shift influences allow this conclusion the time dependent shape as displayed in Fig. 5.3.3.1 did not seem to be dependent on the wavelength of the induced feature.

A spectrum was obtained by measuring this effect at discrete points and normalizing them against the direct transmission signal. The amplitude of the effect was taken from the threshold that was caused when the light was shone onto the sample, and which was very fast and, therefore, less influenced by instabilities. To minimise further errors each measurement was repeated. The result is displayed in Fig. 5.3.3.2 and Fig. 5.3.3.3, respectively. The errors were estimated from reading errors of the amplitude of the effect since these errors were dominant. Even a shift of the total signal because of the instabilities had a negligible influence. The effect had a very small magnitude. Around $\lambda = 550$ nm the ratio between it and the direct transmission was about 5‰. The band has a peak near 575 nm. In the absorption against energy plot (Fig. 5.3.3.3), it seems to have an asymmetric shape with a high energy tail. Unfortunately the PbS-cell was not sensitive enough to detect the infrared tail of the band.

To get further information the effect was studied under spectral dependent illumination. Several filters were mounted alternatively behind the heat filter. The amplitude of the induced transmission around 575 nm dependent on these filters is shown in Fig. 5.3.3.4.

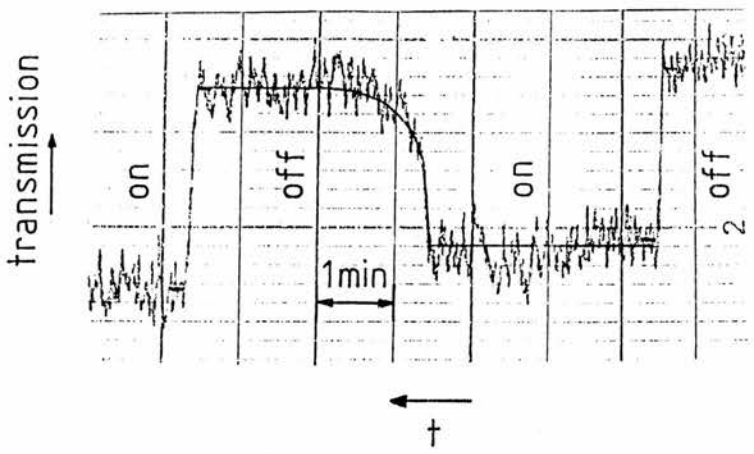

Fig. 5.3.3.1: Trace of the induced absorption at 625 nm, white light inducing illumination

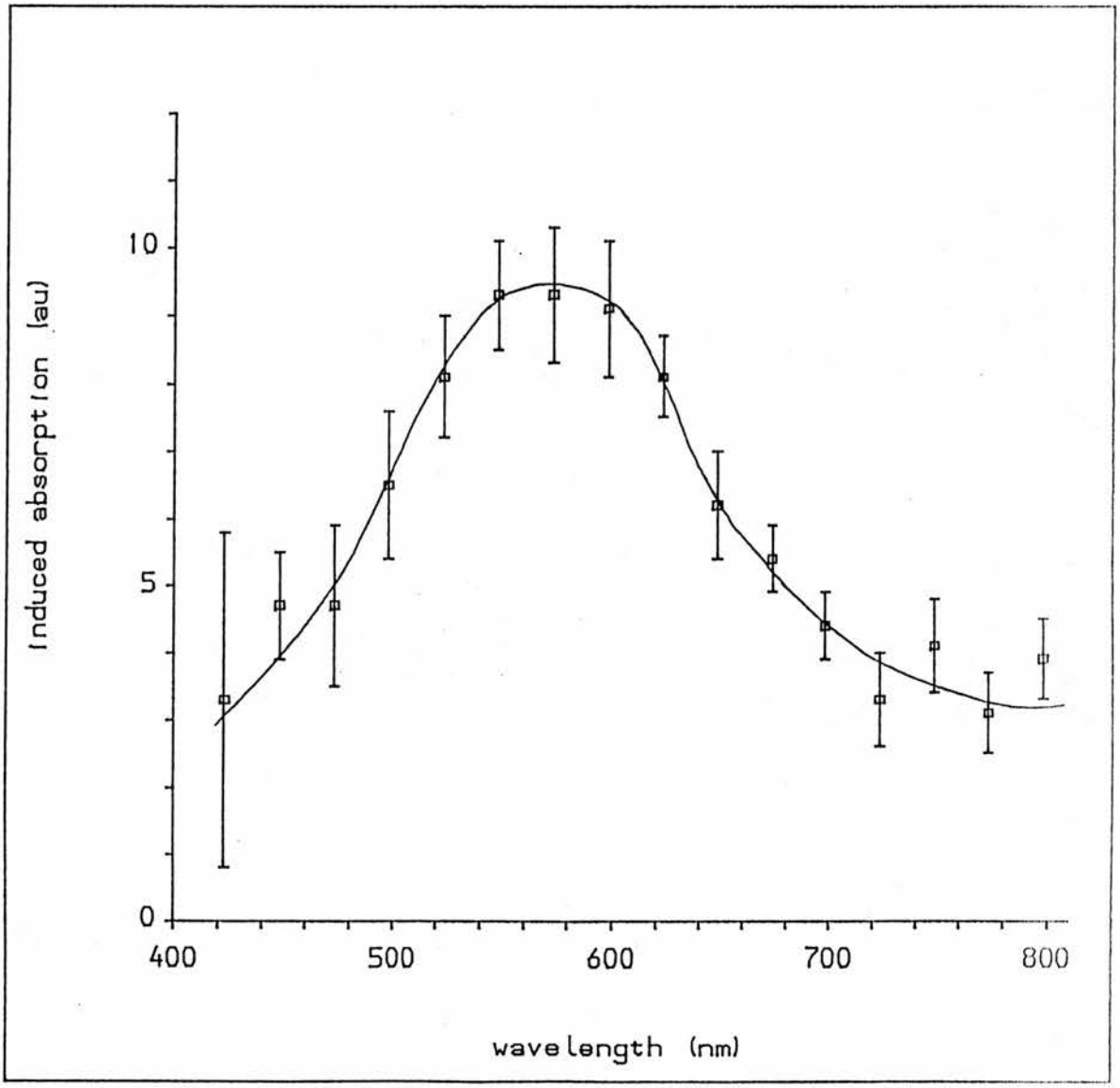

Fig. 5.3.3.2: Spectrum of the induced absorption by white light illumination (against wavelength)

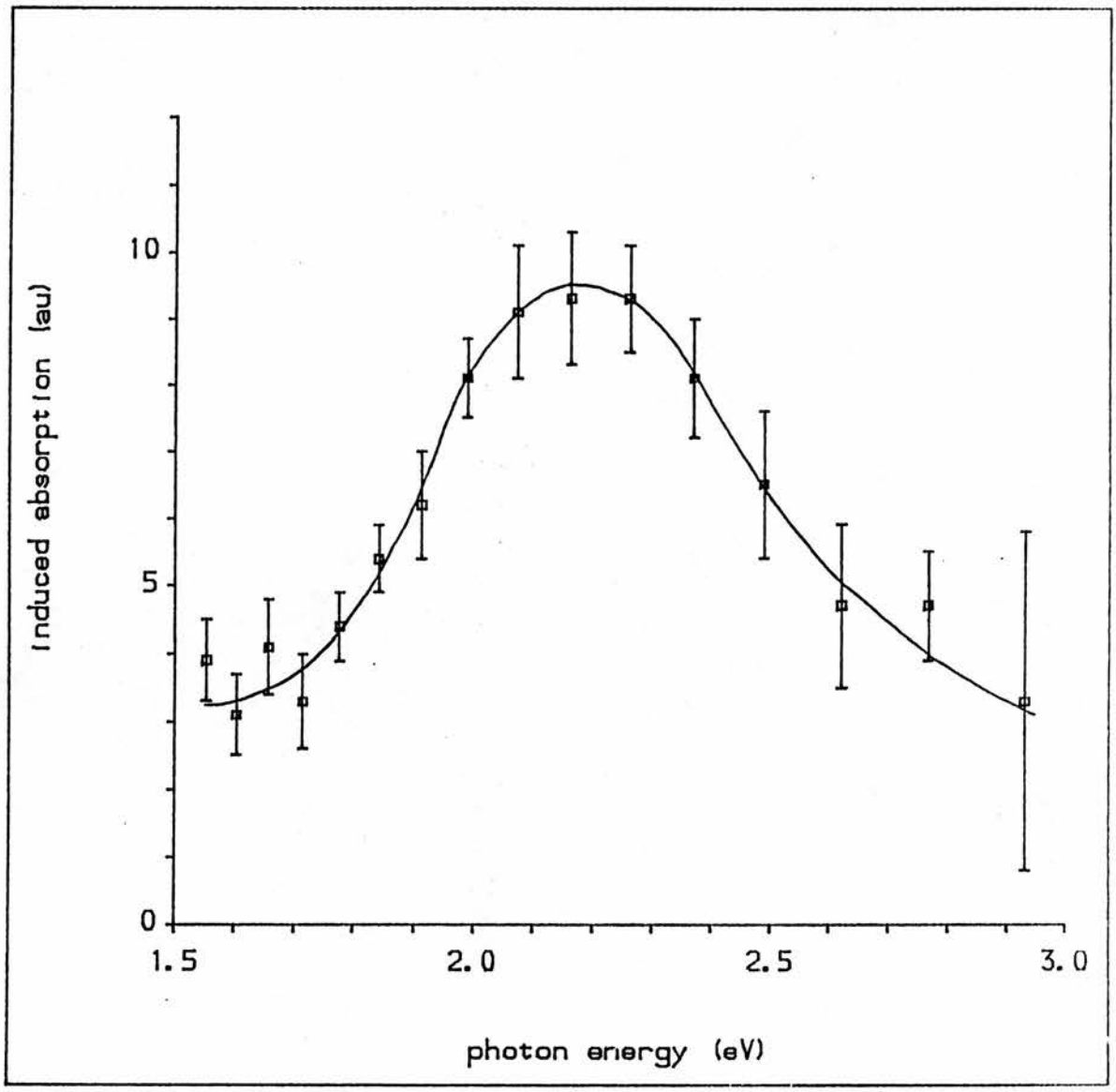

Fig. 5.3.3.3: Spectrum of the induced absorption by white light illumination (against photon energy)

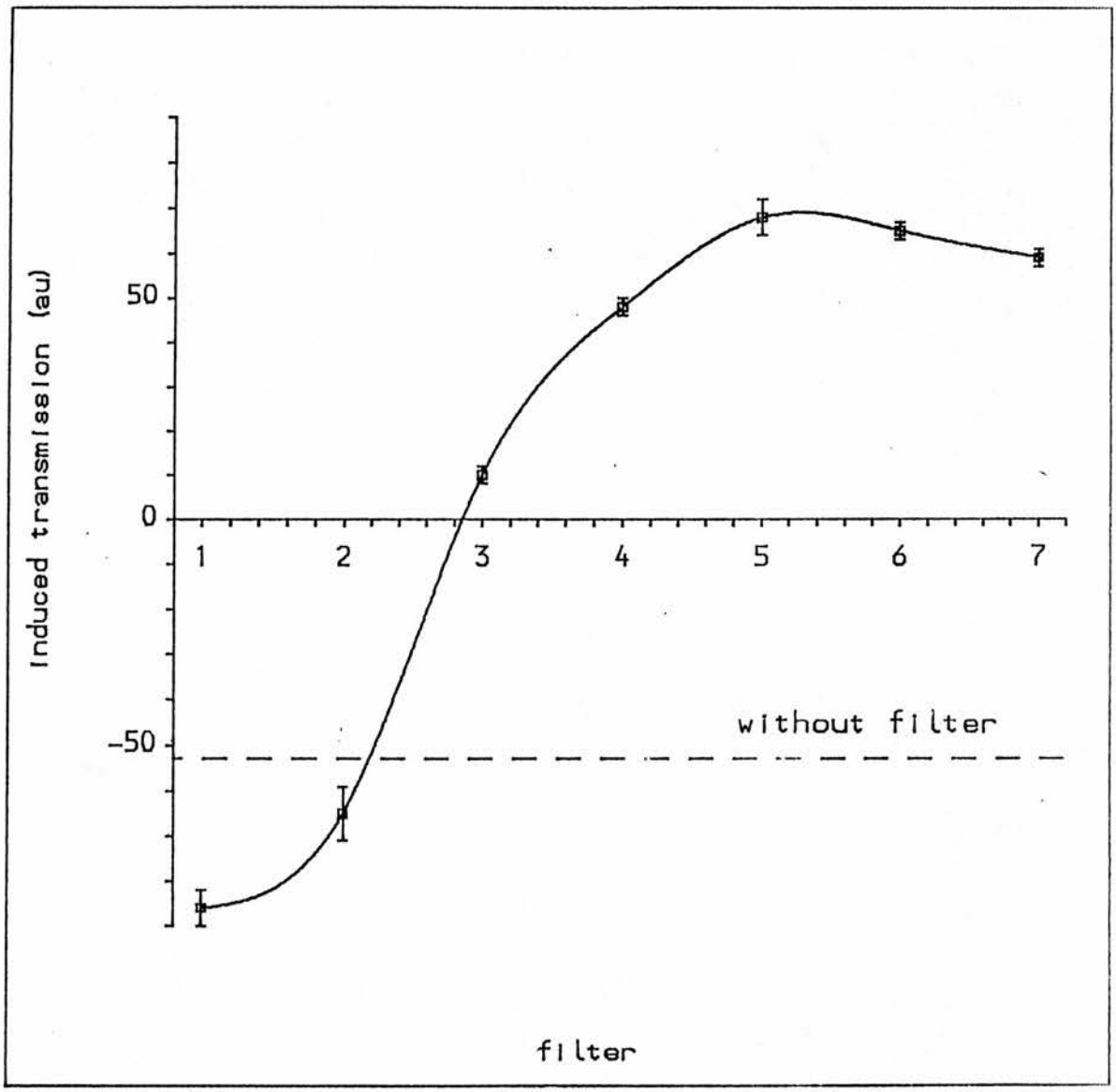

Fig. 5.3.3.4: Induced changes in transmission at 575 nm; filters in the inducing light beam:

1: Wratten 47b (blue-violet)
2: Wratten 38 (blue)
3: Wratten 75 (green-blue)
4: Wratten 58 (green)
5: Wratten 16 (yellow)
6: Ealing 26-3343 (orange)
7: Wratten 29 (red)

Although the spectral windows were not of the same shape in each case, it is obvious that the effect changed from a drop in transmission to an increase in transmission as the exciting light changed from blue to red. For white exciting light the blue part seemed to have been prevailed, though the red part was of much higher intensity as the intensity of the bulb spectrum follows Planck's law with a maximum in the infrared. The time dependent shape of the processes looked quite similar for all the filters and the white light.

To investigate the spectral dependence of the extreme cases a rough spectrum was taken for white, red (Wratten filter 29) and blue (Wratten filter 47b) light illumination. The data can be seen in Fig. 5.3.3.5. The shape of the induced processes seems to be the same for all three cases.

5.4 ORDINARY OPTICAL PROPERTIES OF THE SAMPLE: PHOTOLUMINESCENCE

From now on a different experimental structure was arranged. A laser served as inducing light source as shown in Fig. 4.3.1b). By looking for the induced absorption (s. section 5.5) I also had to record the thereby excited luminescence since the absorption features would be superposed with it. It also showed whether the sample had the usual ZnS:Mn properties.

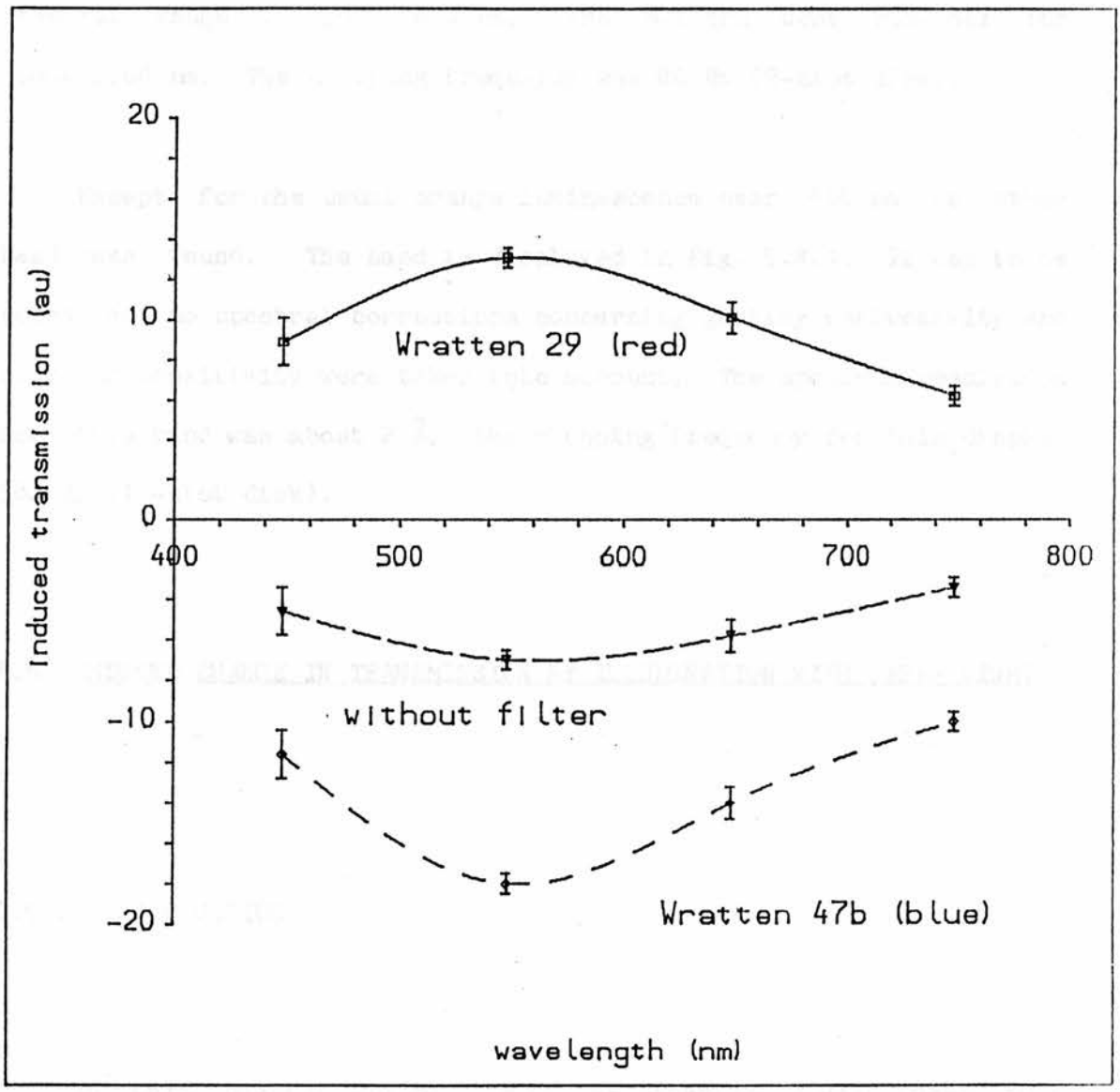

Fig. 5.3.3.5: Rough spectrum of the induced changes in transmission by white, red (Wratten 29) and blue (Wratten 47b) light illumination

The laser beam was perpendicular to the optical axis of the monochromator. The EMI 9558B pm-tube was employed as detector for a spectral range of 350 - 850 nm, the Mullard 62SV PbS-cell for 600 - 2700 nm. The chopping frequency was 80 Hz (2-slot disk).

Except for the usual orange luminescence near 580 nm no other band was found. The band is displayed in Fig. 5.4.1. It has to be noted that no spectral corrections concerning grating reflectivity and detector sensitivity were taken into account. The spectral resolution for this band was about 2 Å, the chopping frequency for this display 380 Hz (10-slot disk).

5.5 INDUCED CHANGE IN TRANSMISSION BY ILLUMINATION WITH LASER LIGHT

5.5.1 INTRODUCTION

In this chapter the results of the experiments with laser light (λ = 514.5 nm) as inducing light source are described. Thus the $^4T_1(G)$ state of the manganese was pumped directly. There is a slight difference to the conditions that Kushida et al [2] employed for their experiments since they used the 488 nm line of an Ar-ion laser. I was not able to change to this wavelength from the 514.5 nm line because my laser was the property of another research group and we had to

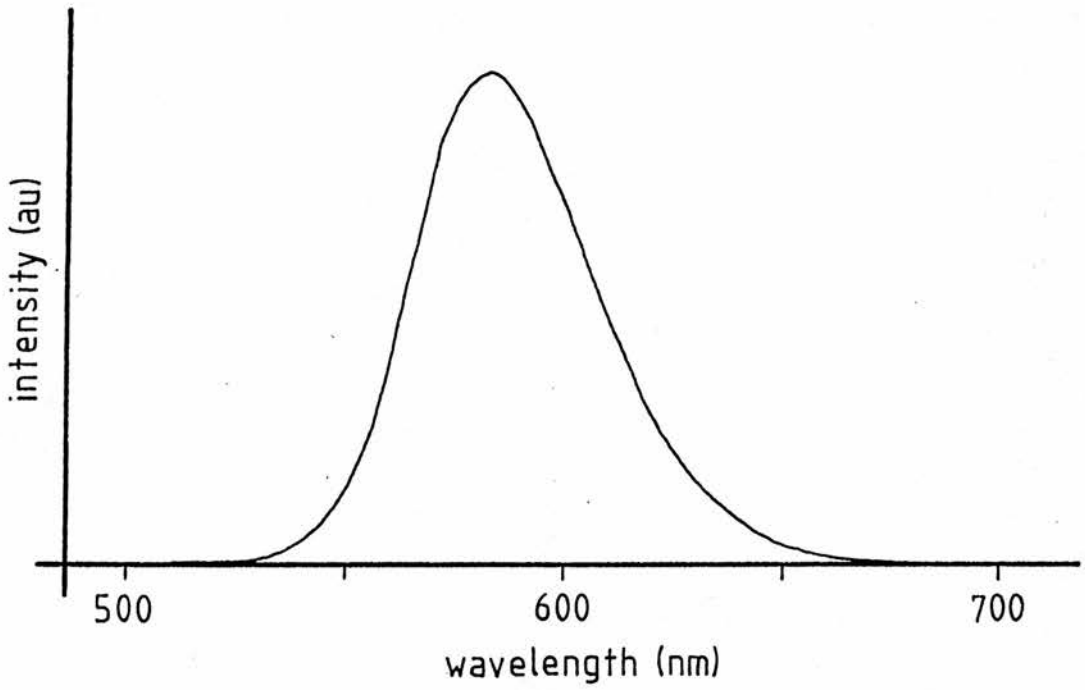

Fig. 5.4.1: Luminescence of the sample near 580 nm (not corrected by spectral distorting effects like grating reflectivity or pm sensitivity)

avoid periodic realignments of the laser. Still, there should be no considerable differences. The only property that changes concerning the manganese impurities is the absorption coefficient and hence the efficiency of the pumping.

The aim of these experiments should be, of course, to look for any manganese correlated bands and to answer the question whether the bands that were observed by Kushida et al could be confirmed. A further aim was to produce spectra that cover large spectral regions so that the intensities of the bands could be easily compared. It was interesting, too, to see whether there would be any photo-ionization like features. If it is possible to determine the depth of the $^4T_1(G)$ state, the ground state of the manganese relative to the ZnS band structure could be found.

The experiments were divided into three parts: first the spectral dependence of any induced effects was investigated. Then the frequency behaviour of the induced signals and the luminescence was used to distinguish the induced features. Thus it was possible to separate bands of different origin and to determine the Mn correlated structures. Finally a different kind of experiment was performed to get further information about one specific feature. This is explained more explicitly in the appropriate section (5.5.4).

Except for section 5.5.4 the experimental outline was that of Fig. 4.3.1b). The first experiments were performed with the chopper being on the same table as the rest of the experiment (except the laser). However, it turned out that the chopper could cause

mechanical vibrations of some parts of the optical equipment and thus mimicked an induced signal (as it was only visible with the probe light). After that had been recognized the chopper was placed separately. Still, already obtained results were not worthless. It showed that because of the lock-in characteristics the effect penetrated the signals only for one disk (2-slot), and only under certain circumstances. This will be discussed in section 5.5.3. The mirrors for the guiding of the laser beam were sited on places where operations within the experiment did not influence them. As already mentioned in section 4.3 the reproducibility of the laser illumination was not very good. Hence each experiment was done in one run to assure equal conditions. When different experiments had to be compared only qualitative aspects were considered.

Another inhomogenity within the experiments was the usage of the second aperture behind the sample to assure that the luminescence came from the same part of the sample as the induced absorption. During the first experiments it was not mounted. This could have caused two problems:

- the luminescence was too bright, it could have masked other signals;

- inhomogenities in the impurity concentration could have caused different effects.

The first problem deals particularly with the spectral search for the induced absorption features. Since these experiments were all

performed or repeated with the second aperture mounted this point can be excluded. The second problem concerns only some experiments under section 5.5.3 and is discussed there.

For the experiments of the sections 5.5.2 and 5.5.3 the laser output power was approximately 1 W, for section 5.5.4 250 mW. The density of the incoming power at the sample is estimated to have been about 2 Wcm^{-1} and 0.5 Wcm^{-1}, respectively.

5.5.2 SPECTRA OF INDUCED BANDS

Similar to section 5.3 I used the EMI 9558B pm-tube as detector for 350-850 nm whereas the Mullard 62SV PbS-cell covered the region 0.6-2.7 μm. A chopping frequency of 80 Hz proved to be an efficient frequency, giving good signals with not too much noise.

I pursued the following method for the scanning of the induced bands: a spectrum of the induced signals from the probe light was obtained first, the phase of the lock-in amplifier being maximized for the luminescence at 580 nm. Then a pure luminescence scan was taken with the probe light shut off. This was done not only for the band at 580 nm but for the whole spectrum. Hence any other possible luminescence could have been considered. The difference of the two scans gave the induced signals only. To test whether there are any other induced signal out of phase a scan with the probe light was taken with the phase being shifted by 90°, too. The induced spectra

were finally normalized against the chopped direct transmission signals that were obtained in the same run as well. Since the time dependent shape of the transmission and the induced signals were different, the ratio of these does not really represent the absolute strength of a signal. Still, it is a good approximation to get an idea of the magnitude of the induced features.

The obtained spectra are shown in Fig. 5.5.2.1-3. Spectra as a function of energy can be seen in Fig. 5.5.2.4,5. In context to the note above, the relative strength of the induced bands can be estimated by multiplying the arbitrary units that are used in the diagrams by 10^{-4}. The spectral resolution was approximately:

wavelength [nm]	Fig.	resolution [nm]
350 - 850	5.5.2.1	0.1
600 - 2400	5.5.2.2	4.5
2200 - 2700	5.5.2.3	9

The diagrams yield the following features:

- a sharp threshold is visible for ≈ 380-520 nm, it is not quite clear whether the signal declines for shorter wavelengths as the transmittance of the crystal dropped sharply and the errors are large, the signal reaches ≈ 1.7 % of the transmittance signal at 380 nm;

- from 550-615 nm the transmittance is rising, the spectral region coinciding with the orange luminescence;

- around 650 nm (1.91 eV) there is an induced absorption band with

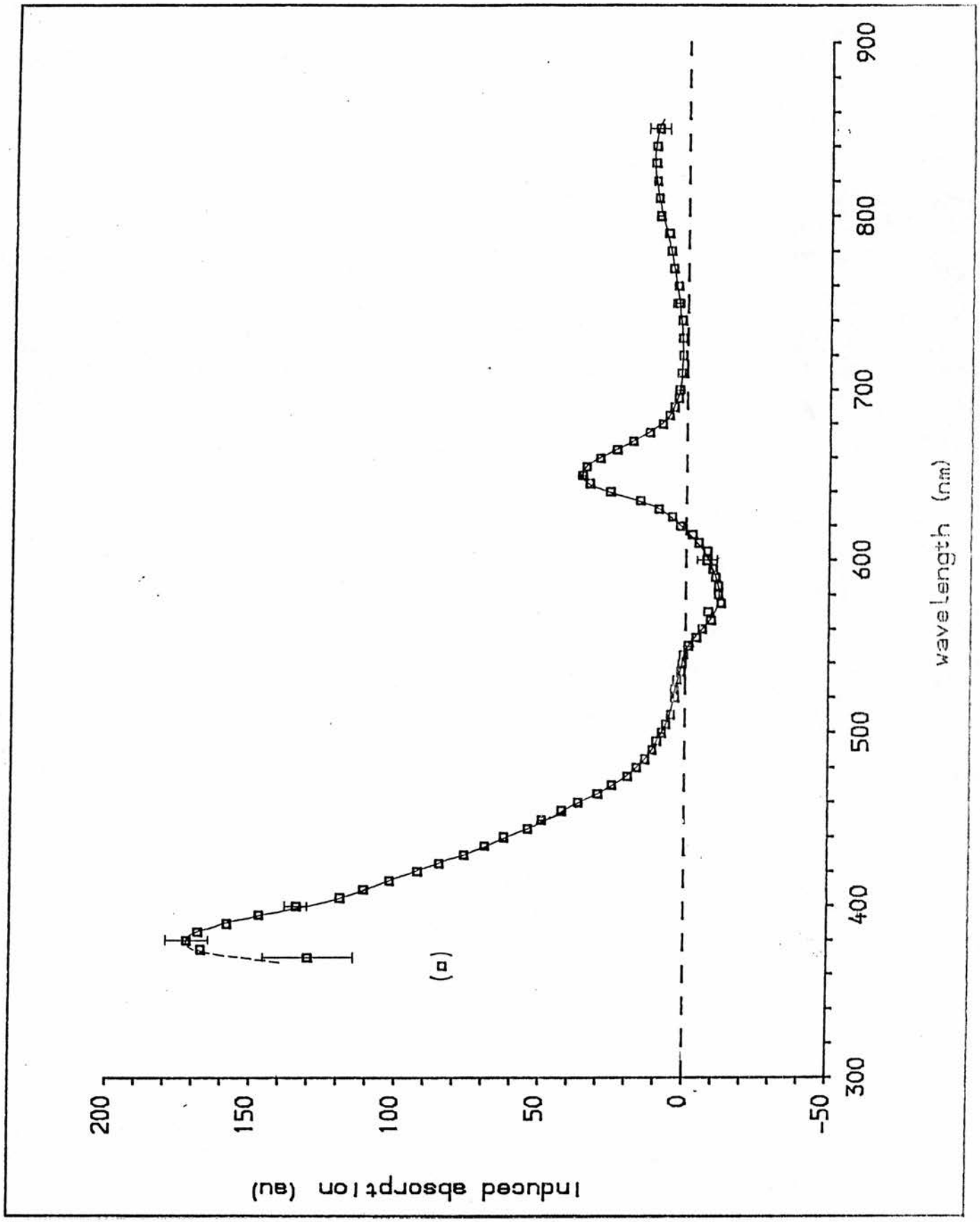

Fig. 5.5.2.1: Spectrum of induced features for 350 - 850 nm, detected by the EMI 9558B photomultiplier, pumping laser chopped at 80 Hz (2-slot disk)

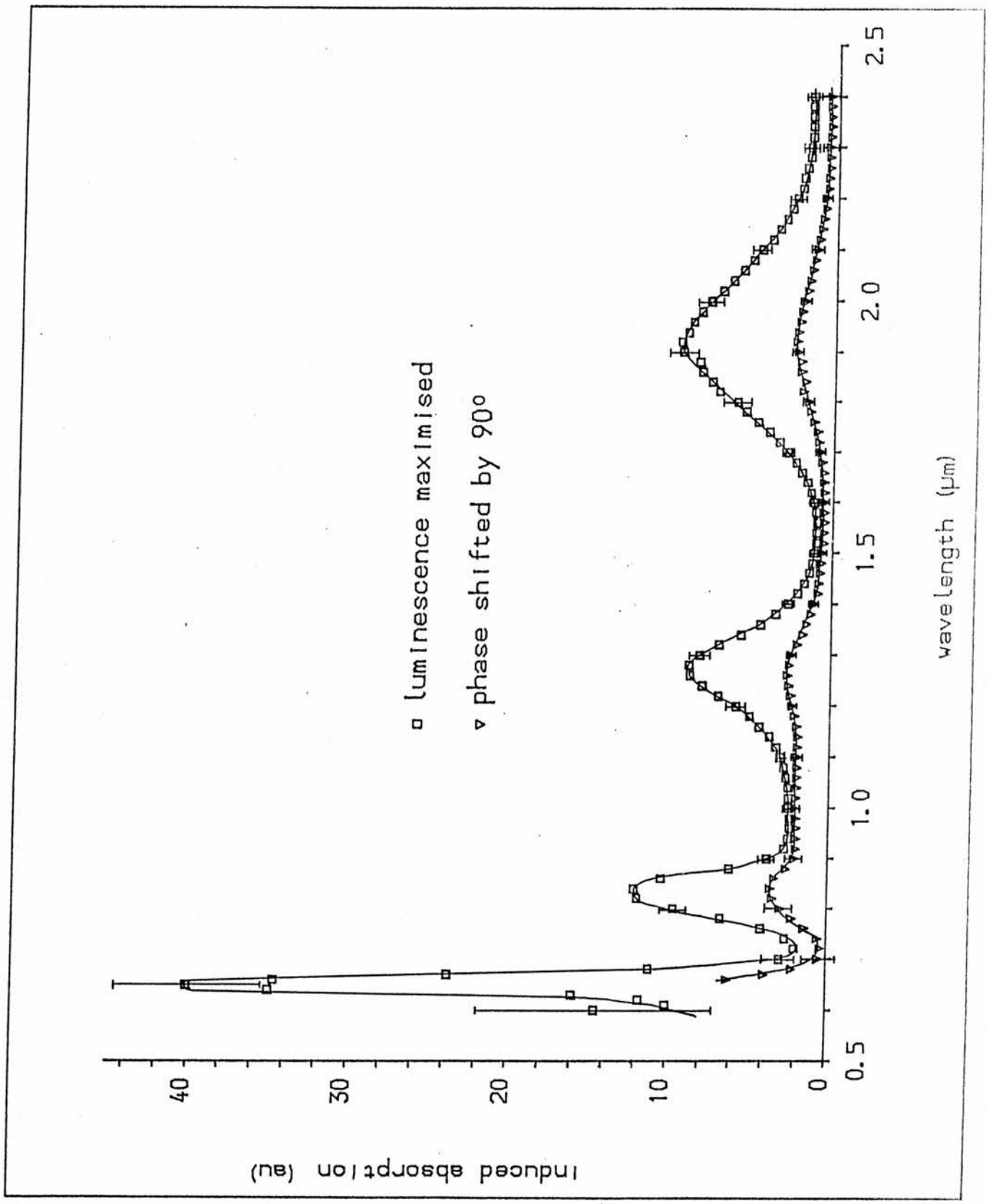

Fig. 5.5.2.2: Spectrum of induced features for 600 - 2400 nm, detected by the Mullard 62SV PbS-cell, pumping laser chopped at 80 Hz (2-slot disk)

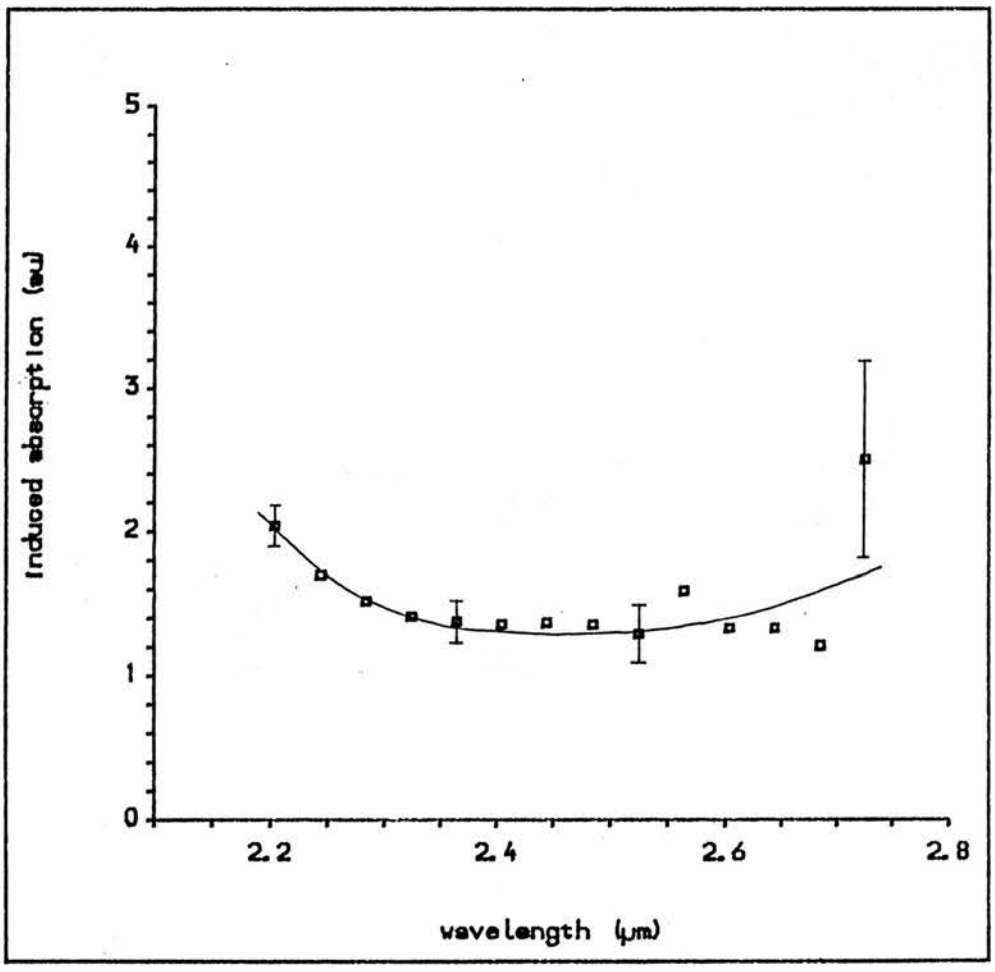

Fig. 5.5.2.3: Spectrum of induced features for 2200 - 2700 nm, detected by the Mullard 62SV PbS-cell, pumping laser chopped at 80 Hz (2-slot disk)

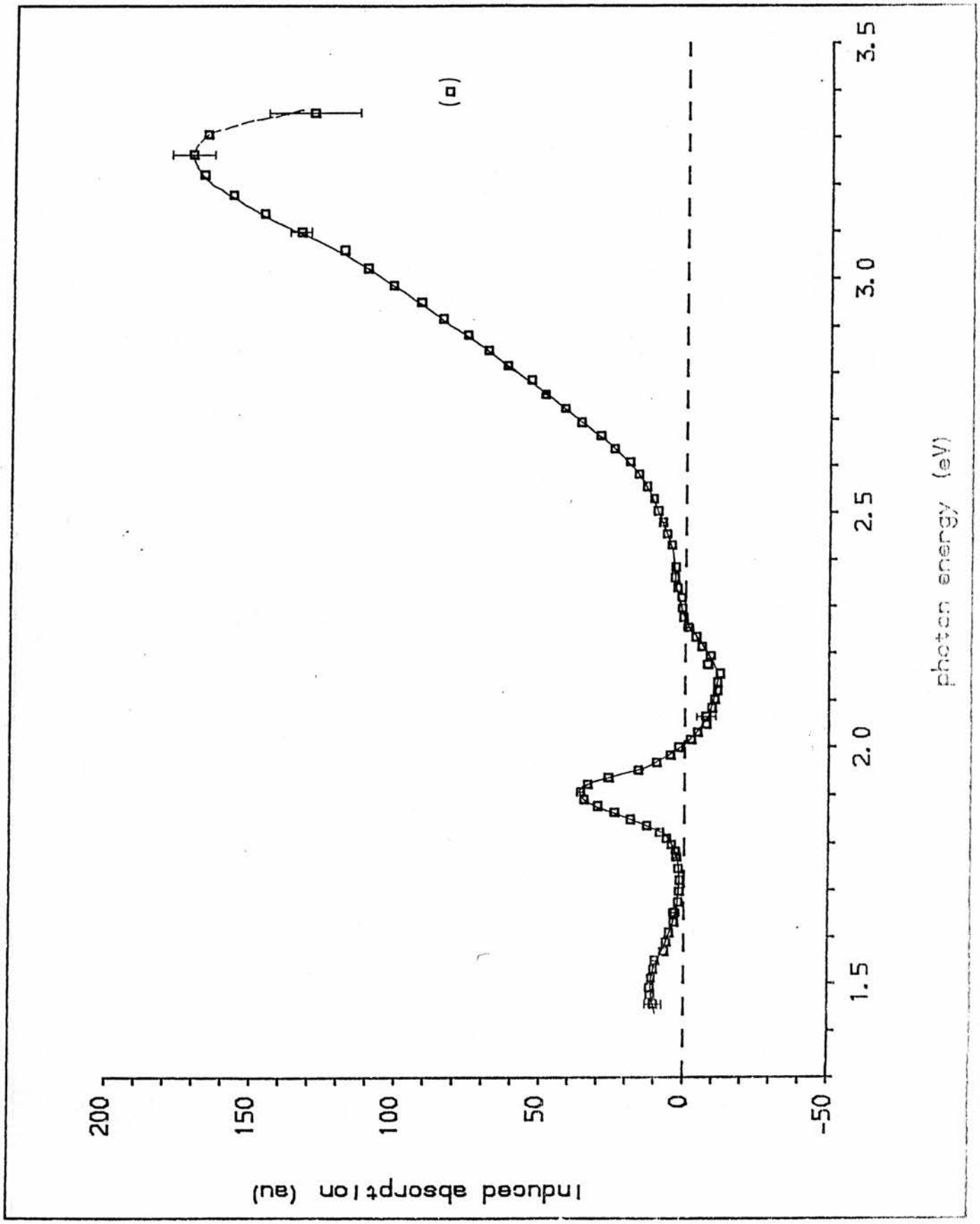

Fig. 5.5.2.4: Energy dependence of the spectrum shown in Fig. 5.5.2.1

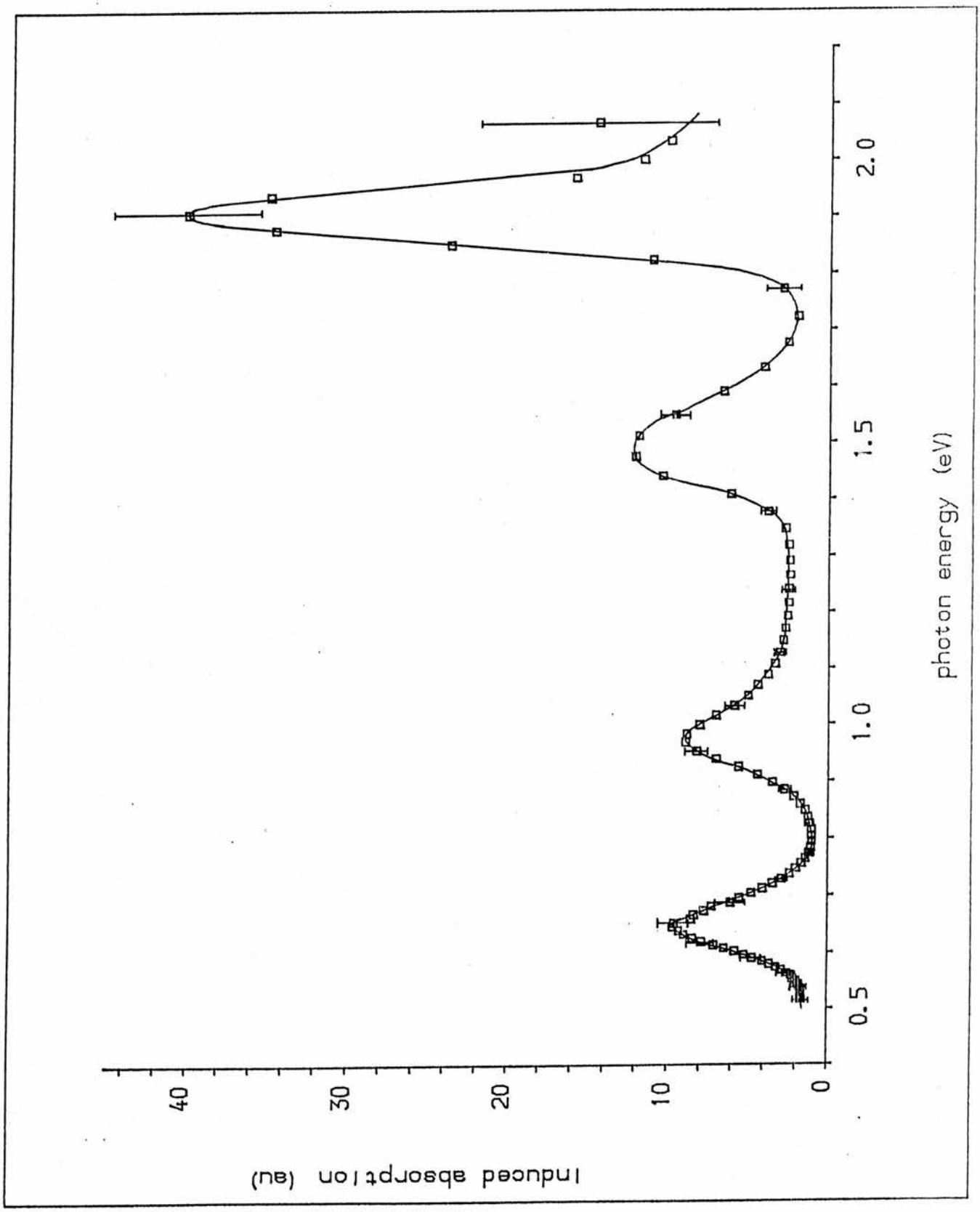

Fig. 5.5.2.5: Energy dependence of the spectrum shown in Fig. 5.5.2.2

a band width of 0.10 eV;

- around 830 nm (1.49 eV) an induced absorption band having a band width of 0.16 eV can be seen;

- at 1000 nm (1.24 eV) a broad band being out of phase was detected, it seems to superpose with other bands on both of its flanks;

- at 1270 nm (0.98 eV) another induced absorption band with a width of 0.13 eV appeared;

- around 1910 nm (0.65 eV) a last induced band with a width of 0.11 eV was discovered.

The bands at 830, 1270 and 1910 nm were of equal intensity whereas the band at 650 nm was three times as intense (≈ 4 ‰ of the direct transmission). The shape of the first three bands seems to be slightly asymmetric with a high energy tail.

The rising of the transmittance near 580 nm was observed at a very late experimental stage. The other features had been detected in a previous but less sensitive scan. Therefore the experiments for section 5.5.3 (frequency dependence) did not cover this structure. On the other hand it can be assured that the effect was not due to an accidental disalignment of optical parts for the excitation since I looked again for this behaviour directly after the experiment that had revealed it. The effect was still visible, but less strong.

5.5.3 FREQUENCY DEPENDENCE OF THE INDUCED FEATURES

The structures around 380-520 nm and 650 nm were discovered first (although the 830 nm band was seen as well within the first results it was too weak for further investigations). Thus the next experiments dealt with these features first. For chopping frequencies of 80, 380 and 780 Hz the signals for the induced absorption at 400, 450 and 650 nm and the luminescence at 580 nm were recorded for different phases of the lock-in amplifier. Two points within the threshold structure were chosen to assure that this feature is behaving homogenously.

The traces for λ = 400, 580 and 650 nm are shown in Fig. 5.5.3.1-3. For λ = 450 nm the behaviour was similar to that at 400 nm. The fitted line was done by a cubic spline, thus giving a rough idea of the shape. A normalization was not applied since only the general phase dependence was of interest. The shapes are more or less sinusoidal, but it is difficult to recognize whether there are any differences between the curves. However, at all three of the frequencies it is obvious that the zero-value of the phase is smaller for the induced absorption than for the luminescence. For the used lock-in amplifier a shorter phase value means a delayed signal. Averaging the two zero-values for each curve and calculating the shift $\Delta\Psi$ to the values for the luminescence one gets the data displayed in Tab. 5.5.3.1. Within the error-bars the shift is quite the same for all three wavelengths. The high value of the errors (compared to later experiments) were generated by the insensitivity of the system

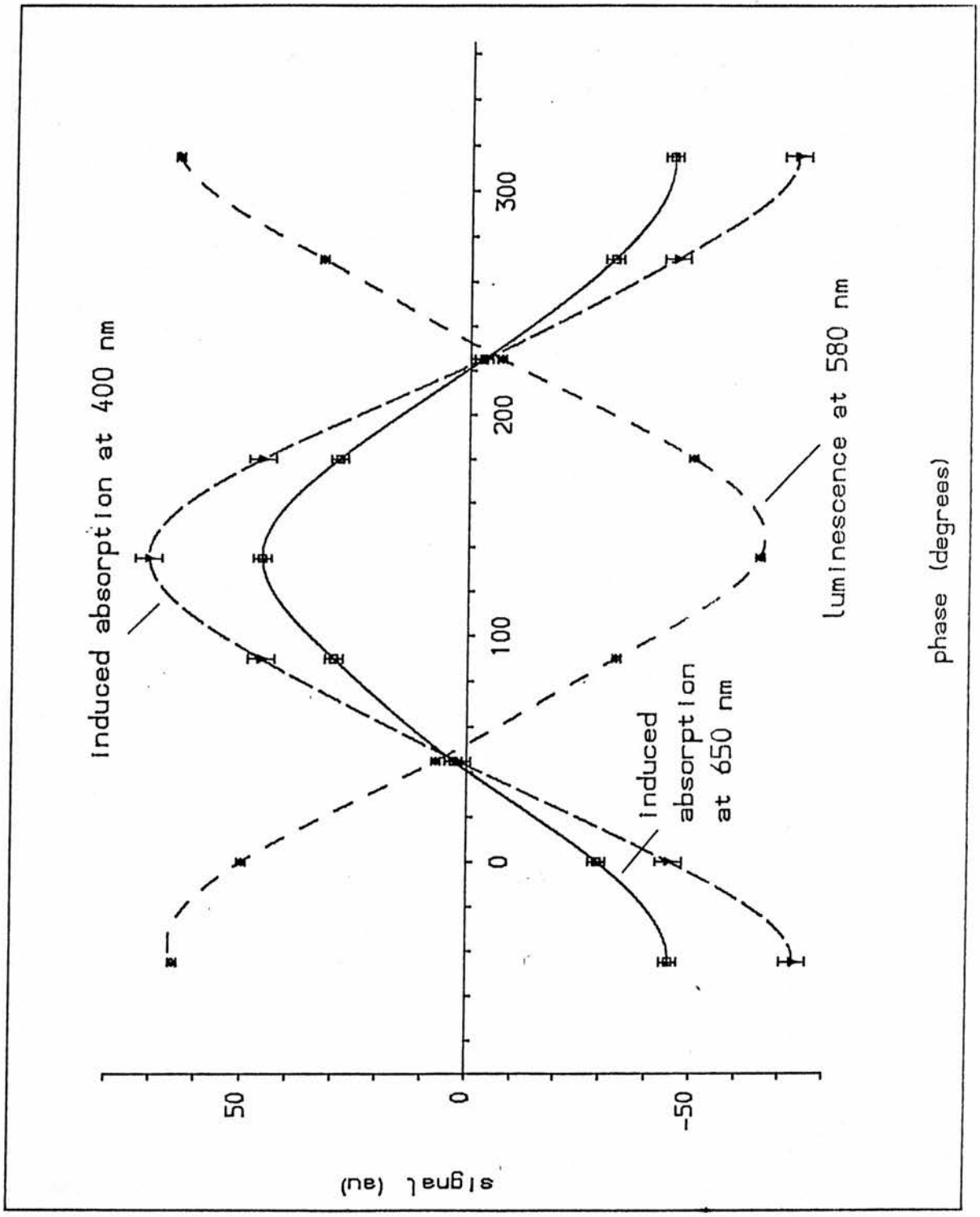

Fig. 5.5.3.1: Phase dependence of the induced absorption at 400 and 650 nm and of the luminescence at 580 nm with the pumping light being chopped at 80 Hz (2-slot disk)

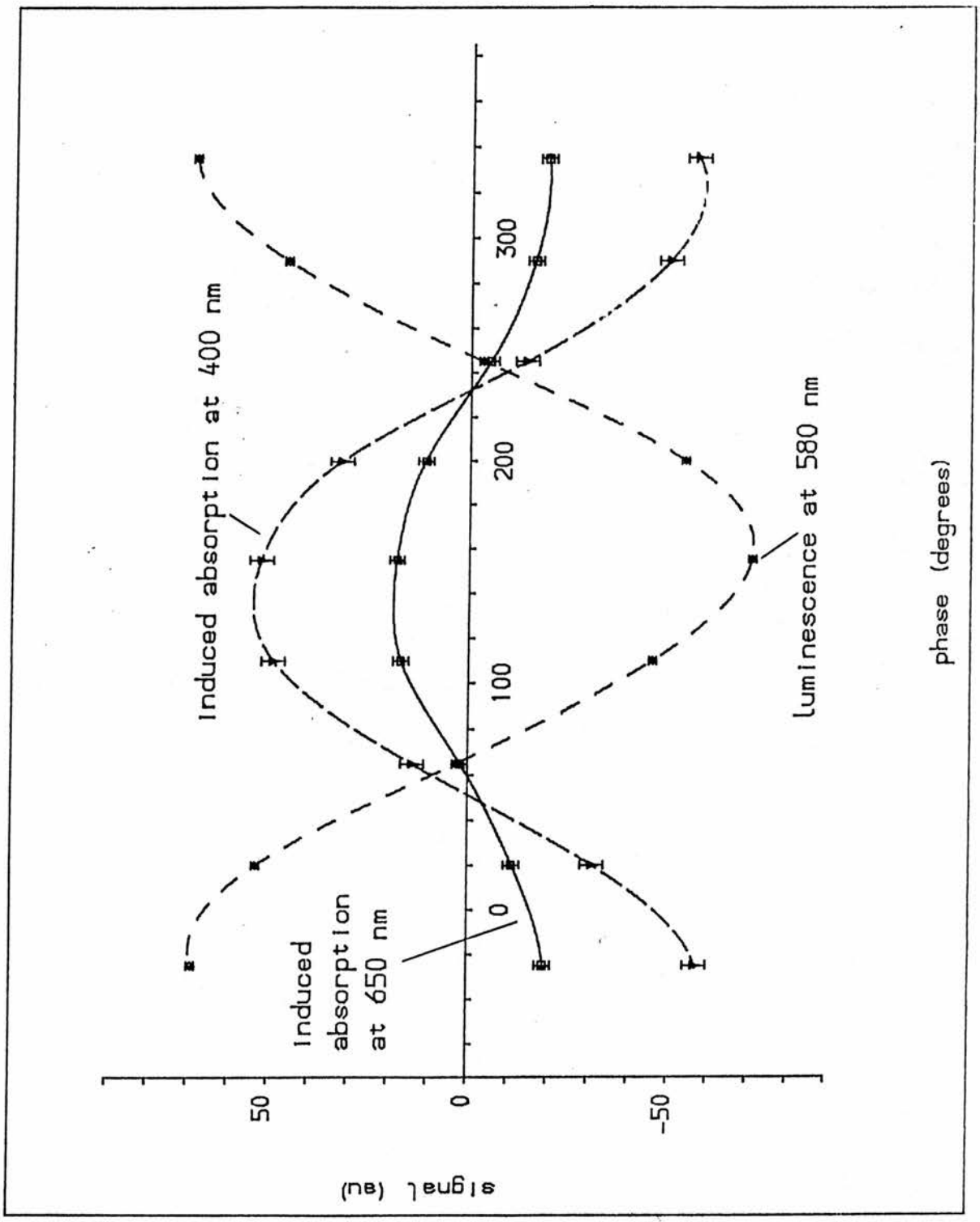

Fig. 5.5.3.2: Phase dependence of the induced absorption at 400 and 650 nm and of the luminescence at 580 nm with the pumping light being chopped at 380 Hz (10-slot disk)

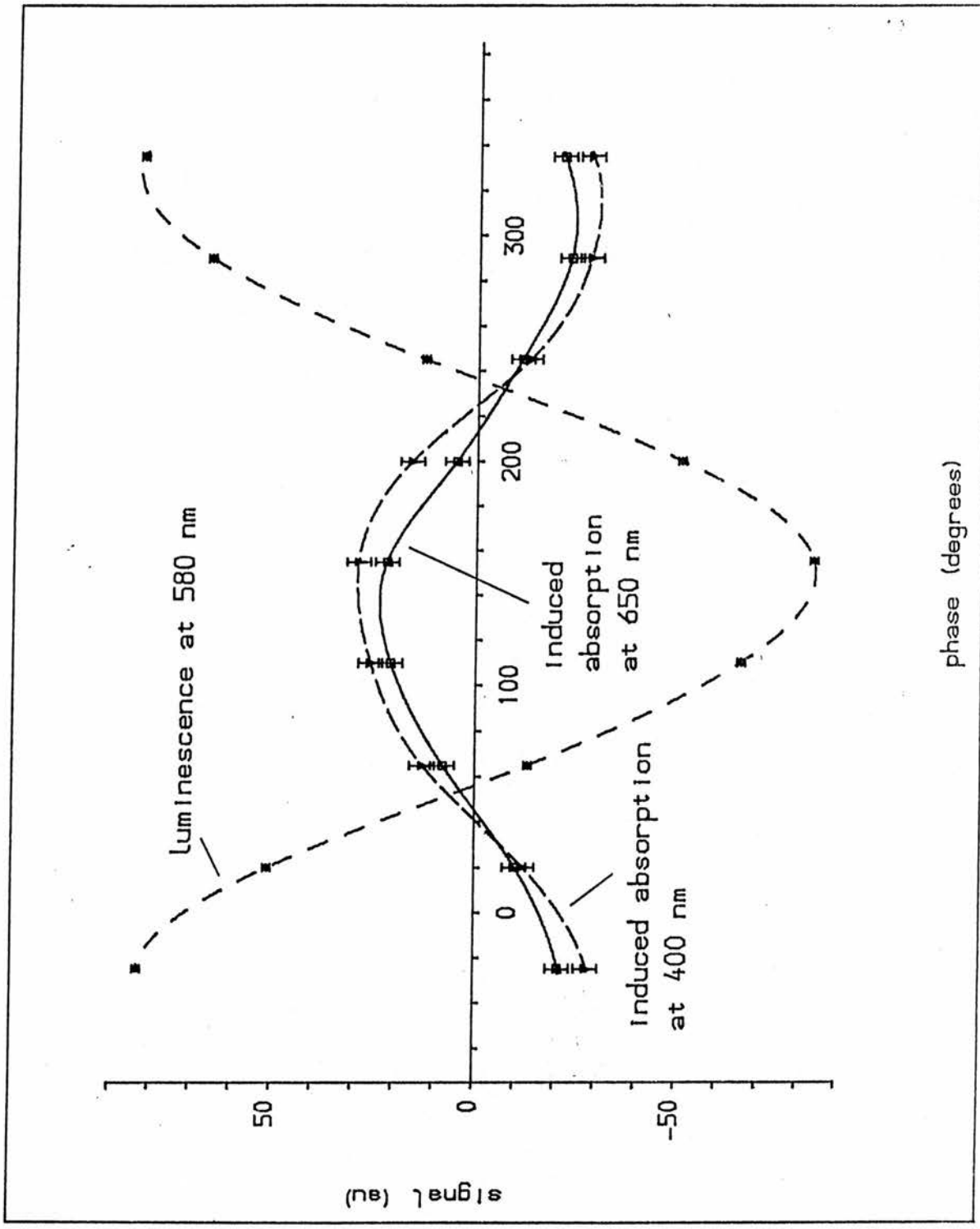

Fig. 5.5.3.3: Phase dependence of the induced absorption at 400 and 650 nm and of the luminescence at 580 nm with the pumping light being chopped at 780 Hz (10-slot disk)

Tab. 5.5.3.1: Phase shift of the zero-values for the induced absorption at 400, 450 and 650 nm towards the luminescence at 580 nm

f [Hz]	wavelength [nm]	$\Delta\Psi$ [°]
80	400	8 ± 4
	450	8 ± 4
	650	10 ± 4
380	400	17 ± 4
	450	17 ± 4
	650	14 ± 7
780	400	12 ± 6
	450	15 ± 5
	650	17 ± 8

at that stage.

To get further evidence for this common characteristic the following experiment was performed: for several frequencies between 80 and 980 Hz the induced signals and the luminescence were measured for the phase where the luminescence was maximized. The obtained amplitudes were normalized against their value at 80 Hz. The results can be seen in Fig. 5.5.3.4. Errors were of the order of 4 au for the induced signals and 1 au for the luminescence (units the same as for the signals in Fig. 5.5.3.4). It is clearly seen that the signals decline with frequency. The signals for the induced absorption behave similarly altogether, decreasing faster than the luminescence. This does indicate that the structure for $\approx$ 380-520 nm behaves roughly homogenously, hence it is not a superposed feature, and the band at 650 nm shows the same characteristics. Both structures seem to have the same origin. Of course, the faster decline of the signals in Fig. 5.5.3.4 does not necessarily mean that the maximum signals are decreasing. It is more likely that an increasing phase shift is the reason for the phenomena.

It was at this stage that the second aperture behind the sample was mounted. Any inhomogenity within the sample could have influenced only the results for the luminescence. However, the basic information that can be extracted from these experiments covers the absorption features. Additionally the next experiment investigated the phase shift, and this was still of the same order. Therefore, I do not think that inhomogenities could have troubled the experiment.

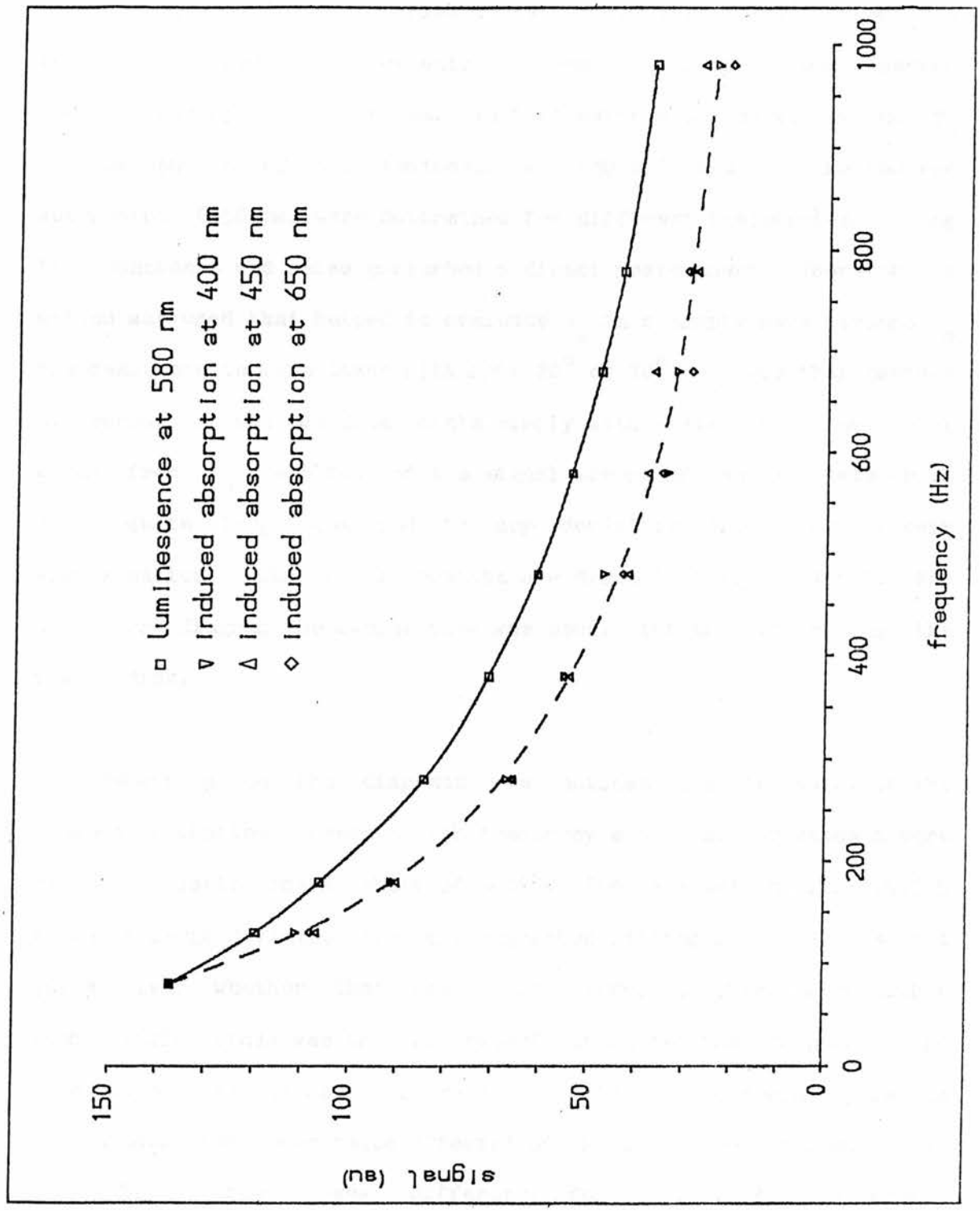

Fig. 5.5.3.4: Signals for the induced absorption at 400, 450 and 650 nm and the luminescence at 580 nm with the phase for maximal luminescence for different frequencies (10-slot disk), normalized for the signals at 80 Hz

For the following experiment only the signal at 450 nm was measured, since it represents the behaviour of the by now observed induced absorption structures. In this experiment the zero-values Ψ_o of the phases of the luminescence (580 nm) and of the induced absorption (450 nm) were determined for different frequencies. Long time constants and noise perturbed a direct measurement. Therefore, a method was used that helped to evaluate Ψ_o in a simple way: around Ψ_o two measurements were taken with $\Delta\Psi = 20^o$ or 30^o. Ψ_o was then derived by connecting the two data points simply with a straight line. The error from Ψ_o resulted of the signal errors of the data sets which were quite large compared to any deviation from the linear approximation. The final results are drawn in Fig. 5.5.3.5,6. For the first diagram the 2-slot disk was used, for the other one the 5-slot disk.

Referring to the diagrams one notices that the delay of the induced absorption increases with frequency and finally reaches a more or less stable phase shift of $\approx 15^o$. One data set in Fig. 5.5.3.5 shows a large deviation from the suggested fitting line. It is not quite clear whether that was a real effect or a resonance either mechanically (this was the only experiment where the chopper could have caused vibrations, s. section 5.1.1) or electronically (since there could have been 'site effects' of the mains for 100 Hz). In Fig. 5.5.3.7 the phase difference for Fig. 5.5.3.5 is drawn. Additionally there is the phase difference for the luminescence between the signal with (w) and without (wo) probe light. It should be noted that all other luminescence signals were measured without

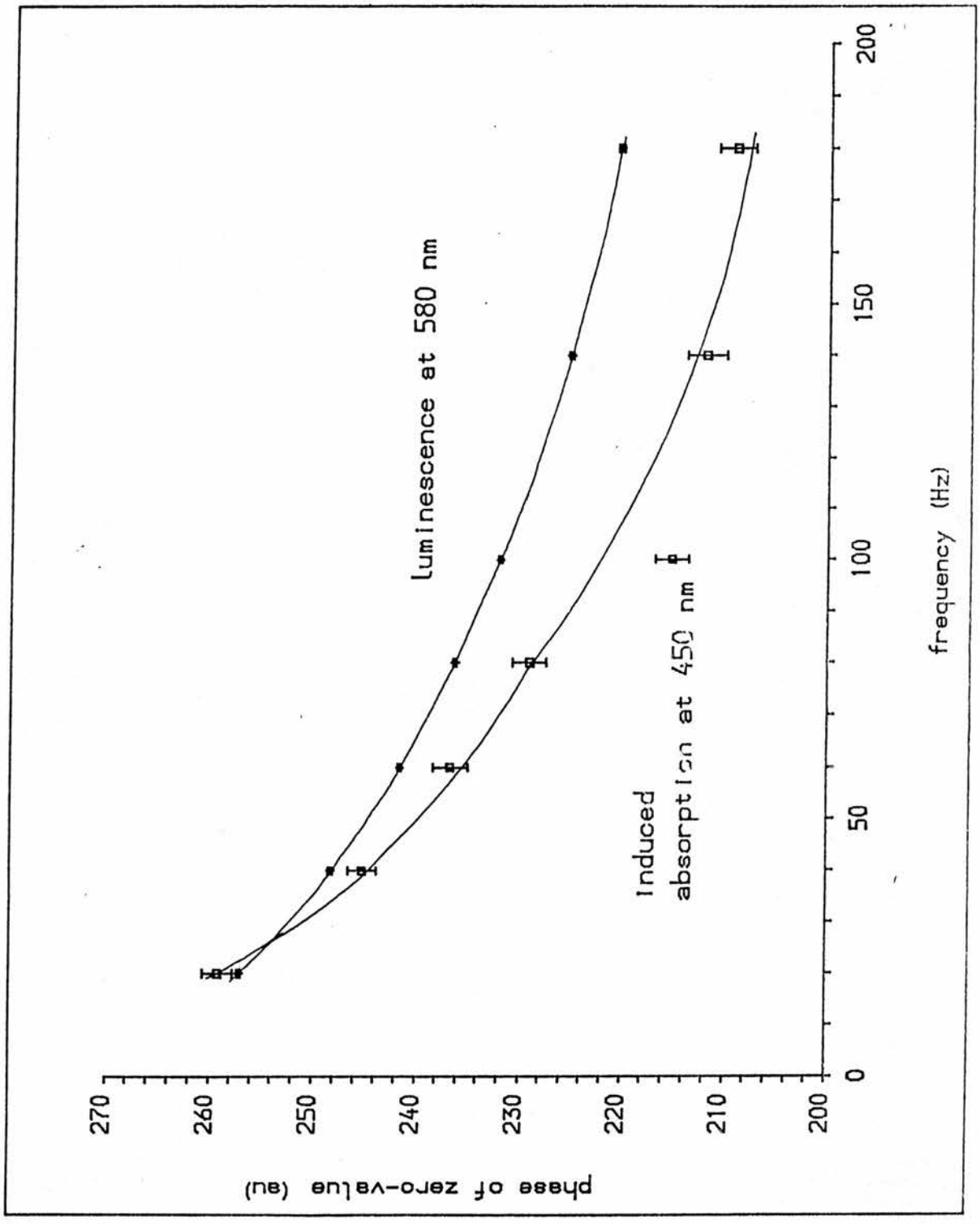

Fig. 5.5.3.5: Zero-values for the induced absorption at 450 nm and the luminescence at 580 nm between 20 and 180 Hz (2-slot disk)

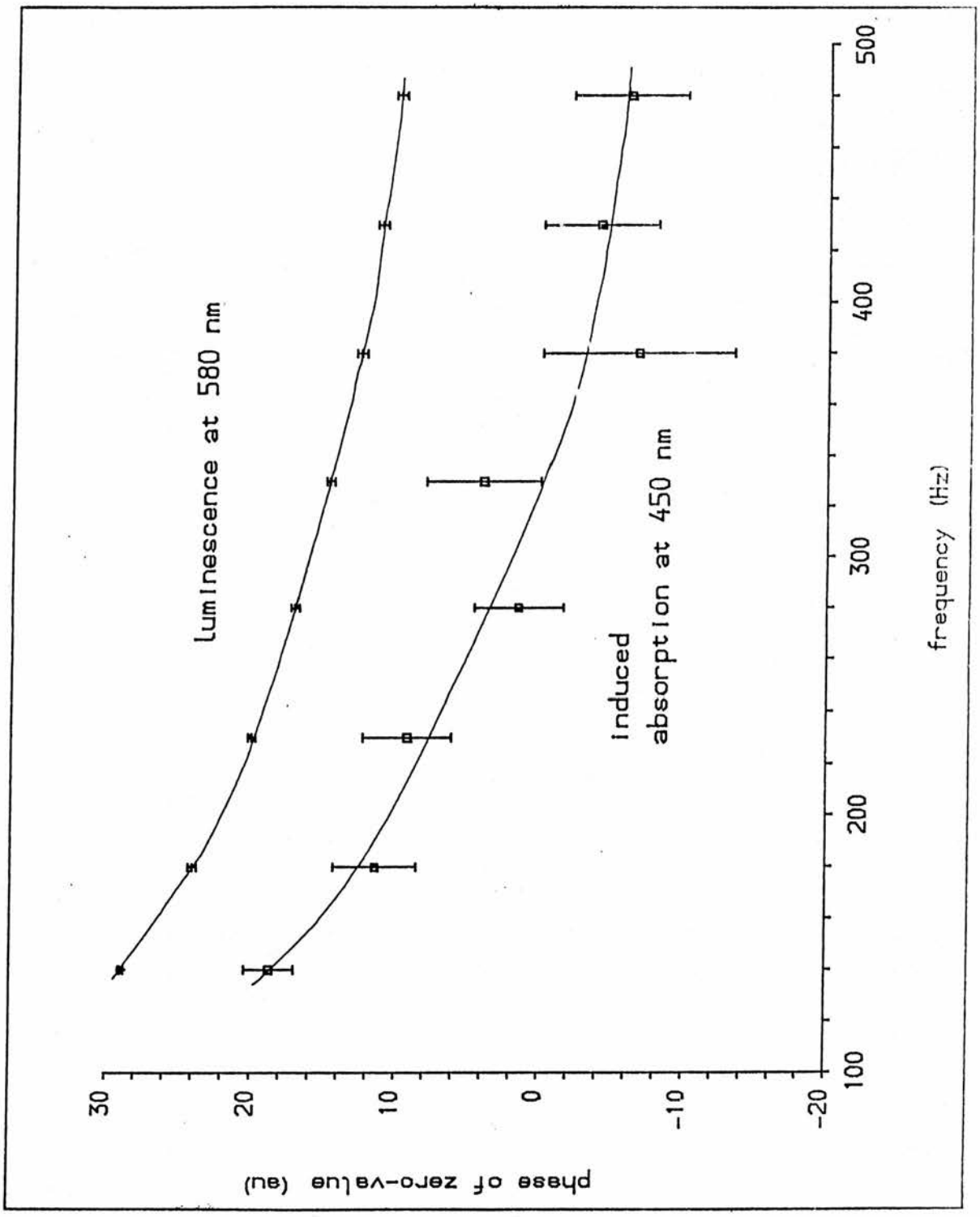

Fig. 5.5.3.6: Zero-values for the induced absorption at 450 nm and the luminescence at 580 nm between 140 and 480 Hz (5-slot disk)

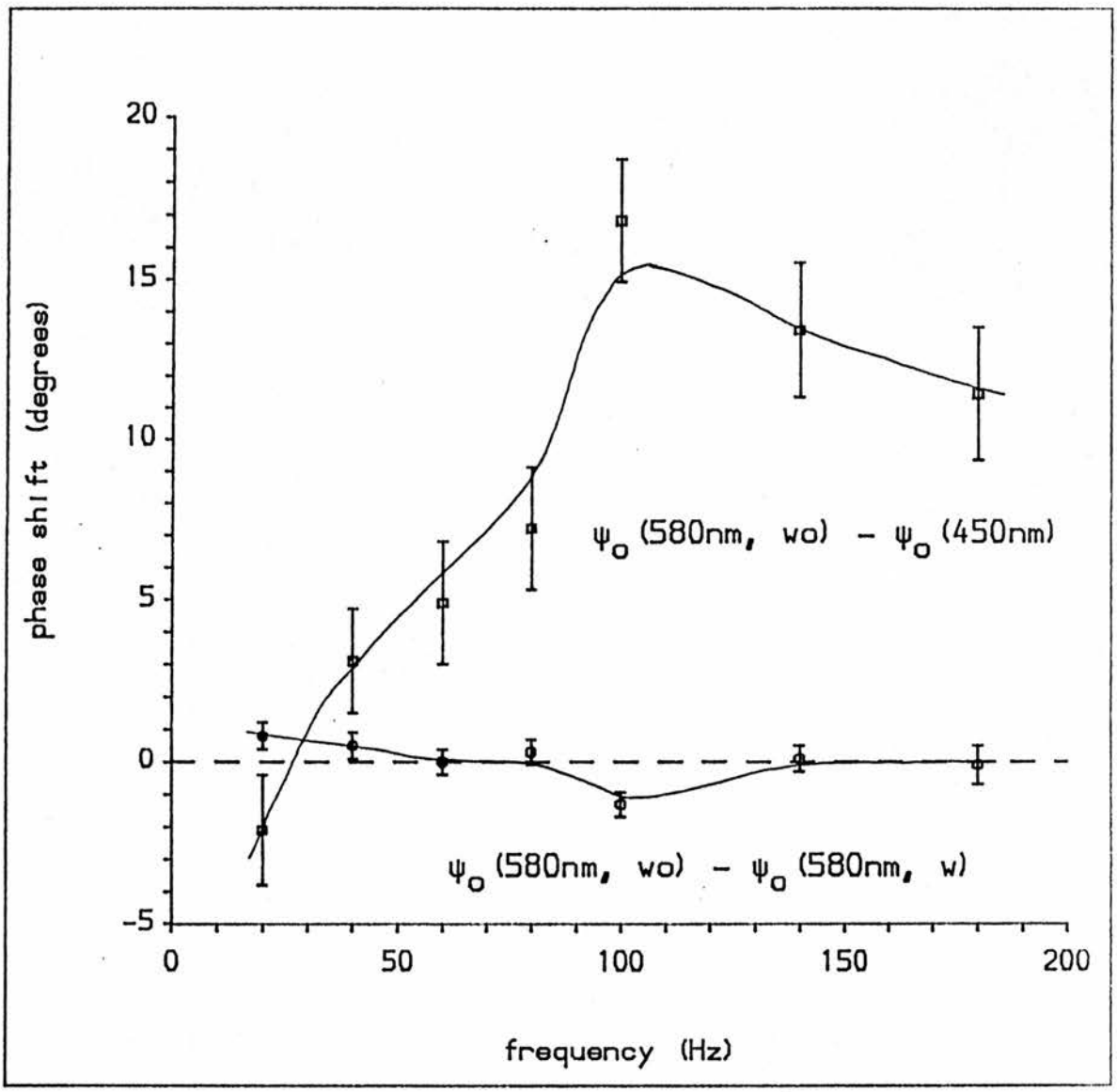

Fig. 5.5.3.7: Phase shift for Fig. 5.5.3.5 and shift of the luminescence at 580 nm between the signals with (w) and without (wo) probe light

probe light. For this second graph a peak is visible for 100 Hz as well, but it is small.

To test the influence of any inhomogenities different parts of the sample were illuminated with a narrow part of the laser beam. No measureable shift of the luminescence was detected.

I now proceed to the other induced absorption bands. With the PbS-cell it was possible to investigate the phase shift of all the structures at 650, 830, 1000, 1270 and 1910 nm. With the 2-slot disk ($f \leq 160$ Hz) and the 5-slot disk ($f \geq 160$ Hz) results were obtained for several frequencies, similar to the previous experiment. The data can be seen in Fig. 5.5.3.8, the error-bars would be of the order of 2°. The bands at 650 and 1910 nm show a behaviour like former results for 450 nm. The phase shift increases with frequency reaching a constant shift around 13°. However, the bands at 830 and 1270 nm give a nearly constant phase shift for all frequencies, being around 15°. Finally, the band at 1000 nm behaves totally differently. The phase shift starts with a high value ($\approx 45^{\circ}$), declines with frequency and joins the other graphs for 460 Hz, the highest employed frequency. It has to be borne in mind that the three bands at 830, 1000 and 1270 nm were superposing on each other. Therefore, it is suggested that the bands at 830 and 1270 nm have the same characteristics as the 650 and 1910 nm band. On the other hand the 1000 nm band gets very inefficient for fast processes so that finally the flanks of the two nearby bands dominate giving this band the same phase characteristics.

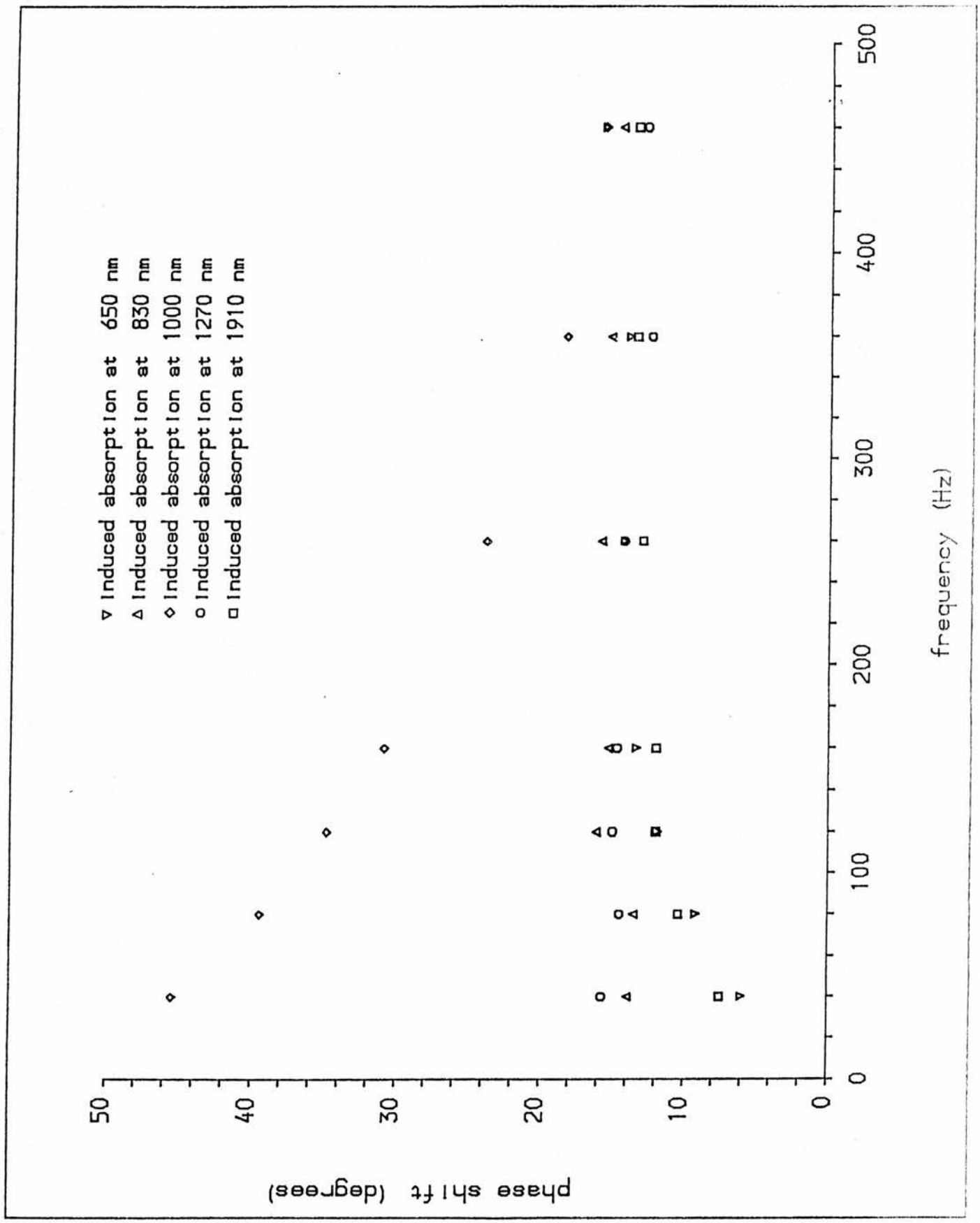

Fig. 5.5.3.8: Phase shift relative to the luminescence at 580 nm for the induced absorption at 650, 830, 1000, 1270 and 1910 nm for several chopping frequencies (f ≤ 160 Hz: 2-slot disk, f ≥ 160 Hz): 5-slot disk)

In Fig. 5.5.3.9 the slopes m of the signals at the zero-value are displayed. They are normalized against their value at 460 Hz. This yields information about the decline of the signal. Errors are of the order of 20 % of the data. The very fast decline of the signal at 1000 nm is well visible. Again the 830 and 1270 nm bands show a behaviour that is a bit different from the one for the other two bands at 650 and 1910 nm, indicating the probable superposition. The luminescence seems to 'decay' more slowly.

5.5.4 INDUCED EXCITATION OF THE Mn LUMINESCENCE AT 400 - 500 nm

As will be discussed later the induced absorption at short wavelengths could represent the photo-ionization of the $^4T_1(G)$ state. To get further evidence for this suggestion the following idea arose: the population of the $^4T_1(G)$ state causes a certain amount of luminescence. If the Mn atom undergoes an electronic transition from the $^4T_1(G)$ state to a state within the conduction band auto-ionization will happen and one electron will be removed from the Mn shell. In this case there would be no instant luminescence. Instead, it is quite probable that the hole in the d-shell of the manganese is removed to the valence band. The hole in the valence band and the electron in the conduction band could recombine somewhere in the crystal, and finally the situation would be the same as before the Mn was pumped to the $^4T_1(G)$ state, the Mn atom being in the $^6A_1(S)$ ground state again without having emitted any light. Thus a possible

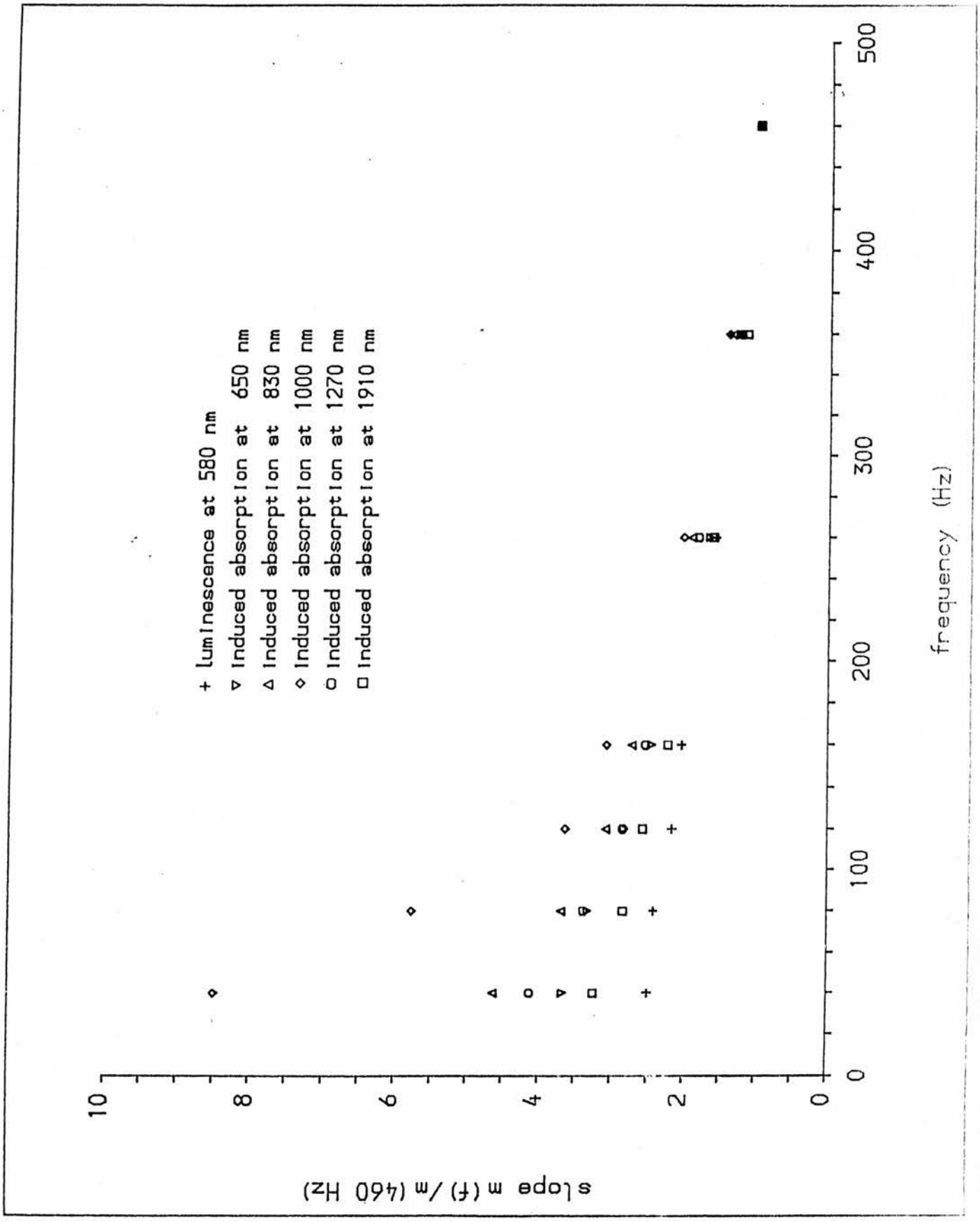

Fig. 5.5.3.9: Ratio of the slopes m at the zero-value at a frequency f and at f = 460 Hz for the induced absorption at 650, 830, 1000, 1270 and 1910 nm and for the luminescence at 580 nm (used disks as in Fig. 5.5.3.8)

photo-ionization would give a quenching of the luminescence.

The experimental layout of the subsequent experiment was the one described in the end of section 4.3: as quenching light source, although not very strong, the probe light source was used. Laser light and quenching light were shone on opposite directions onto the sample. The quenching light passed interference filters (FWH = 10 nm) to allow strong enough light intensities. The luminescence along the cross-section of the two beams was directly recorded by the EMI 9558B pm-tube. A similar interference filter as the other ones with the central transmittance at 580 nm was fixed in front of the pm-tube. The signals of the luminescence reached around 15 V dc. The quenching light was chopped at 80 Hz. A maximum signal was expected to be around a phase of 0° since the light was in phase with the chopper. Nevertheless signals for $\Psi = 90^{\circ}$ were recorded as well.

Surprisingly the ac-signal within the luminescence band that was measured by shutting on and off the laser beam showed a rise of the luminescence in the investigated range of 400 - 500 nm for the quenching light. The normalized signals that were evaluated by considering the dc-signals of the quenching light detected by a thermopile are drawn in Fig. 5.5.4.1. The signals stay nearly constant with wavelength, a slow decline with wavelength is suggested. Coming back to the phase these signals were nearly zero for $\Psi = 90^{\circ}$.

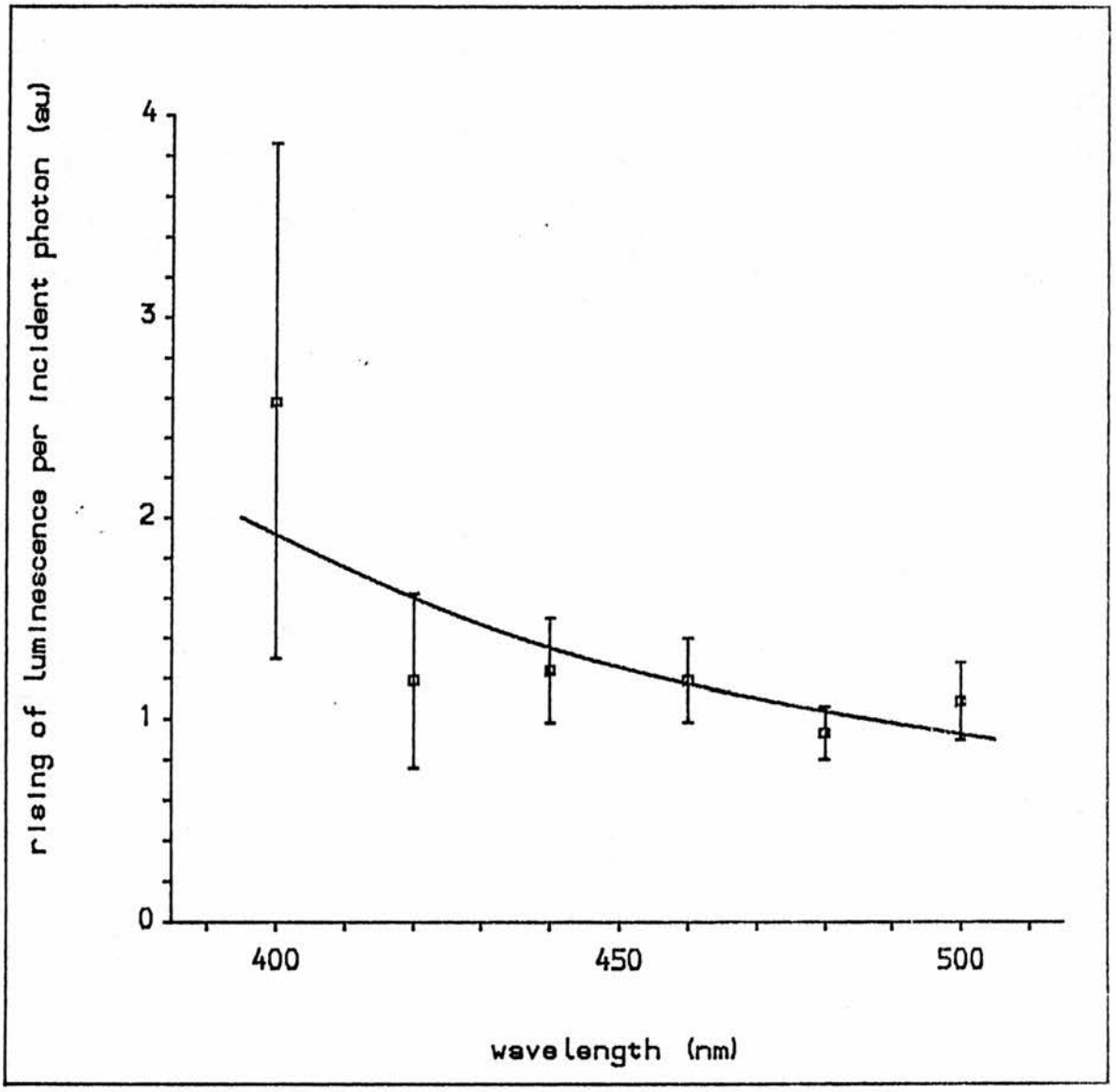

Fig. 5.5.4.1: Rising of the luminescence around 580 nm by light between 400 and 500 nm (chopped at 80 Hz, 2-slot disk) when the constant laser light is shone onto the sample

6 DISCUSSION

6.1 ORDINARY OPTICAL PROPERTIES OF THE SAMPLE

The results of the sections 5.2 and 5.4 are to be discussed in this section. First I turn to the absorption properties of the sample. Referring to Fig. 5.2.2-5 the sample got transparent around 370 nm, four absorption maxima are clearly visible up to ≈ 520 nm, a weak fifth one seems to be near 535 nm and finally the absorption decreases slowly with wavelength up to 2.7 µm. The errors are too large to ascribe any other variations in the curves to real absorption features. These five bands coincide with the usual absorption structures in ZnS:Mn (s. section 3.1). Tab. 6.1.1 shows a comparison to the wavelengths obtained by Kushida et al [2] and Gumlich et al [24].

In [24], Fig. 4, an absorption spectrum for a wurtzite ZnS:Mn crystal (doped with 7.3 at% Mn) is displayed. According to the same article the different crystal structure is of minor importance. Qualitatively that spectrum exhibits a behaviour that is a bit different from Fig. 5.2.2. Very striking is the characteristic that in [24] the sample got very transparent after 550 nm. At 600 nm the absorption was around 7 % for the thickness of the sample having been 1 mm. Assuming this rest absorption was due to ZnS host absorption one gets for a sample being 9 mm thick an absorption of 48 %, whereas

Tab. 6.1.1: Wavelength of the Mn absorption bands in ZnS:Mn (all in nm)

Fig. 5.2.2	Kushida et al [2]	Gumlich et al [24]
390	390	387
428	430	426
467	465	463
497	498	494
533 - 541	535	-

Tab. 6.1.2: Observed absorption in % ($a_\%$) and the calculated absorption coefficient a for the first four absorption bands in Fig. 5.2.2

wavelength [nm]	$a_\%$ [%]	a [mm^{-1}]
390	97	0.23
428	92	0.19
467	92	0.19
497	93	0.20

a value of 78 % has been observed. This could be explained by both scattering by damages within the sample and the employed measuring method having been rather crude. Eg the beam focusing was a bit different between the signals with and without sample since refraction occurred. Thus a bigger absorption was mimicked that continued up to the infrared. The decline in the signals in Fig. 5.2.2-5 could be explained by the decreasing of both the refractive index and of the scattering by the damages.

Coming back to the absorption features the first four absorption maxima in Fig. 5.2.2 yield the absorption coefficients displayed in Tab. 6.1.2. Referring to Fig. 5 in [24] the latter are far too high for a concentration of 0.5 at% Mn. However, it is more likely to ascribe this to scattering and other losses as well than to doubt the concentration value.

It does not surprise that the sample seemed to be black up to near 370 nm. The band gap is around 340 nm, but thermal broadening and a relative large thickness were responsible for this virtual shift of the band gap. There were similar results in [24], Fig. 4, where the sample was just 1 mm thick.

I conclude that the sample used for this thesis showed the typical absorption characteristics of a ZnS:Mn sample and that no additional absorption peaks were observed.

Furthermore the expected orange luminescence near 580 nm was seen in photoluminescence (Fig. 5.4.1). Although the curve in Fig. 5.4.1 is not corrected according to spectral distorting effects (eg pm sensitivity, grating reflectivity), the typical asymmetric shape with a low energy tail in an emission-over-wavelength diagram can be suggested. The orange band is the only band that should be seen at low Mn concentrations (s. chapter 3). Of course, any luminescence at shorter wavelengths than the laser's one could not have been seen. Nevertheless the result gives further evidence that the sample exhibited usual ZnS:Mn properties.

6.2 INDUCED CHANGE IN TRANSMISSION BY ILLUMINATION WITH BULB LIGHT

The long time exposure experiments of section 5.3.2 did not show any effects. Of course, this statement is only valid in respect of the sensitivity of the system. Nevertheless there is one conclusion of importance: there was no significant darkening.

On the other hand the more sensitive short time experiments revealed a very broad band around 575 nm (2.2 eV)(Fig. 5.3.3.2,3). In an absorption against energy diagram it seems to have an asymmetric structure with a high energy tail. The wavelength coincides with the luminescence but the induced band is far broader than it. It is interesting that the effect was a superposition of two opposite effects: the transmittance decreased by blue light illumination and

increased by red light illumination (Fig. 5.3.3.4), both having the same spectral shape (Fig. 5.3.3.5).

Accidentally, Noras [42] had used the same sample as I did. He was looking for induced changes in the transmission by white light illumination, too, but he worked at low temperatures and employed monochromatic light as probe light. He saw a broad induced absorption structure beginning around 3000 cm^{-1} (0.4 eV) and continuing to shorter wavelengths. The effect was one order stronger at 6 K than at 77 K. Unfortunately he seemed to have looked at the induced signal only in the infrared. Kushida et al [2] found in their work that at 4.2 K a broad absorption feature appeared and masked all the Mn correlated induced absorption bands from the visible to the infrared. It had a much longer lifetime than the Mn luminescence.

Noras' further experiments brought an interesting result: the induced absorption was always visible when light with $\lambda = 500$ nm was shone onto the crystal unless red light with 600 nm $< \lambda <$ 700 nm was used for the induced light in between. Then it took blue light again to see the induced absorption under 500 nm illumination. For this blue light he got an excitation spectrum with a threshold near 22000 cm^{-1} (2.7 eV)(Fig. 3 in [42]). He proposed this possible explanation: an optical centre gets ionized by this 22000 cm^{-1} threshold. The electron is recaptured by some kind of metastable state. Any illumination of 500 nm excites this centre and the observed induced absorption are the subsequent transitions from this level to others above. After the 500 nm light is switched off, the centre returns to its ground state. Unfortunately his theory lacks an

explanation why the metastable states were emptied by red light.

Provided that his observations and my results are about the same centres this could mean that I saw the induced transition from the metastable state to the one where he had seen the induced infrared absorption (Fig. 6.2.1, centres B and C). From C the electrons were thermally removed to the conduction band since I worked at room temperature. By the blue light the centres A got ionized and the population in B increased. On the other hand B was emptied by red light as this was of the same energy as the induced transition itself. Since I employed white light as probe light both processes occurred already without the inducing light. The latter just enhanced one or the other effect. However, this does not explain why Noras' effect vanished after having used 600 nm < < 700 nm illumination. Unfortunately Noras gave no information about any variation of the effects relative to a spectral change of the 500 nm and red light illumination.

It is still possible that other processes, more or less similar, have occurred and that Noras' results concerned another centre. If one took the model by Dieleman et al [43] as explained in section 3.3 (s. also Fig. 3.3.2), one would have a very large energy E_{id} or E_{ia}, respectively. The induced absorption is then either the transition E_{id} or E_{ia}. The pumping would work via E_a, E_d or even E_o by the blue light.

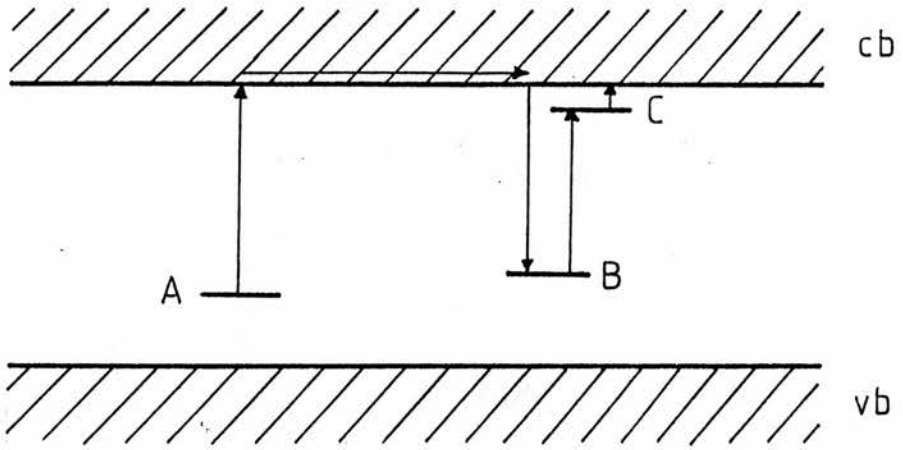

Fig. 6.2.1: Model for observed induced absorption: center A is ionized by blue light, electron is trapped by B, which gives the induced transition to C, then the electron is thermally removed to the conduction band

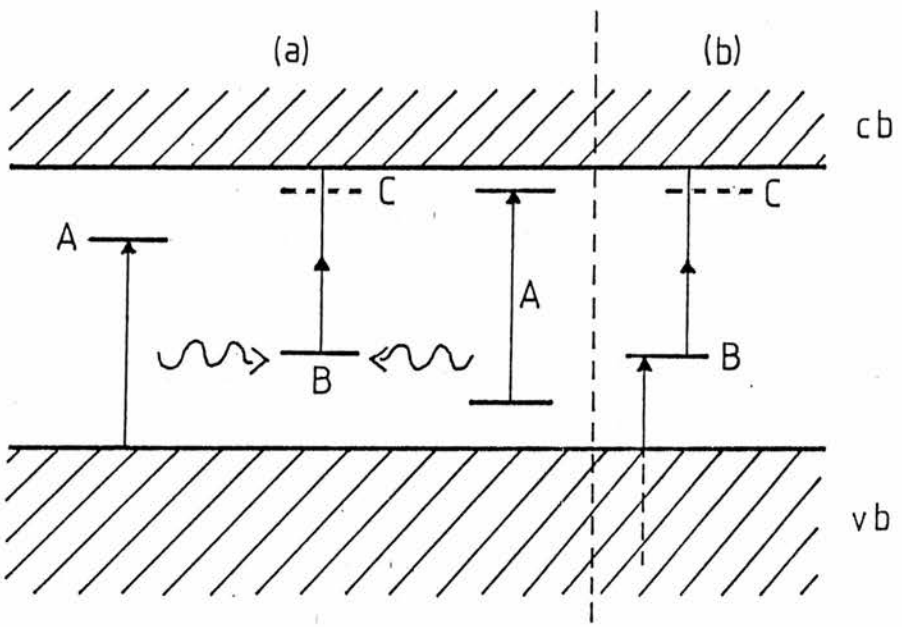

Fig. 6.2.2: Other models for the induced absorption:
(a) center A is exicted either by an electronic transition from the valence band or by an internal transition, then energy transfer occurs to center B which gives the induced transition directly to the conduction band or via center C
(b) center B is excited directly from the valence band, especially from the deeper parts, then like in (a)

Other possibilities are shown in Fig. 6.2.2: centres B get populated either via centres A by energy transfer (a) or directly from the valence band (b). The induced absorption is the transition to the conduction band or to another centre C close to it, from where the electron is moved thermally to the conduction band. For (b) this would mean that the transition from the valence band to B is too improbable at low energies compared to the transitions departing from B. For higher energies, however, it dominates.

For all this one has to bear in mind that the inducing light was not normalized. However, one tendency can be established: the pumping process was far more efficient than the other one since within the white light the red fraction dominated over the blue one, but the effect showed still the induced absorption.

One characteristic has not been considered yet: the time dependency of the effect seemed to have been the same for all illumination types. A stable signal was fast achieved when the light was shone onto the sample. However, when it was shut off a relaxation of the order of half a minute was recorded. This could mean that the B centres are easily saturated by the blue light and emptied by the red light. When only the probe light is switched on neither saturation nor total emptying takes place. A balance has to be achieved which takes time. There could be differences for blue and red light but since the signals were very noisy and sometimes even unstable (s. section 5.2) this was not recognized. If the red light fully empties and the blue light fully fills B the adjusting of a

balance has to be expected for white light illumination. This was not seen either. Maybe it was still a result of the large light intensities (compared to the probe light).

Yet nothing was said about the actual nature of the participating centres. It is unclear whether they are really physically different or part of a sort of complex. Maybe some of the levels are even from the same centre. Era et al [46] found broad luminescence bands in ZnS phosphors due to acceptor-donor transitions. Although none of their investigated dopings had the appropriate spectral shape, that work showed that transitions between centres near to the conduction and valence bands can cause very broad optical bands. Recently Matsuura et al [47] suggested that F^+ centres in ZnS cause a broad absorption band near 2.3 eV. The centres were introduced by neutron and electron irradiation and by heat treatments in Zn vapor or liquid. Then the centres got thermally annealed. Since EPR signals due to F^+ centres and the 2.3 eV band behaved the same way the authors derived the above conclusion. Furthermore they found that the signal was enhanced by 355 nm but quenched by 430 nm light. As this is quite different from the behaviour found in my experiments this type of centre can be ruled out.

Could it be possible that the Mn centres are involved in the process? The observed induced transition is certainly not an internal Mn transition. It is far too broad, and the estimated concentration of excited Mn atoms was around 10^{10}-10^{11} mm^{-3}. However, a possible pumping via the Mn cannot be excluded that easily. The wavelength of the induced band coincides with the wavelength of the luminescence.

Subsequently a resonant energy transfer from the excited Mn centres could happen and thus explain the results of Rigby [36].

Summarized this section yields the following conclusions: although models for the observed structure are suggested the problem is far from a detailed solution. Further experiments are necessary. More detailed excitation spectra and samples with other dopings as well as temperature dependent experiments could give more clues. On the other hand the observed effect can be very important for the proceeding laser experiments which are the main subject of this thesis.

6.3 INDUCED CHANGE IN TRANSMISSION BY ILLUMINATION WITH LASER LIGHT

6.3.1 INTRODUCTION

A lot of features were detected in the experiments of section 5.5. The threshold structure around 400 nm and the bands at 650, 830, 1270 and 1910 nm shared the same dependence on frequency. This indicates that the mechanisms that were responsible for these structures had the same origin. Therefore, these features are discussed in section 6.3.2 which is called 'Mn correlated features'. The reason for this specification will be given in that section. The remaining structures, the band at 1000 nm and the apparent rise of the

luminescence are dealt with in section 6.3.3.

6.3.2 Mn CORRELATED FEATURES

The emphasis for the laser experiments was to see whether there are any induced transitions from the $^4T_1(G)$ state of the Mn centres to higher electronic levels. Hitherto it was essential to achieve a sufficient concentration of excited Mn atoms. To estimate the latter, formula (6.3.2.1) was derived from the conditions of static equilibrium by cw laser illumination:

$$N^* = \tau (1-r)\, I\, a(\lambda_1)\, e^{-a(\lambda_1)\, x}\,, \quad (6.3.2.1)$$

where N^* : density of excited states

τ : lifetime of the excited state

r : reflectivity of the sample

I : incoming photon flux

$a(\lambda_1)$: absorption coefficient of the sample at the laser wavelength (it is assumed that all transitions under this absorption contribute to the excited state)

x : depth where N^* shall be calculated for .

(6.3.2.1) is only valid when there are no saturation problems, but here the pumping was far from saturation. With τ = 1.6 ms [37] (including energy transfer), r = 0.17 (n = 2.41, s. Fig. 4.2.3), $I = P/(h\nu A)$ with $P \approx 1$ W, λ = 514.5 nm and $A = (4\ \text{mm})^2\pi$,

$a(\lambda_1) = 0.19\ mm^{-1}$ (derived from Fig. 2 in [24] and calculated for 0.5 at% Mn) and $x \approx 2$ mm, and considering the density N of Mn centres in ZnS for a doping of 0.5 at% Mn one finally has for the fraction of excited Mn atoms:

$$N^*/N \approx 7 \cdot 10^{-5} .$$

Surprisingly this is of the same order as the one Kushida et al [2] estimated for their experiments though they had employed a maximal laser intensity of 45 Wcm^{-2} (compared to 2 Wcm^{-2} for these experiments). Anyway, this fraction is not very large. However, as the expected transitions are thought to be spin allowed transitions to higher quartet states (the transitions to the doublet states should be too weak to be recognizable among the induced bands), unlike the usual transitions from the $^6A_1(S)$ ground state, the transition probability is expected to be far higher than for the ordinary transitions. Therefore, it is reasonable to look for any induced Mn bands (although ac pumping was used and the actual concentration was, therefore, a bit lower).

Furthermore the question arises whether luminescence and induced absorption should be in phase. Already Kushida et al [2] observed a delay for the 650 nm band that decreased with Mn concentration. Their samples had been doped with 1, 2 and 4 at% Mn. They attributed the effect to the circumstances that with higher Mn concentration Mn pairs got important. Their conclusion was that for high enough concentrations only pairs contributed to both luminescence and absorption whereas at smaller concentrations the single Mn centres got

more influence. As singles behave different in luminescence but not necessarily in induced absorption this can cause the delay.

It is actually possible to discuss this delay in more detail, especially for more dilute samples when energy transfer via the Mn centres can be neglected. For a sample with 0.5 at% Mn this is fairly fulfilled [37]. According to Behringer [34] (s. also Fig. 3.2.1) 3 % of the Mn centres are associated in pairs at this concentration (higher associates are negligible). Pairs are known to have a quite shorter lifetime. In [18] one finds:

singles: τ_s = 1.8 ms, pairs: τ_p = 0.15 ms (in [18]: 0.1-0.2 ms).

Since the induced transitions are no longer spin forbidden it is quite reasonable to assume nearly equal transition probabilities for both singles and pairs (this nomenclature shall be used for single Mn centres and Mn centres associated in pairs). Thus one always had a superposition for the luminescence and induced absorption that was of different character and resulted in a phase shift. It is possible to estimate the phase shift if one assumes a square wave signal for the excitation with a period long enough. Fig. 6.3.2.1 shows this kind of signal together with an exponential decaying luminescence. To put it exactly the next period would have a slightly varied shape for the luminescence since the starting conditions were different then. After some cycles the luminescence would gain stability. However, if the period is long enough one can approximate the final luminescence by the curve displayed in Fig. 6.3.2.1.

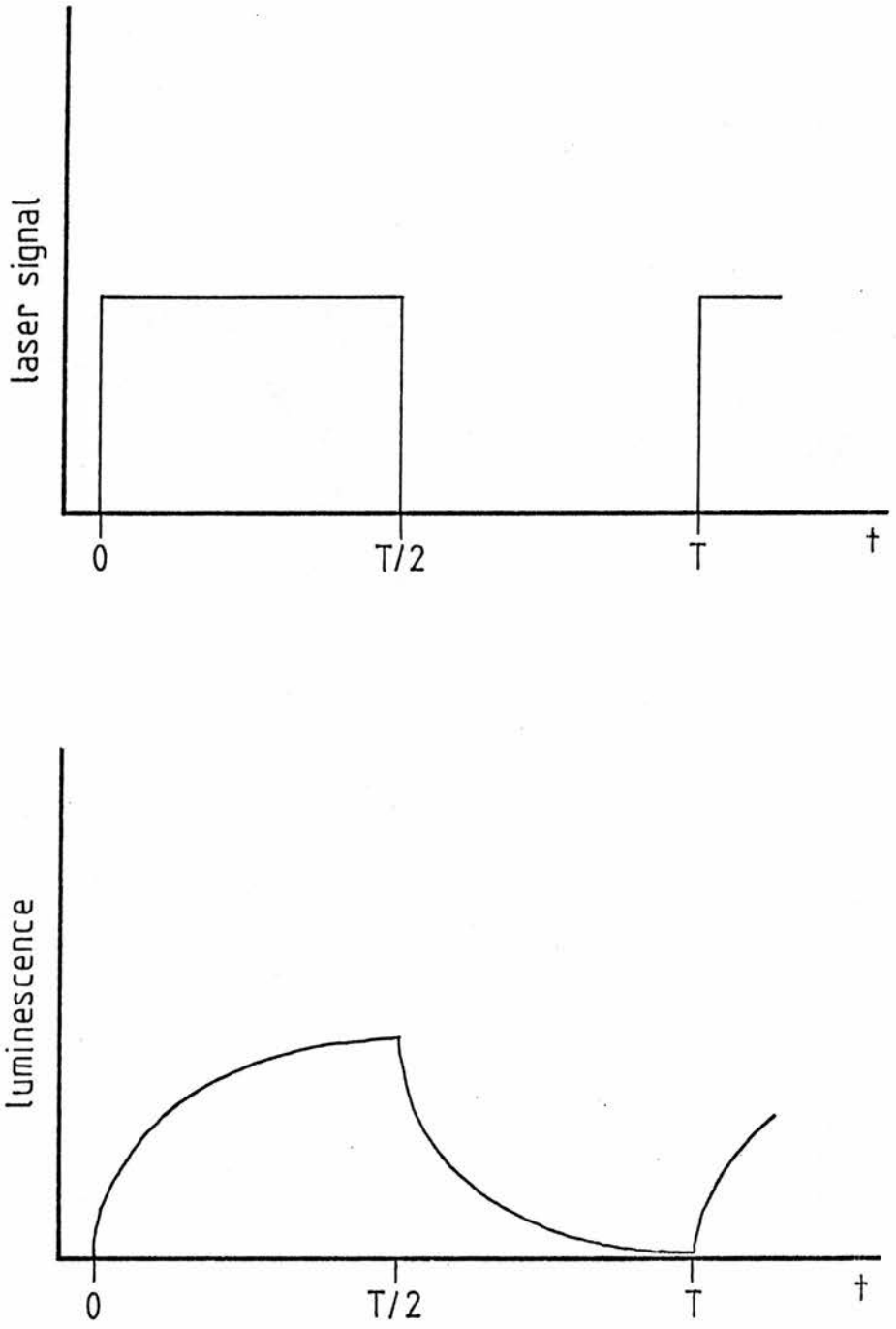

Fig. 6.3.2.1: Square wave exciting laser signal and the exponential response of luminescence (that is proportional to the density of excited centres); strictly the graph is only valid for the first period, for long enough periods the shown shape is a good approximation for the stationary case

The actual luminescence is a superposition of two such curves. Its shape is obtained by solving first order differential equations for $N_s^*(t)$ and $N_p^*(t)$ (concentrations of excited singles/pairs) and writing out equation (6.3.2.2):

$$f_l(t) = N_s^*(t)/\tau_s + N_p^*/\tau_p \ . \quad (6.3.2.2)$$

The detailed form of $f_l(t)$ is given in (6.3.2.3) on the next page. Similar one has to proceed for the induced absorption. A function $f_a(t)$ that gives the shape of the induced absorption is given by (6.3.2.4):

$$f_a(t) = \alpha_{es} N_s^*(t) + \alpha_{ep} N_p^*(t) \ . \quad (6.3.2.4)$$

where α_{es} and α_{ep} are standing for the transition probabilities to higher states. The final expression is given in (6.3.2.5) on the separate page as well. The signal that is detected by the lock-in amplifier is to a first order the Fourier transform of the sin(x) component. Depending on a phase shift Ψ one has for a term $I_{l,a}$ that is proportional to this Fourier component of $f_{l,a}(t)$:

$$I_{l,a}(\Psi) = \int_o^T \omega f_{l,a}(t) \sin(\omega t+\Psi) \, dt \ , \quad (6.3.2.6)$$

where $\omega = 2\pi/T$. After having inserted the results of (6.3.2.3) and (6.3.2.5), respectively, and solved the integrals one gets $I_{l,a}(\Psi)$ explicitly. The phase shift $\Delta\Psi$ between luminescence and induced absorption is obtained by finding the Ψ_o values where

$$f_l(t) = \begin{cases} \phi \alpha_{gs} N_s \left(1 - e^{-\frac{t}{\tau_{gs}}}\right) + \phi \alpha_{gp} N_p \left(1 - e^{-\frac{t}{\tau_{gp}}}\right), & 0 \le t \le \frac{T}{2} \\ \phi \alpha_{gs} N_s \left(e^{\frac{T}{2\tau_{gs}}} - 1\right) e^{-\frac{t}{\tau_{gs}}} + \phi \alpha_{gp} N_p \left(e^{\frac{T}{2\tau_{gp}}} - 1\right) e^{-\frac{t}{\tau_{gp}}}, & \frac{T}{2} < t < T \end{cases} \qquad (6.3.2.3)$$

$$f_a(t) = \begin{cases} \phi \alpha_{gs} \alpha_{es} N_s \tau_{gs} \left(1 - e^{-\frac{t}{\tau_{gs}}}\right) + \phi \alpha_{gp} \alpha_{ep} N_p \tau_{gp} \left(1 - e^{-\frac{t}{\tau_{gp}}}\right), & 0 \le t \le \frac{T}{2} \\ \phi \alpha_{gs} \alpha_{es} N_s \tau_{gs} \left(e^{\frac{T}{2\tau_{gs}}} - 1\right) e^{-\frac{t}{\tau_{gs}}} + \phi \alpha_{gp} \alpha_{ep} N_p \tau_{gp} \left(e^{\frac{T}{2\tau_{gp}}} - 1\right) e^{-\frac{t}{\tau_{gp}}}, & \frac{T}{2} < t < T \end{cases} \qquad (6.3.2.5)$$

$$\tan \psi_{ol} = \frac{2\alpha_{gs} N_s + 2\alpha_{gp} N_p - \left(2 + e^{-\frac{T}{2\tau_{gs}}} - e^{-\frac{T}{\tau_{gs}}}\right) \frac{\alpha_{gs} N_s \omega^2 \tau_{gs}^2}{1 + \omega^2 \tau_{gs}^2} - \left(2 + e^{-\frac{T}{2\tau_{gp}}} - e^{-\frac{T}{\tau_{gp}}}\right) \frac{\alpha_{gp} N_p \omega^2 \tau_{gp}^2}{1 + \omega^2 \tau_{gp}^2}}{\left(2 + e^{-\frac{T}{2\tau_{gs}}} - e^{-\frac{T}{\tau_{gs}}}\right) \frac{\alpha_{gs} N_s \omega \tau_{gs}}{1 + \omega^2 \tau_{gs}^2} + \left(2 + e^{-\frac{T}{2\tau_{gp}}} - e^{-\frac{T}{\tau_{gp}}}\right) \frac{\alpha_{gp} N_p \omega \tau_{gp}}{1 + \omega^2 \tau_{gp}^2}} \qquad (6.3.2.8)$$

$$\tan \psi_{oa} = \frac{2\alpha_{gs} \alpha_{es} N_s \tau_{gs} + 2\alpha_{gp} \alpha_{ep} N_p \tau_{gp} - \left(2 + e^{-\frac{T}{2\tau_{gs}}} - e^{-\frac{T}{\tau_{gs}}}\right) \frac{\alpha_{gs} \alpha_{es} N_s \tau_{gs}^3 \omega^2}{1 + \omega^2 \tau_{gs}^2} - \left(2 + e^{-\frac{T}{2\tau_{gp}}} - e^{-\frac{T}{\tau_{gp}}}\right) \frac{\alpha_{gp} \alpha_{ep} N_p \tau_{gp}^3 \omega^2}{1 + \omega^2 \tau_{gp}^2}}{\left(2 + e^{-\frac{T}{2\tau_{gs}}} - e^{-\frac{T}{\tau_{gs}}}\right) \frac{\alpha_{gs} \alpha_{es} N_s \omega \tau_{gs}^2}{1 + \omega^2 \tau_{gs}^2} + \left(2 + e^{-\frac{T}{2\tau_{gp}}} - e^{-\frac{T}{\tau_{gp}}}\right) \frac{\alpha_{gp} \alpha_{ep} N_p \omega \tau_{gp}^2}{1 + \omega^2 \tau_{gp}^2}} \qquad (6.3.2.9)$$

$f_l(t)$: shape of resulting luminescence
$f_a(t)$: shape of resulting induced absorption
ψ_{ol} : zero-value of phase for the luminescence
ψ_{oa} : zero-value of phase for the induced absorption
τ_{gs} : decay time of luminescence in singles
τ_{gp} : decay time of luminescence in pairs
ϕ : pumping photon flux
T : period of pumping cycle
N_s : density of single Mn centres
N_p : density of Mn centres associated in pairs
α_{gs} : transition propability for the pumping in singles
α_{gp} : transition probability for the pumping in pairs
α_{es} : transition probability for the induced transition in singles
α_{ep} : transition probability for the induced transition in pairs
ω : $2\pi/T$

$$I_{1,a}(\Psi_o) = 0 \; . \qquad (6.3.2.7)$$

In solving (6.3.2.7) one finally has the very obscure formula (6.3.2.8) and (6.3.2.9), displayed again on the separate page. The lifetimes are known, same are the concentrations $N_{s,p}$ (just the ratio is of importance). For the absorption probabilities $\alpha_{gs,gp}$ one can assume (6.3.2.10):

$$\tau_{gs}/\tau_{gp} = \alpha_{gp}/\alpha_{gs} \approx 12 \; . \quad (6.3.2.10)$$

Finally one assumes (explanation s. above)

$$\alpha_{es} = \alpha_{ep} \; . \qquad (6.3.2.11)$$

Now it is possible to calculate the phase shift $\Delta\Psi$ for different frequencies. To assure the approximation of Fig. 6.3.2.1 the frequency should not be higher than 100 Hz. In Tab. 6.3.2.1 the theoretical values a compared with the experimental ones that have been taken from section 5.5.3 (Fig. 5.5.3.7,8). The data of the induced band at 650 nm were chosen from Fig. 5.5.3.8 because they were thought to have not been influenced by other bands. Whereas the results for the 650 nm band give a good agreement the ones for the 450 nm signal seem to be shifted somehow. It has to be reminded that the results of Fig. 5.5.3.7 could have been influenced by perturbing vibrations (s. section 5.5.3). It could also be possible that the difference was caused by slightly different illumination conditions. Still, the error bars of the experimental results are overlapping and,

Tab. 6.3.2.1: Calculated and observed phase shift $\Delta\Psi$ between luminescence and induced absorption

frequency [Hz]	calculated $\Delta\Psi$ [°]	observed $\Delta\Psi$ [°]	
		*	**
20	2.9	-2.1±1.7	-
40	5.6	3.1±1.6	6.0±3.1
60	8.4	4.9±1.9	-
80	11.2	7.2±1.9	9.2±1.7

* : from Fig. 5.5.3.7 for the induced absorption at 450 nm
**: from Fig. 5.5.3.8 for the induced absorption at 650 nm

therefore, consistent. Both signals should behave the same way as Fig. 5.5.3.4 showed plainly. One has to recall all the approximations that have been made for the calculations, eg the signal shape was approximated, energy transfer has been neglected, only the first of the odd harmonics for the Fourier analyse was taken into account and finally equation (6.3.2.11) was assumed. Therefore, I think I can justify the final conclusion that the features I talk about in this section are due to processes involving the $^4T_1(G)$ state of the Mn centres.

The fact that all signals including the luminescence declined with frequency does not surprise as with a higher frequency the maximal population of the excited state decreases. It was that reason why 80 Hz was chosen to be a good frequency for the spectral search of the features. The nearly stable phase shift for higher frequencies than 100 Hz could mean that by approaching $2\tau_s$ in T the different characteristics of pairs and singles do not change significantly. Still, the peak in Fig. 5.5.3.7 remains a problem though it could indicate just this threshold.

According to (6.3.2.3) and (6.3.2.5) the shapes of the luminescence and induced absorption signals are different. Hence the Fourier analysis by the lock-in amplifier will be different. This explains the results of Fig. 5.5.3.9 where the luminescence did not behave like the induced absorption structures.

I now come to the discussion of the induced features themselves. The three bands Kushida et al [2] had seen appeared again. Thus I can confirm these bands. I also obtained their result that the 830 nm and 1270 nm bands were approximately equal in intensity whereas the 650 nm band was three times as intense as those two. Additionally I got a band around 1910 nm that, surprisingly, was not detected by the former Japanese work. The threshold in the shorter wavelength region was not reported either. Since the phase behaviour of those two structures clearly indicates a Mn participation their new discovery is even more amazing.

First I want to deal with the bands only. To allow a possible assignment for these bands Tanabe-Sugano diagrams [7,8,10] (s. also section 2.1.3) have been calculated for different sets of Racah parameters B and C. For reasons explained above doublet states were not of concern. The following three diagrams were evaluated with B and C values that were chosen from various authors:

Fig. 6.3.2.2: B and C were taken from Kushida et al [1,2] who tried to fit the first three ordinary bands and to maintain thereby the ratio C/B of the free ion;

Fig. 6.3.2.3: B and C were taken from O'Neill [48] according to a best fit to the five ordinary bands;

Fig. 6.3.2.4: B and C were taken from Pohl et al [22] to fit the zpl's of the first four ordinary absorption bands.

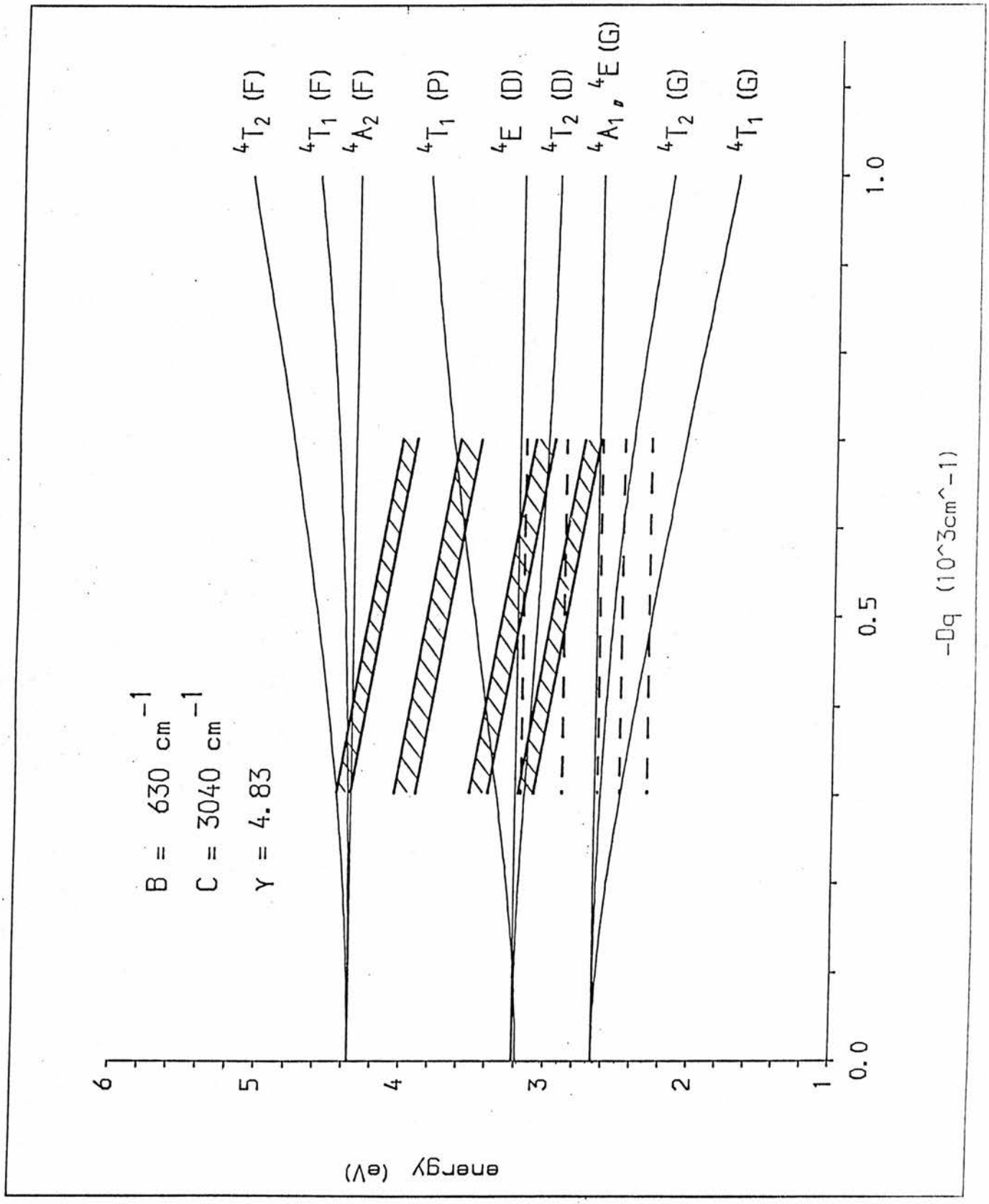

Fig. 6.3.2.2: Tanabe-Sugano diagram of Mn in ZnS with data from [1], induced bands indicated by shaded area, ordinary bands by dashed line

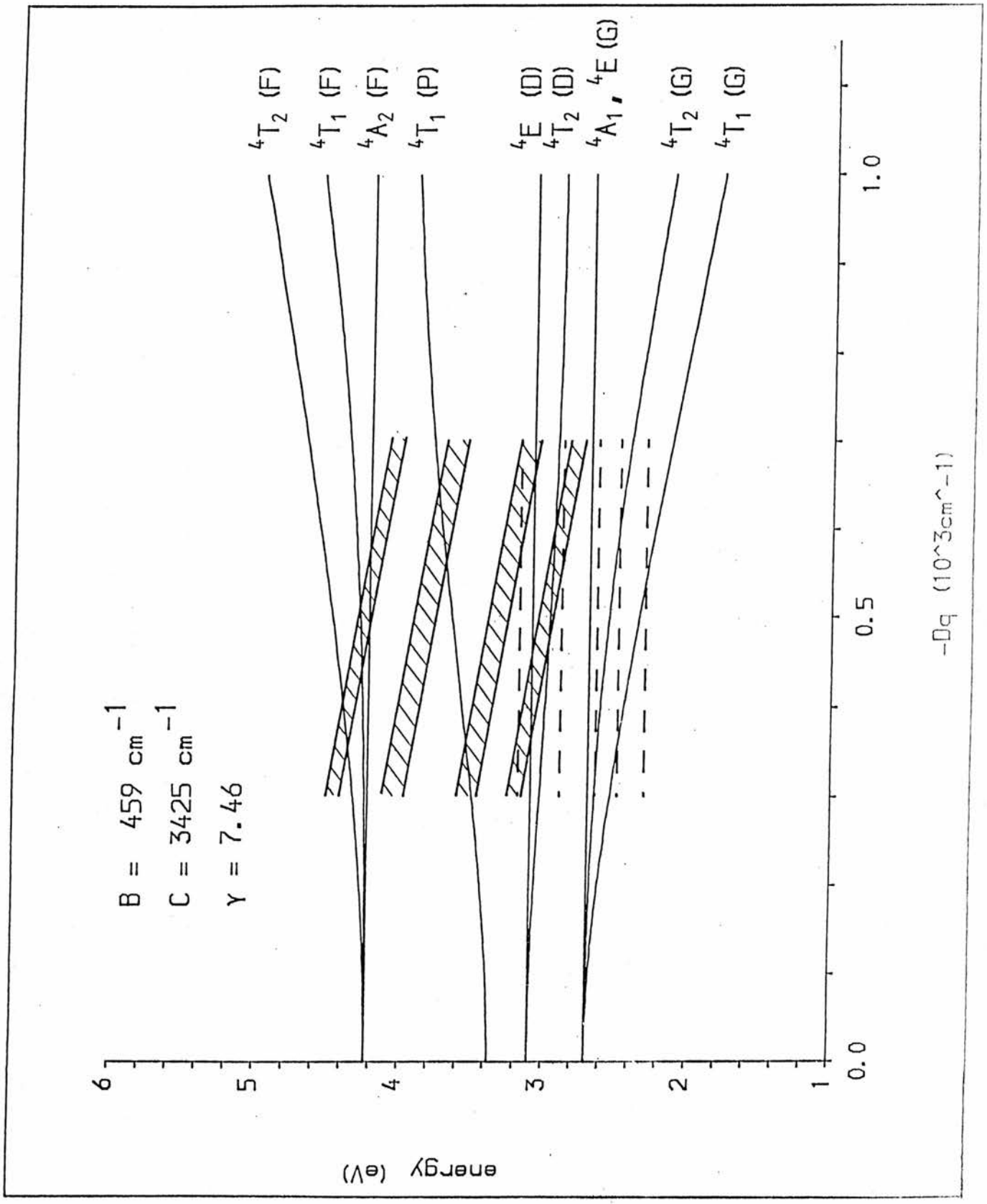

Fig. 6.3.2.3: Tanabe-Sugano diagram of Mn in ZnS with data from [48], induced bands indicated by shaded area, ordinary bands by dashed line

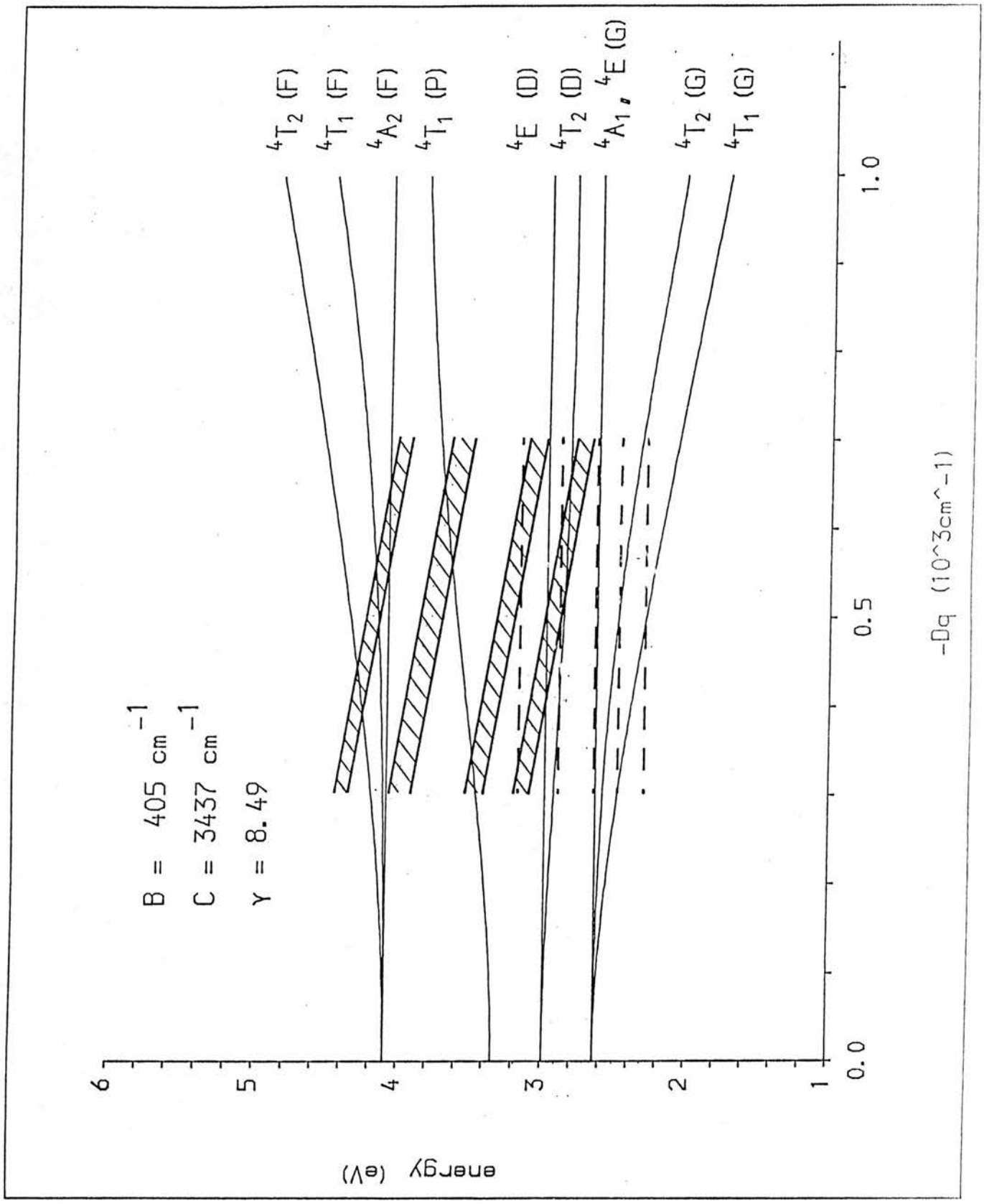

Fig. 6.3.2.4: Tanabe-Sugano diagram of Mn in ZnS with data from [22], induced bands indicated by shaded area, ordinary bands by dashed line

In each diagram the position of the induced bands relative to the $^4T_1(G)$ state is represented by the shaded area, the position of the ordinary absorption bands as obtained by Fig. 5.2.2 by the dashed lines. The last two figures give very unusual C/B ratios. The method used by Pohl et al [22] astonishes a bit since the actual transitions that shall be described by crystal field theory are the ones that terminate directly above the minimum of the ground state in a configuration coordinate diagram, and which are represented by the maximum of the temperature broadened bands (s. section 2.3) and not by the zpl's. This explains the bad agreement to the dashed lines in this diagram.

For the discussion of the induced bands the use of these diagrams is controversial. It is not only Dq but B and C that can be changed. Since already for the usual absorption one gets very unusual B and C values it is obvious that within the crystal the conditions can be quite different from the free ion case. Provided that crystal field theory is still applicable, it could be that B and C are different for the excited state as any shielding effects could have changed. On the other hand one has to get first clues about the nature of the induced processes, and since the theory even seems to be too simple to describe all bands of the ordinary absorption as it neglects covalency any evaluation of other fitting does not look very reasonable.

It has to be pointed out that there are no symmetry forbidden transitions from the $^4T_1(G)$ state to the states above (except to the $^4A_1(G)$ state, but this is degenerate with the $^4E(G)$ state). For electric dipole transitions one has for the direct product of the symmetry of the dipole operator (T_2) and the symmetry of the initial state (T_1):

$$T_2 \otimes T_1 = A_2 + E + T_1 + T_2 \ .$$

Kushida et al [2] assigned the 650 nm band to the $^4A_2(F)$, the 830 nm band to the $^4T_1(P)$ and the 1270 nm band to the $^4E(G)$ state. Referring to Fig. 6.3.2.2 those assignments are not very self-evident. Considering all three diagrams one has one obvious problem: neither all ordinary bands are fitted exactly nor is that the case for the induced bands. The situation is worse in Fig. 6.3.2.2 than in the other two diagrams. However, if one uses the observed energy values for the fourth and fifth ordinary band instead of the calculated ones for the $^4E(D)$ and $^4T_2(D)$ states the agreement between the four observed lines and those two bands together with the calculated ones for the $^4T_1(P)$ and $^4A_2(F)$ states is fairly good around Dq = -600 cm^{-1} in Fig. 6.3.2.3 and especially in Fig. 6.3.2.4. Although any assignments to actual states are far from certainty I share Kushida et al's opinion that the 1270 nm band represents the transition between the two outermost ordinary absorption bands. Furthermore the band around 1910 nm should be the transition to the next of the ordinary absorption bands. If one takes the energy difference of the ordinary bands and the energy of the appropriate induced band one gets:

energy difference 390 nm band - 537 nm band : 0.87 eV
energy of induced absorption band at 1270 nm: 0.98 eV

energy difference 428 nm band - 537 nm band : 0.59 eV
energy of induced absorption band at 1910 nm: 0.65 eV

As already suggested in the Japanese paper (for their single band) the possible shift could be explained by a configuration coordinate scheme (Fig. 6.3.2.5). If one assumes the same parabolic shape for the ground and the excited states and the minimum for the two upper curves to be at the middle of the two others, it yields a much better agreement. Now one has to subtract the energy of the zpl of the first state from the band energies, which is 2.22 eV [25]:

energy difference 390 nm band - 2.22 eV : 0.96 eV
energy of induced absorption band at 1270 nm: 0.98 eV

energy difference 428 nm band - 2.22 eV : 0.68 eV
energy of induced absorption band at 1910 nm: 0.65 eV

A shift in a configuration coordinate diagram can be motivated as well from the circumstances that the width of the induced bands is comparable to those of the ordinary bands. There, however, the shift can be explained as the radial parts of the wavefunctions change after a transition from a sextet to a quartet. For the induced absorption such a displacement must have another explanation. The reason could be that the influence of covalency is different for the two states,

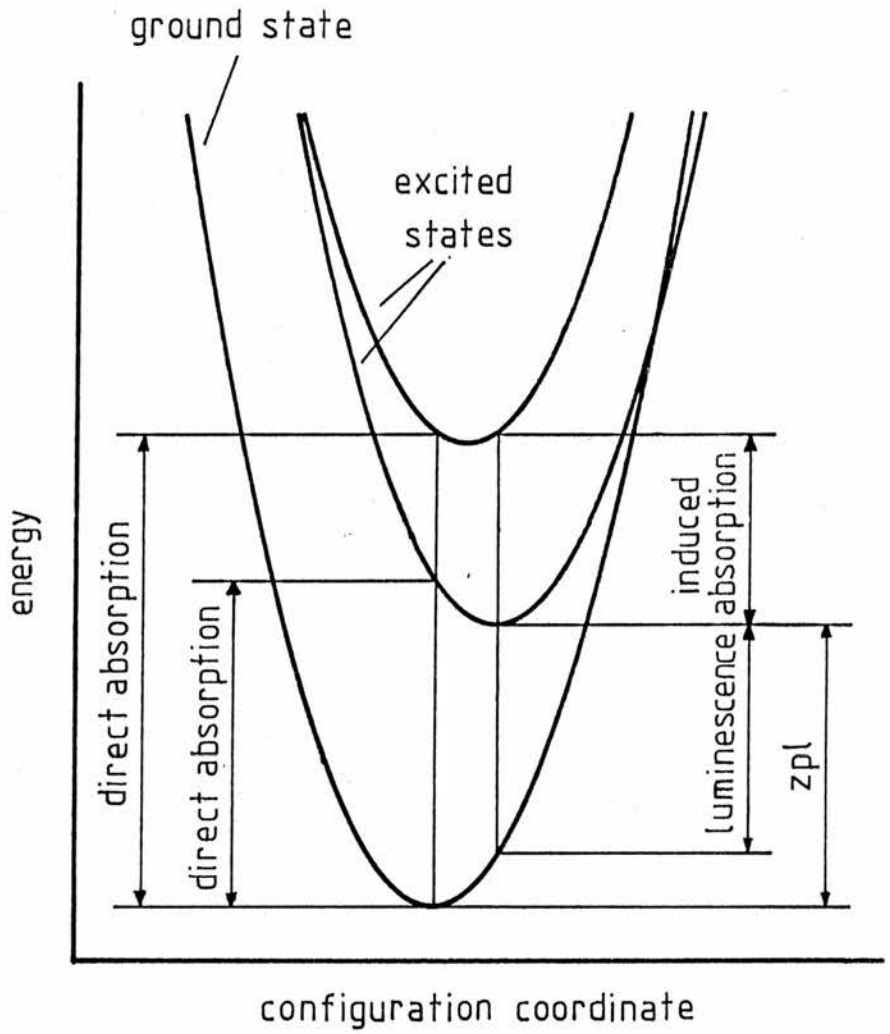

Fig. 6.3.2.5: Configuration coordinate diagram to explain the shift from the energy of the induced absorption band to the energy difference of the ordinary absorption bands

giving different radial parts of the wavefunctions.

The interpretation of the other two bands is much more difficult. The assignment of the 830 nm band to the $^4T_1(P)$ state is less controversial than one for the 650 nm band as the graph for the $^4T_1(P)$ state is quite isolated. According to the diagrams the slopes between the $^4T_1(G)$ and $^4T_1(P)$ states are less parallel to each other than for any other possible state nearby. This would be consistent with the fact that the 830 nm band was the broadest of the four bands. Furthermore the $^4T_1(P)$ state would lie close to the bandgap (3.7 eV) where already Gumlich et al [24] suggested it to be. Eventually Theis [49] saw anomalies in the reflectivity of ZnS heavily doped with Mn around 3.6 eV. The effect was stronger the deeper the temperature was. Since he was using the sensitive technique of wavelength modulated reflectivity it could have been that in the heavy doped samples and at very low temperatures it was possible to detect this state among the strong intrinsic signals. Unfortunately he never considered this possibility in his paper.

The situation is different for the 650 nm band. The $^4A_2(F)$ and the $^4T_1(F)$ states are not very well separated. Considering the 650 nm band to be the $^4A_2(F)$ state the question arises: where should have been the other bands? With the parameters of Fig. 6.3.2.3 and Fig. 6.3.2.4 one gets for Dq = -600 cm^{-1} that the difference of the $^4A_2(F)$ to the $^4T_1(F)$ state is 0.10 eV, the difference of the $^4A_2(F)$ to the $^4T_2(F)$ state 0.25 eV. By adding these energies to 1.91 eV, the observed energy of the induced band one gets a rough estimate of the spectral position of the other induced bands:

$$^4T_1(F): \ 620 \text{ nm}, \qquad ^4T_2(F): \ 550 \text{ nm}.$$

Hence both of them should be visible provided the transition probabilities are not too weak. From Fig. 5.5.2.1 it is clearly seen that at these positions no striking features can be recognized. Just around 540 nm there is a glimpse of a structure as there seems to be a dip in the increased transmission region. Still, it would be quite weak. The Japanese work [2] explained the absence of these bands by vanishing transition matrix elements in the strong field limit. The latter, however, is not a very good approximation. Hence their statement is rather doubtful. On the other hand symmetry selection rules do not forbid one of these transitions. Yet their application is at issue since they do not hold for the transitions from the ground state: the direct product of A_1 and T_2 (dipole approximation) representations gives:

$$A_1 \otimes T_2 = T_2 \ .$$

Nevertheless other transitions are as strong as eg the $^6A_1(S) \rightarrow {}^4T_2(G)$ transition. One can say that in the latter case the transitions are already spin-forbidden which complicates the interpretation. But it could be as simple as that: the applied theory is too basic for the ZnS:Mn system. A strong argument is that it does not include covalency more specificly eg it does not distinguish between e and t_2 orbitals concerning the radial parts of their wavefunctions (s. section 2.2.1). As ZnS is not purely ionic the implications are obvious. Especially for very high energy levels the

deviations form the ordinary crystal field theory should be considerable. There have been several attempts to describe the Mn absorption in ZnS with theories that were involving covalency somehow (eg [13,14]). Here I tried to apply O'Neill's theory [13] who had had the following idea: by defining parameters ε and τ to reduce the radial parts of the electron-electron interaction integrals among either e-orbitals or t_2-orbitals one can 'simulate' covalency. Then it is possible to derive expressions for the mixed integrals as well. The more and were less than unity the less localised the impurity orbits would be.

For two sets of ε and τ energy level diagrams have been calculated according to the perturbation matrices by O'Neill [13]. B and C were chosen to the free ion case. For Fig. 6.3.2.6 ε and τ were calculated for a best fit for the ordinary absorption bands [13,48]. In Fig. 6.3.2.7 ε was defined to unity whereas the fit was done for τ [48]. The latter had been performed as the first value of ε had been somehow strange. In both diagrams it is not possible to fit the four induced bands when the two low energy bands are thought to be transitions to the fourth and fifth band of the ordinary absorption, neither when the calculated values are taken nor the experimental ones. As far as other fittings are concerned there is just one in Fig. 6.3.2.6 near Dq = -650 cm^{-1}, but it is not very plausible. Additionally it turned out that there must have been a slight mistake in the calculations of [13,48] as I got a different value for the $^4T_1(G)$ state for each evaluation (even for Fig. 6.3.2.2). Still, this should not alter the basic problems about the actual assignments.

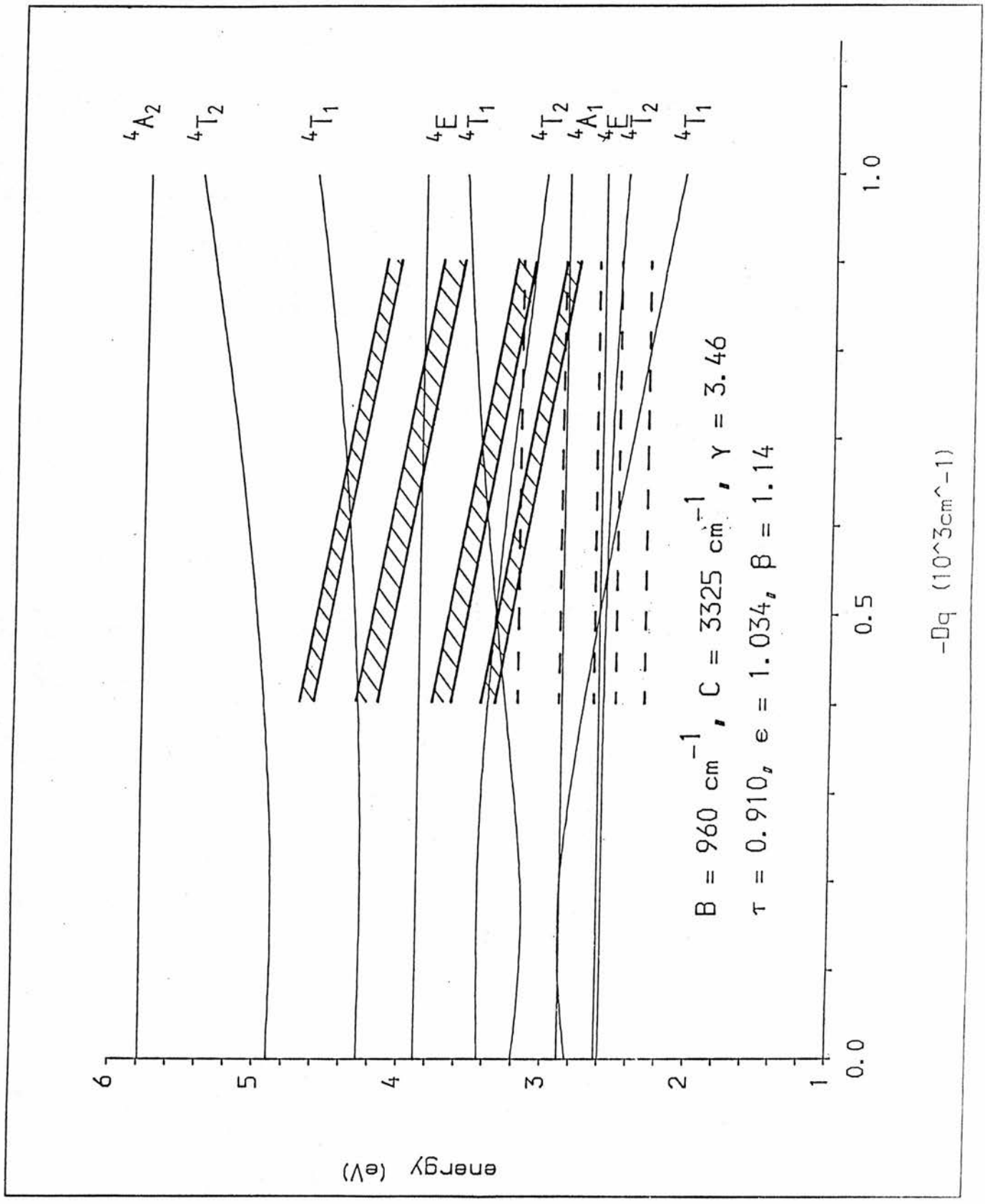

Fig. 6.3.2.6: O'Neill diagram of Mn in ZnS with data from [13,48] induced bands indicated by shaded area, ordinary bands by dashed line

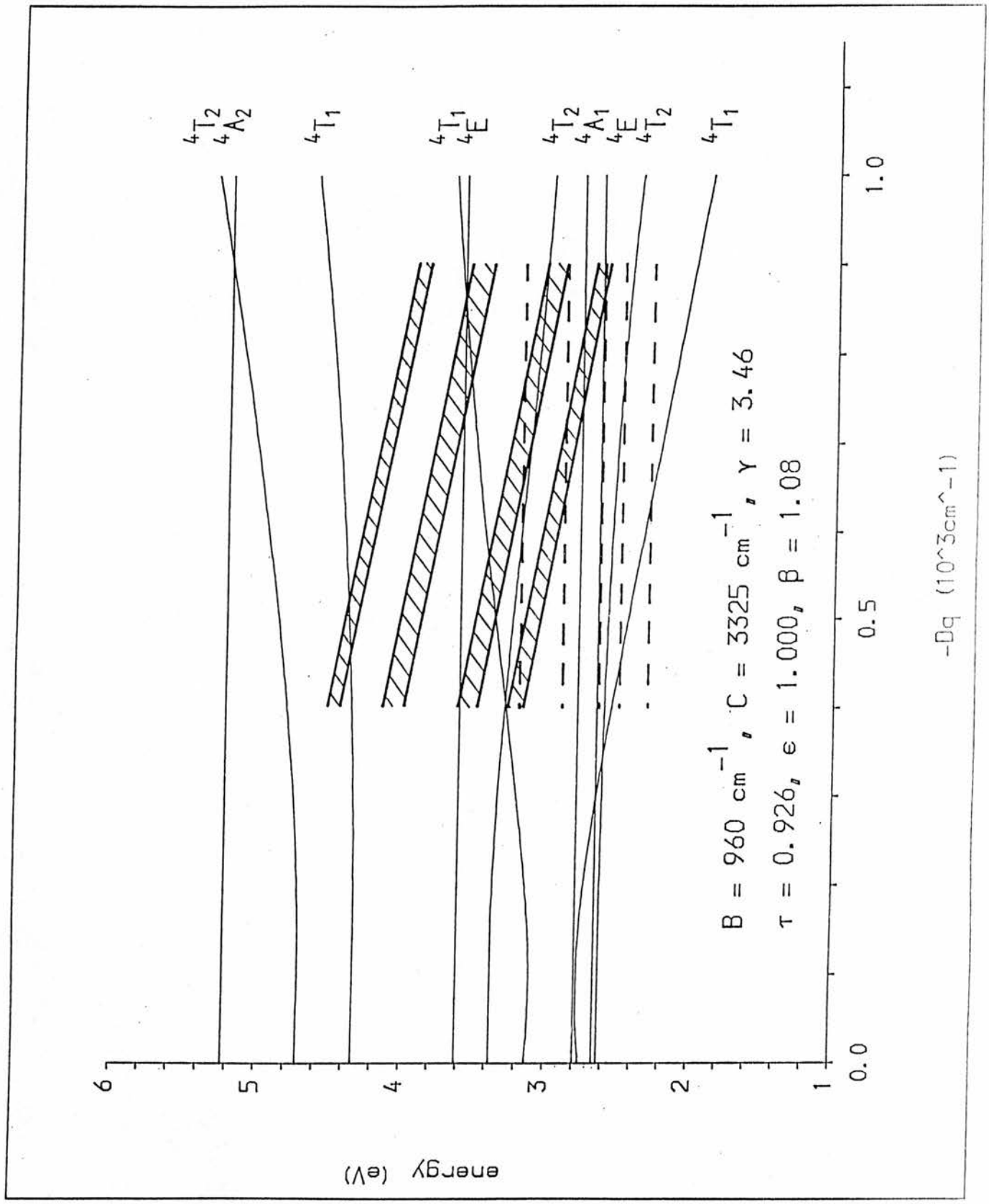

Fig. 6.3.2.7: O'Neill diagram of Mn in ZnS with data from [48], induced bands indicated by shaded area, ordinary bands by dashed line

Concluding I suggest that the four bands observed in induced absorption represent internal transitions within the Mn centres. It is quite probable that transitions from the first band of ordinary absorption to the fourth and fifth band were recorded, but any assignments to actual levels are not very reasonable.

Among the features that have been discussed in this section there is one left: the threshold structure near 400 nm. It has been suggested in section 5.5.1 that a possible photo-ionization of the $^4T_1(G)$ state would show such a feature. Since it also revealed the same properties as the other induced Mn-structures it is connected to the Mn centres. In section 2.4 photo-ionization has been theoretically discussed. This is now applied to the data of Fig. 5.5.2.4. According to (2.4.5) and (2.4.7), the graphs shown in Fig. 6.3.2.8,9 were drawn. The theoretical expected shape of Fig. 2.4.4 can be reasonably suggested in both cases. The fit by a straight line for a part of the graph gives intercepts of 2.45 eV and 2.36 eV, respectively. As the method is rather crude and it is difficult to judge which fit is better, it is sensible to take 2.4 eV for the energy E_{ic} in Fig. 2.4.3. The application of the principle shown in Fig. 2.4.5 was tried resulting in Fig. 6.3.2.10. Although an estimation of the actual energy difference of the $^4T_1(G)$ state to the edge of the conduction band is made, E_{min} = 2.25 eV, the slope of the graph is not steep enough to allow a reasonable interpretation. Hence the phonon interaction was too strong.

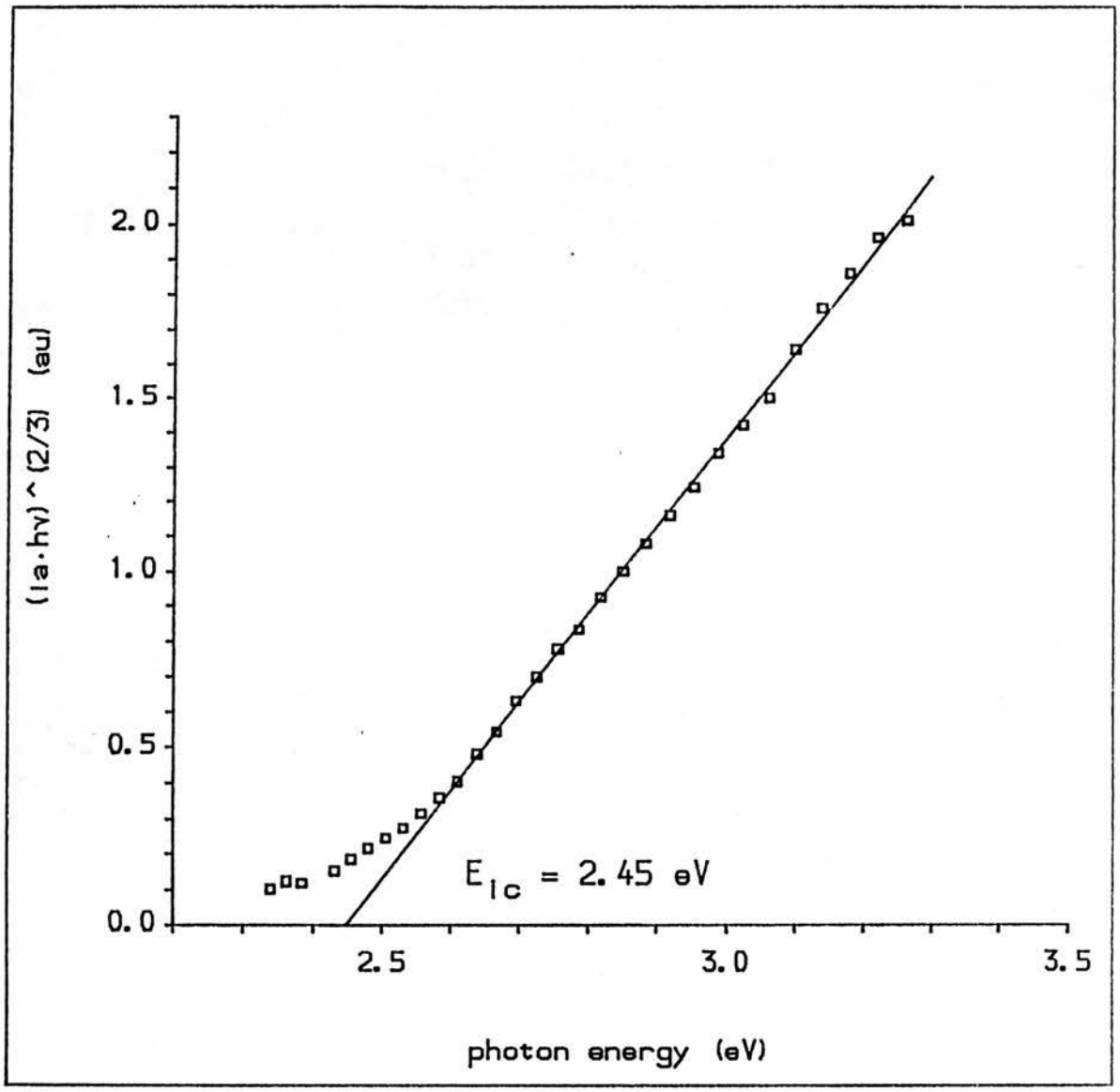

Fig. 6.3.2.8: Fit of induced absorption (ia) threshold according to (2.4.5)

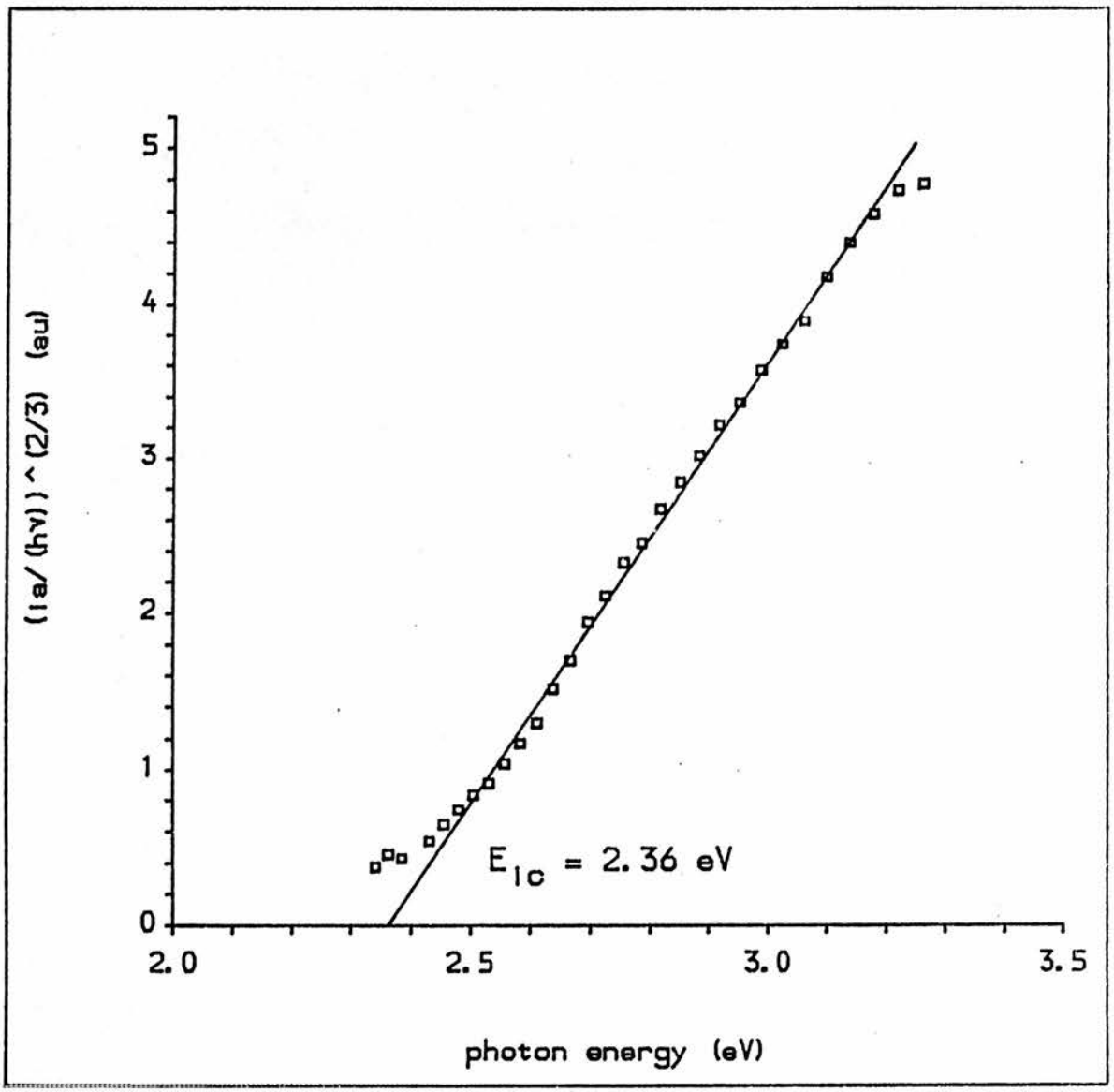

Fig. 6.3.2.9: Fit of induced absorption (ia) threshold according to (2.4.7)

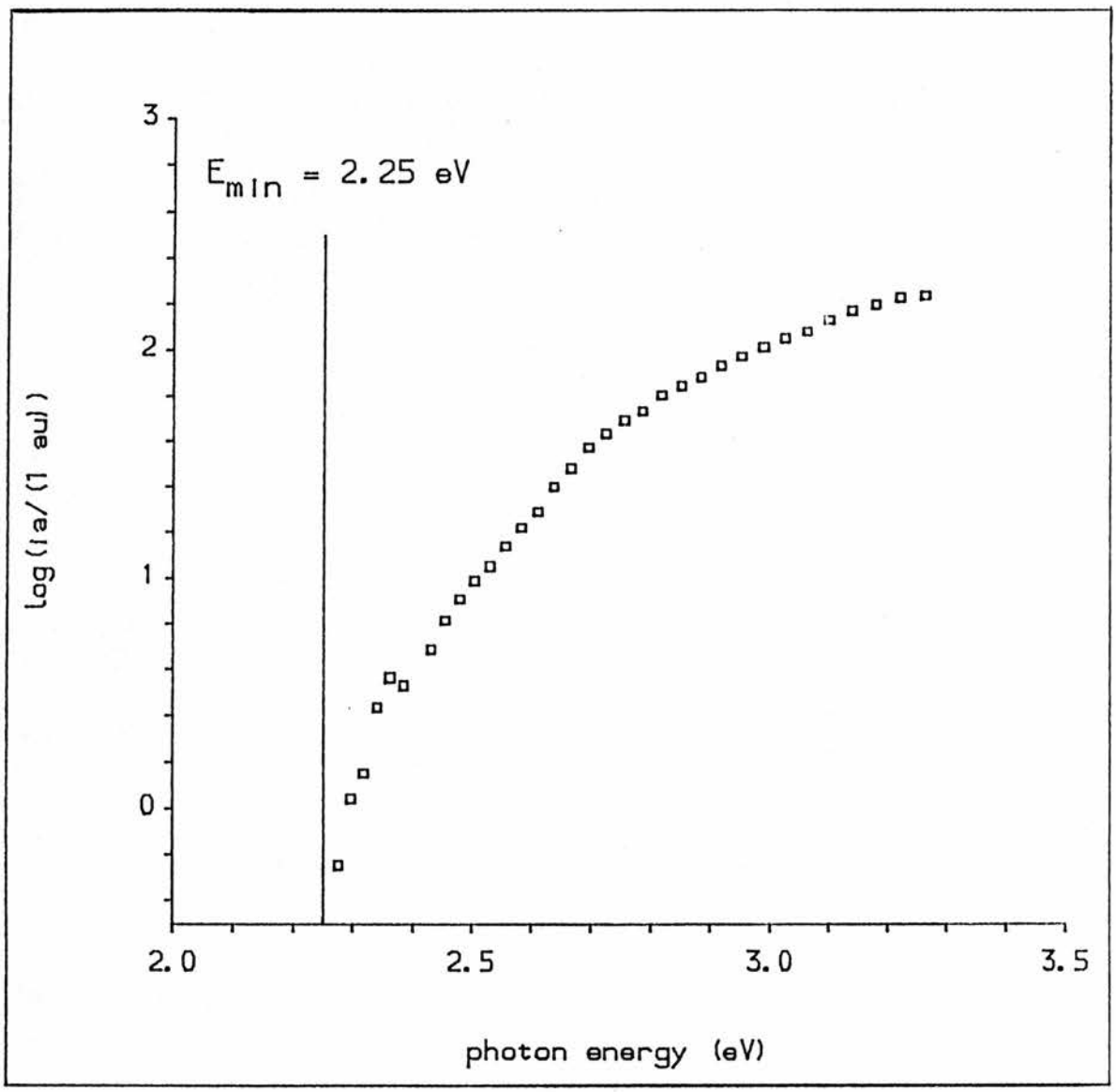

Fig. 6.3.2.10: Logarithmic diagram of induced absorption (ia) threshold to estimate the electronic depth E_{min} of the $^4T_1(G)$ state (s. 2.4)

The points where the graph of Fig. 5.5.2.4 actually declined again were not considered since the theory is only valid for an intermediate part of the curve. Furthermore an energy interval of 0.6 eV for the straight line fit is quite large.

Provided that the feature really represented the photo-ionization of the $^4T_1(G)$ state this would allow an estimate for the depth of the $^6A_1(S)$ ground state: taking 2.4 eV to be the energy depth of the $^4T_1(G)$ state one has with Fig. 6.3.2.11: the $^6A_1(S)$ state is 0.9 eV below the top of the valence band. This figure is different from all the values that have been reported yet (s. section 3.1). On the other hand there has not been a very accurate determination. The results by Allen [30] and Gumlich et al [24] were mere estimations. Langer et al [29] seemed to have experimental evidence but their results remain ambiguous. On the other hand the method employed for the experiments presented in this thesis is quite accurate, leaving an estimated error of around 0.3 eV. The crucial question is now: was it really the photo-ionization of the $^4T_1(G)$ state? It is interesting to note the UV excitation spectra of the orange luminescence in Fig. 10 of Kushida et al's article [2]: near 260 nm, equivalent to 4.8 eV, a sudden threshold is visible that does not seem to be temperature dependent. However, they did not give any importance to that feature. Also, it is not quite sure how the signals had been normalized.

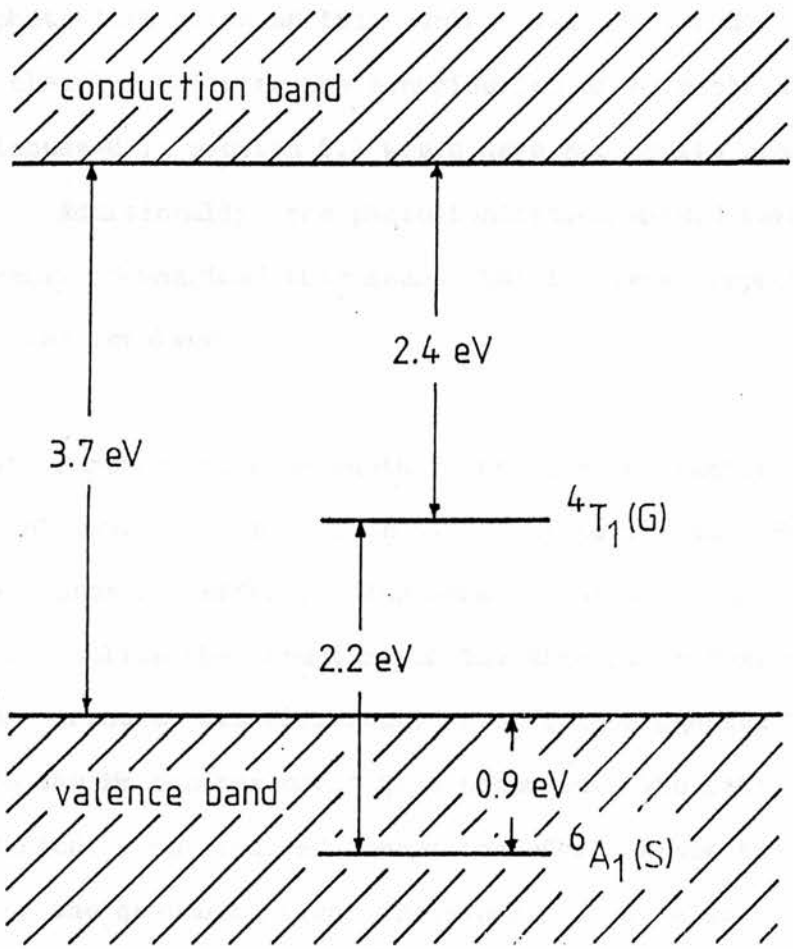

Fig. 6.3.2.11: Possible depth of the Mn states within the band scheme of the ZnS host lattice

In section 6.2 a centre being in the band gap was proposed for the induced absorption discussed in that section. Could it have been that the photo-ionization of this centre was observed? The phase dependence clearly indicates the contribution of Mn centres. Also the process discussed in section 6.2 would have been quite slow for an ac excitation. Additionally the photo-ionization should have been seen there as well. Summarized this means that is very improbable that this centre was involved.

To get further evidence whether the Mn atoms really got ionized the experiment explained in section 5.5.4 was performed. However, it showed the opposite effect. Furthermore the spectral response was rather flat, unlike the structure of the absorption feature. Hence the ongoing process was different, and it is suggested that energy transfer to the Mn centres could have occurred. The latter term has to be modified: an induced energy transfer, since the signal was modulated by the quenching light frequency. It is also possible that the laser was enhancing the transmittance of the sample by the broad band discussed in section 6.2. For green illumination this band exhibited such a behaviour (Fig. 5.3.3.4). The luminescence would have acted as probe light.

It is difficult to say whether the experiment rules out the process it was thought to prove. If one tries to estimate the expected signal one has to do a lot of approximations. Eventually it turns out that the quenching effect would have been at least one order less in magnitude than the observed signal. Hence one cannot exclude

the photo-ionization by the results of the experiment.

One has to bear in mind another important conclusion in the case the $^4T_1(G)$ state really is 2.4 eV below the conduction band: the high energy levels of the $3d^5$ electrons of the Mn centres would be very close to the conduction band and, therefore, the failure of crystal field theory for these levels would not surprise.

I finish the discussion of this section with the remark that it is possible that the photo-ionization of the $^4T_1(G)$ was observed. However, there is not enough evidence to be sure.

6.3.3 OTHER STRUCTURES

This section deals with the induced band around 1000 nm and with the increased transmittance at the spectral region of the luminescence. The first feature clearly had a different frequency behaviour as Fig. 5.5.3.8 showed. The process got very inefficient for high frequencies (Fig. 5.5.3.9). Since the phase shift was far too high at low frequencies the origin of the feature could not have been an internal Mn process. It gives rather evidence of an optical centre other than the Mn centres. Unfortunately I could not derive the proper spectral shape as two of the other bands were close to it. However, it seems to be rather broad (compared to the other induced bands). In section 6.2 it was suggested that there is a centre B somewhere above the valence band (Fig. 6.2.2). Suppose that this band

stands for the transition of an electron from the valence band to the centre B. The energy difference would be around 1 eV which seems to be consistent. Of course, this does not exclude any other kind of process.

For the other feature one has obviously this problem that already arose for the results of section 5.4.4: was it the luminescence that got enhanced or was it another superposing structure? Again the latter could have been the broad band of section 6.2 The fact that it was now rather small in width could be explained as on both sides were structures with the opposite effect. On the other hand an enhancement of the luminescence is also possible. At least the feature seems to be consistent with the observed rise of the luminescence discussed in the previous section. It is, however, confusing why the signal was rather unstable (s. section 5.5.4). Unfortunately I have to leave the discussion to these suggestions.

6.3.4 CONCLUSION

The experiments have revealed a lot of induced processes in the investigated sample of ZnS:Mn. The existence of the three bands first seen by Kushida et al [2] has been confirmed. I also support their suggestion that these bands represent internal induced transitions of the Mn impurities, although I do not follow their certainty about assignments to actual energy levels.

However, a lot of other structures appeared additionally, raising more questions about an apparently very sophisticated system. Since some of the processes are clearly connected to the Mn centres the question remains why they had not been recognized by the former work. The most outstanding result was the possible discovery of the depth of the $^4T_1(G)$ state. To ensure the latter and to bring up more understanding of the other processes more experiments are necessary. It is important to repeat the here described experiment with a view to the following points: different samples have to be used, having the same, differing and no concentration of Mn impurities; similar semiconductors should be used like ZnSe, especially of interest would be a series of ZnS_xSe_{1-x}:Mn samples; photocapacitance measurements could be employed additionally like suggested by Gumlich in [18]; the temperature dependence of the effects could yield even more information; samples that were made conductive by the so-called Zn treatment, where any acceptor and even donor would be well populated and could no longer perturb the experiment, should be used as well.

7 SUMMARY

A sphalerite ZnS sample doped with 0.5 at% Mn was investigated by means of induced absorption. By populating the first excited state of the Mn centres, $^4T_1(G)$, it should be possible to see subsequent absorption to higher excited states that are usually hidden in direct absorption by the fundamental band gap absorption. Kushida et al [1,2] did first work on this field. They pumped the $^4T_1(G)$ state by the 488 nm line of an Ar-ion laser and saw induced absorption bands at 655, 830 and 1280 nm. Since the signals were very weak they used the sensitive method of modulating the laser signals by a chopper and recovering the correlated signals in the direct dc probe beam. They recognized as well that one has to consider the contribution of Mn centres in pairs at high enough concentrations which can result in a phase shift between luminescence and induced absorption. Still, those results needed some kind of confirmation. This was why the research presented in this thesis was carried out.

The sample used here showed ordinary properties in direct absorption and in photoluminescence (excited by the 514.5 nm line of an Ar-ion laser). A spectral region of 350 - 2700 nm was covered by detectors as a photo-multiplier and a PbS-photocell. All experiments were done at room temperature. Before the laser experiments were started white light by a halogen-tungsten bulb had been employed as inducing light. Any revealed structure could not have been due to internal Mn transitions since the concentration of excited centres was too low. However, any discovered process would be due to other

effects that could perturb the later laser experiments and mimic any Mn participation. In these first experiments the probe light beam was chopped and the change in the transmission signal was recorded.

Eventually a broad induced absorption band was found having its peak near 575 nm (2.2 eV). It turned out that the effect was much stronger under blue light but reversed under red light illumination. Although the signal responded very quickly when the inducing light was shone onto the crystal, the signal took time of an order of half a minute to relax after the light was shut off.

For the laser experiments the laser beam (Ar-ion, λ = 514.5 nm) was chopped, like in the former Japanese experiment. A lot of structures have been revealed in these experiments (chopping frequency: 80 Hz). The frequency behaviour of five structures showed a common tendency and was consistent with a calculated phase shift for the expected induced absorption. Therefore, it is very likely that these structures represent transitions departing from the $^4T_1(G)$ state of the Mn centres. There were four bands at 650, 830, 1270 and 1910 nm. They had a FWHM of a bit more than 0.1 eV. The last three were nearly of the same intensity whereas the first one was as three times as intense. A threshold appeared around 520 nm, rising up to near 380 nm. It was then slowly decreasing again but as the intrinsic absorption was getting very intense this remains dubious. Additionally there was a signal around 1000 nm that was totally out of phase and nearly disappeared for high enough frequencies. Surprisingly the transmittance around the wavelength of the orange luminescence rose. Unfortunately no information was obtained about

the phase behaviour of this feature since it was discovered at a very late stage.

For the broad band seen under bulb light illumination several models were worked out and discussed. Although it is obvious that states in the forbidden gap were involved it is not exactly clear what had happened and what the nature of these centres was.

The four bands attributed to Mn transitions were discussed in terms of crystal field theory. It seems to be quite sure that the two low energy bands correspond to transitions within the outermost bands seen in direct absorption. A shift between the energy difference of the ordinary bands and the energy of the induced bands can be explained by a configuration coordinate scheme. Though, actual assignments are difficult. It seems to be plausible to ascribe these bands to the $^4T_2(D)$ and $^4E(D)$ states. The two high energy bands could be the $^4T_1(P)$ and $^4A_2(F)$ state as suggested by Kushida et al [2]. However, from my point of view these assignments are far from certainty.

The most important result of this work is the possible discovery of the depth of the $^4T_1(G)$ state within the host band structure. The threshold at short wavelengths was discussed in terms of some basic theory of photo-ionization, which gave at least some evidence that photo-ionization really had occurred. Since the phase behaviour of this feature was the same as the one of the other Mn bands one gets the possible conclusion that the photo-ionization of the $^4T_1(G)$ was observed. This would mean that the latter state is around 2.4 eV

below the edge of the conduction band, the $^6A_1(S)$ ground state 0.9 eV below the edge of the valence band. The position of the ground state has never been determined very accurately. There was a wide range of estimations, and one experiment seemed to show the ground state being 3 eV below the top of the valence band. But there was still uncertainty.

Another experiment was performed to get more information about this specific feature. It was tried to quench the luminescence by the light which corresponded to the wavelengths of the threshold (further explanation s. section 5.5.4). The opposite effect was observed, the luminescence rose. However, this did not rule out the suggested photo-ionization. The effect could have been too weak and superposed by a different process. The rise of the luminescence could be consistent with the one reported above and due to energy transfer. It is also possible that the feature detected under bulb illumination could have been involved. Finally there is still the band at 1000 nm which was discussed in connection to the white light induced absorption as well without having resulted in a clear model.

Concluding the experiments have confirmed the existence of the three bands that were observed by Kushida et al [2] first. However, other features were revealed as well. Further experiments as suggested in the sections of chapter 6 have to be performed to get more information. In particular it is important to put the emphasis on the electronic ground state energy of the Mn centres in ZnS, which is essential for the understanding of the excitation process in electroluminescence.

Another important result seems to be that the application of ordinary crystal field theory to Mn in ZnS is rather restricted.

REFERENCES

[1]: T Kushida, Y Tanaka and Y Oka, Solid State Comm 14, 617 (1974)

[2]: T Kushida, Y Tanaka and Y Oka, J Phys Soc Japan 37, 1341 (1974)

[3]: G Destriau, J de Chimie Physique 33, 587 (1936)

[4]: H A Bethe, Ann Physik 3, 133 (1929)

[5]: G Gliemann and H L Schläfer, 'Einfuehrung in die Ligandenfeldtheorie', 2nd edition, Aula Verlag, Wiesbaden (1980)

[6]: C J Ballhausen, 'Introduction to Ligand Field Theory', McCraw-Hill, New York (1962)

[7]: Y Tanabe, S Sugano and H Kamimura, 'Multiplets of Transition-Metal Ions in Crystals', Academic Press, New York (1970)

[8]: D S McClure, Solid State Phys 9, 399 (1959)

[9]: G Racah, Phys Rev 63, 367 (1942)

[10]: Y Tanabe and S Sugano, J Phys Soc Japan 9, 753, 766 (1954)

[11]: L E Orgel, J Chem Phys 23, 1004 (1955)

[12]: S Koide and M H L Pryce, Phil Mag 8, 607 (1958)

[13]: A G O'Neill, PhD thesis, Univ of St Andrews (1984)

[14]: A Zunger, Solid State Phys 39, 275 (1986)

[15]: J W Allen, unpublished

[16]: J W Allen, unpublished

[17]: J W Allen, J Phys C 2, 1077 (1969)

[18]: H E Gumlich, J Lum 23, 73 (1981)

[19]: Atomic Energy Levels, vol II, Circular of the National Bureau of Standards 467, 37 (1952)

[20]: F A Kroeger, Physica 6, 369 (1939)

[21]: R A Ford, E Kauer, A Rabenau and D A Brown, Ber Bunsenges phys Chem 67, 460 (1963)

[22]: U W Pohl, H E Gumlich and W Busse, phys stat sol (b) 125, 773 (1984)

[23]: Y Uehara, Bull Marianna Univ 3, 57 (1974)

[24]: H E Gumlich, R L Pfrogner, J C Shaffer and F E Williams, J Chem Phys 44, 3929 (1966)

[25]: D Langer and S Ibuki, Phys Rev 138, A809 (1965)

[26]: E Neumann, Thesis D 83, Techn Univ Berlin (1971)

[27]: D S McClure, J Chem Phys 39, 2850 (1963)

[28]: A Mehra, J Electrochem Soc 118, 136 (1971)

[29]: D W Langer, O C Helmer and N H Weichert, J Lum 1,2, 341 (1970)

[30]: J W Allen, Proceedings of the International Conference on the Physics of Semiconductors, Paris, edited by M Hulin (Academic, New York), 781 (1964)

[31]: J Xue-yin, Y Jia-qi, Y Bao-jun, F Shu-fen and H Ying, Faguang Yu Xianshi, No 1, 1 (1983)

[32]: H Ying, Y Jia-qi and Y Bao-jun, J Phys C 19, 5405 (1986)

[33]: N D Borisenko and F F Kodzhespirov, Sov Phys Semicond 5, 114 (1971)

[34]: R E Behringer, J Chem Phys 29, 537 (1958)

[35]: W Busse, H E Gumlich, B Meissner and D Theis, J Lum 12,13, 693 (1976)

[36]: N E Rigby, PhD thesis (to be submitted), Univ of St Andrews

[37]: O Goede and D D Thong, phys stat sol (b) 124, 343 (1984)

[38]: O Goede, W Heimbrodt and D D Thong, phys stat sol (b) 126, K159 (1984)

[39]: P Sviszt, phys stat sol 4, 631 (1964)

[40]: P E Simmonds and L Eaves, Appl Phys Lett 39, 558 (1981)

[41]: J M Noras, phys stat sol (a) 76, K53 (1983)

[42]: J M Noras, J Phys C 16, 5517 (1983)

[43]: J Dieleman, C Z van Doorn, S H de Bruin and J H Haanstra, Proceedings of the International Conference on the Physics of Semiconductors, Paris, edited by M Hulin (Academic, New York), 941 (1964)

[44]: H Kukimoto, R Hioki and T Koda, Phys Lett 19, 551 (1965)

[45]: Handbook of Optical Constants of Solids, edited by E D Palik (Academic Press Handbook Series), 597 (1985)

[46]: K Era, S Shionoya and Y Washizawa, J Phys Chem Solids 29, 1827 (1968)

[47]: K Matsuura, S Kishida and I Tsurumi, phys stat sol (b) 140, 347 (1987)

[48]: A G O'Neill, private correspondence

[49]: D Theis, Phys Lett 59A, 154 (1976)